

**Antitumoral polymeric siRNA nanoformulation and
pretubulysin-based combination therapies**

von Sarah Verena Kern

Inaugural-Dissertation zur Erlangung der Doktorwürde
der Tierärztlichen Fakultät der Ludwig-Maximilians-Universität
München

**Antitumoral polymeric siRNA nanoformulation and
pretubulysin-based combination therapies**

von Sarah Verena Kern

aus Bühl (Baden)

München 2019

Aus dem Veterinärwissenschaftlichen Department der Tierärztlichen Fakultät
der Ludwig-Maximilians-Universität München

Lehrstuhl für Molekulare Tierzucht und Biotechnologie

Arbeit angefertigt unter der Leitung von Univ.-Prof. Dr. Eckhard Wolf

Angefertigt an:

Fakultät für Chemie und Pharmazie, Lehrstuhl für Pharmazeutische
Biotechnologie der Ludwig-Maximilians-Universität München

Mentor: Univ.-Prof. Dr. Ernst Wagner

Gedruckt mit Genehmigung der Tierärztlichen Fakultät
der Ludwig-Maximilians-Universität München

Dekan: Univ.-Prof. Dr. Reinhard K. Straubinger, Ph.D.

Berichterstatter: Univ.-Prof. Dr. Eckhard Wolf

Korreferenten: Univ.-Prof. Dr. Johannes Hirschberger
Univ.-Prof. Dr. Dr. h.c. Hans-Joachim Gabius
Univ.-Prof. Dr. Bernd Kaspers
Univ.-Prof. Dr. Heidrun Potschka

Tag der Promotion: 25. Februar 2019

Meiner Familie

TABLE OF CONTENTS

I.	INTRODUCTION.....	1
1.	Nucleic acid therapy using siRNA.....	2
1.1.	Obstacles in siRNA delivery.....	3
1.2.	Carrier systems for siRNA and drug delivery.....	4
1.2.1.	Precise sequence-defined oligomers.....	6
1.3.	Surface shielding of nanoparticles.....	7
1.4.	Active and passive targeting of nanoparticles.....	8
2.	Combination chemotherapy as therapeutic approach.....	10
2.1.	Methotrexate.....	10
2.2.	Pretubulysin.....	11
3.	Aims of this thesis.....	13
3.1.	Shielded and targeted nanoparticles for effective siRNA delivery..	13
3.2.	Combinatorial treatment of PT and MTX.....	13
II.	MICE, MATERIALS AND METHODS.....	15
1.	Mice.....	15
1.1.	Mouse strains.....	15
1.1.1.	NMRI-nude mice.....	15
1.1.2.	BALB/c mice.....	15
1.2.	Housing conditions.....	15
1.3.	Health monitoring.....	16
2.	Materials.....	16
2.1.	Cell culture.....	16
2.2.	<i>In vivo</i> experiments.....	17
2.3.	Oligomers.....	17
2.4.	siRNAs.....	17
2.5.	Compounds.....	18
2.6.	Instruments.....	18
2.7.	Software.....	18
3.	Methods.....	18
3.1.	Cell culture.....	18
3.2.	<i>In vivo</i> experiments.....	18

3.2.1.	Biodistribution study with PSar shielding.....	19
3.2.2.	Biodistribution of Fola-targeted lipopolyplexes	20
3.2.3.	Intratumoral <i>EG5</i> gene silencing after systemic application.....	20
3.2.4.	Clinical biochemistry after systemic application	21
3.2.5.	Combinatorial treatment with Fola-targeted siEG5 lipopolyplexes and PT	21
3.2.6.	Treatment with GE11-targeted, PT containing siEG5 lipopolyplexes.....	21
3.2.7.	Intratumoral treatment with E4-MTX-H-PT conjugate	22
3.2.8.	Effect of intravenous injections of PT+MTX on L1210 tumor growth	22
3.2.8.1.	MTX dose finding	22
3.2.9.	Effect of intravenous injections of PT+MTX on KB tumor growth...	23
3.2.10.	Effect of intravenous injections of PT+MTX on HUH7 tumor growth	23
3.2.11.	Oligomer-based micellar encapsulation of PT+MTX for systemic administration.....	23
3.3.	Statistical analysis.....	24
III.	RESULTS	25
1.	Shielded and targeted lipopolyplexes for effective siRNA delivery	25
1.1.	Exploiting click chemistry for the modification of lipopolyplexes with functional domains.....	25
1.1.1.	Comparison of PSar and PEG as shielding agents.....	27
1.2.	Fola receptor-targeted lipopolyplexes for gene silencing <i>in vivo</i> ...	28
1.2.1.	Biodistribution study	30
1.2.2.	Clinical biochemistry evaluation	36
1.2.3.	Tumoral gene silencing <i>in vivo</i>	37
1.2.4.	Combinatorial treatment with Fola-targeted lipopolyplexes and PT	41
1.2.5.	Treatment with GE11-targeted, PT containing siEG5 lipopolyplexes.....	44
2.	Combinatorial treatment of PT and MTX.....	48
2.1.	Intratumoral treatment with E4-MTX-H-PT conjugate	48

2.2.	Combined antitumoral effects of PT and MTX after systemic application	51
2.2.1.	Effect of PT+MTX combination therapy on L1210 tumor growth....	52
2.2.1.1.	Dose finding of MTX.....	54
2.2.2.	Effect of PT+MTX combination therapy on KB tumor growth	56
2.2.3.	Effect of PT+MTX combination therapy on HUH7 tumor growth	57
2.3.	Oligomer-based micellar encapsulation of PT+MTX for systemic administration.....	60
IV.	DISCUSSION.....	65
1.	Shielded and targeted lipopolyplexes for effective siRNA delivery	65
1.1.	PEG and PSar as shielding agents	65
1.2.	Targeted lipopolyplexes for gene silencing <i>in vivo</i>	67
2.	Combinatorial treatment of PT and MTX.....	72
2.1.	Intratumoral treatment with E4-MTX-H-PT conjugate	72
2.2.	Combined antitumoral effects of PT and MTX	73
2.3.	Oligomer-based micellar encapsulation of PT+MTX for systemic administration.....	75
V.	SUMMARY	77
VI.	ZUSAMMENFASSUNG.....	79
VII.	REFERENCES	83
VIII.	APPENDIX.....	101
1.	Publications.....	101
2.	Abstracts and Posters	102
2.1.	Poster.....	102
2.2.	Abstract.....	102
IX.	ACKNOWLEDGEMENTS.....	103

ABBREVIATIONS

°C	degree Celsius
µL	microliter
ALT	alanine transaminase
AST	aspartate transaminase
BUN	blood urea nitrogen
CCD	charge-coupled device
cDNA	complementary DNA
CholA	cholanic acid
CLSM	confocal laser scanning microscopy
Cy7	cyanine 7
(D)CT	(delta) cycle threshold
DBCO	dibenzocyclooctyne
DHFR	dihydrofolate reductase
DMEM	Dulbecco's Modified Eagle's Medium
DNA	deoxyribonucleic acid
e.g.	exempli gratia (for example)
EG5	eglin 5, kinesin spindle protein
EDTA	ethylenediamine tetraacetic acid
EGF	epidermal growth factor
EGFR	epidermal growth factor receptor
EPR effect	enhanced permeability and retention effect
FCS	fetal calf serum
FELASA	Federation of European Laboratory Animal Science Associations
FoIA	folic acid

FR	folate receptor
G	gauge
g	gravity
GADPH	glyceraldehyde 3-phosphate dehydrogenase
h	hour(s)
HBG	HEPES buffered glucose
HPLC	high performance liquid chromatography
i.t.	intratumoral(ly)
i.v.	intravenous(ly)
IVIS [®]	<i>in vivo</i> imaging system
LPEI	linear polyethylenimine
mRNA	messenger RNA
MTT	3-(4,5-dimethylthiazol-2-yl)-2,5-diphenyltetrazolium bromide
MTX	methotrexate
N/P	polymer nitrogen to nucleic acid phosphate ratio
NIR	near infrared
OleA	oleic acid
PBS	phosphate buffered saline
pDNA	plasmid DNA
PEG	polyethylene glycol
POMP	6-mercaptopurine (=Purinethol), vincristine (=Oncovin), methotrexate, prednisone
PSar	polysarcosine
PT	pretubulysin

qRT-PCR	quantitative reverse transcription polymerase chain reaction
RES	reticuloendothelial system
RFC	reduced folate carrier
RISC	RNA-induced silencing complex
RNA	ribonucleic acid
RNase	ribonuclease
s.c.	subcutaneous(ly)
S.E.M.	standard error of the mean
siRNA	small interfering RNA
Sph	succinoyl-pentaethylene-hexamine
ssbb	disulfide building block
Stp	succinoyl-tetraethylene-pentamine
TfR	transferrin receptor
UPL	universal probe library
wt	wildtype

I. INTRODUCTION

Cancer remains the second leading cause of death worldwide with almost 1/6th of deaths being related to cancer [1]. In 2012, the WHO recorded 14.1 million of new diagnoses and 8.2 million of cancer related deaths [2]. Among men, lung cancer is globally the most commonly diagnosed form and most common cause of cancer death, whereas in women, breast cancer occurs most frequently [3]. About every third case is attributed to an unhealthy lifestyle which includes obesity, lack of physical activity and excessive consumption of alcohol or tobacco. The latter has emerged a major risk factor being responsible for 22% of cancer deaths [1].

Cancer arises when healthy cells degenerate and transform into malignant tumor cells. The underlying cause encompasses genetic predisposition and external parameters like physical, chemical or biological factors, but also dietary habits or chronic infections like hepatitis B and C or human papillomavirus (HPV) [1]. Another important aspect is ageing: A drastic ascent in the incidence can be found with an increase of age. This finding can be explained by an accumulation of risk factors, but also by the fact that the cells' repair mechanisms become less effective over time [1]. Consistent with this tendency, Germany experienced a rise of cancer cases between 2002 and 2012 that ranged around 13% in men and 10% in women, which is traced back to the demographic change with a growing proportion of older people [4].

In terms of therapeutic outcome and prognosis, the time of diagnosis is essential. Various forms of cancer like breast cancer or cervical cancer show promising cure rates when diagnosed at an early stage [1]. Certainly, each type of cancer requires a specific treatment protocol. Most established treatment methods include surgery, radiation and chemotherapy. However, once the primary tumor has started to metastasize to distant sites of the body, surgery becomes inconvenient. Another major weakness is the growing development of chemoresistance that hampers success rates of chemotherapy. Considering these drawbacks that conventional methods are confronted with, the need for innovative treatment options becomes

crucial. Therefore, this thesis deals with the establishment of efficient carrier systems for the delivery of small interfering RNA (siRNA) and introduces a novel drug combination as alternative to conventional treatment regimens.

1. Nucleic acid therapy using siRNA

Nucleic acid therapeutics are gaining more and more attention in the treatment of several diseases. There are two main groups with opposite effects to be distinguished: On the one hand, messenger RNA (mRNA) and plasmid DNA (pDNA) promote the expression of a gene product [5], thus enhance a gene function, while antisense oligonucleotides and siRNA on the other hand, lead to a knockdown of the target gene product [6], thus hamper a gene function.

siRNA, as a non-coding RNA, interferes directly with the expression of a gene product by specifically downregulating the target mRNA, and therefore represents a promising therapeutic tool in combatting various diseases [7-11]. It consists of two strands, one guide strand (antisense strand) and one passenger strand (sense strand) with 21 to 23 nucleotides. Once it has reached the cytosol of its target cell, the two strands are cleaved and the guide strand is incorporated into the RNA induced silencing complex (RISC), while the passenger strand is degraded. Through the incorporation of siRNA, RISC gets enabled to detect the target mRNA, which will subsequently be cleaved by the activated RNase part of the complex (referred to as argonaute protein 2, or Ago2). Finally, this degradation results in a knockdown of the disease-associated gene product (**Figure 1**) [6, 12, 13].

To the present day, several siRNA-based therapeutics have entered clinical trials [14]. In August 2018, the US FDA approved Patisiran (Onpattro™, a PEGylated liposomal transthyretin (TTR) siRNA formulation) as first siRNA drug for the treatment of hereditary transthyretin-mediated amyloidosis (hATTR) [15]. However, siRNA therapeutics in general are repeatedly confronted with drawbacks regarding their tolerability [14, 16], so more effort has to be made in designing stable and efficient, nevertheless biocompatible carrier systems.

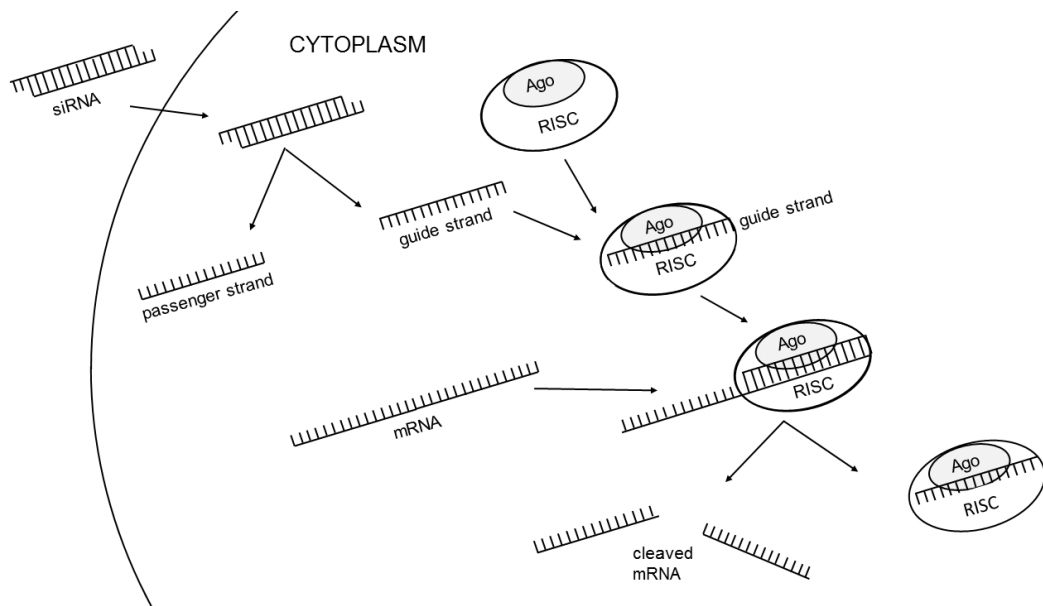


Figure 1: Gene silencing mediated by siRNA. After reaching the cytoplasm, double-stranded siRNA is cleaved. The passenger (=sense) strand is degraded, while the guide (=antisense) strand is incorporated into the RISC complex. This leads to an activation of Ago 2, the RNase part of the complex. The matching mRNA sequence can be identified and subsequently cleaved resulting in a knockdown of the disease-associated gene product.

1.1. Obstacles in siRNA delivery

Despite very encouraging advances in siRNA research and the great potential of this attractive tool in the therapy of various diseases, siRNA delivery faces some major drawbacks. Naked siRNA presents very poor pharmacokinetic properties and gets cleared from the circulation already a few minutes after intravenous injection [17]. In fact, siRNA is confronted with several hurdles after systemic application that an ideal carrier should overcome. First, siRNA containing nanoparticles have to prevent their content from recognition by macrophages and other immune cells. Also, degradation by serum nucleases can pose a threat. Therefore, an optimal delivery system should shield siRNA from unwanted interactions with blood components and by that prolong its circulation time [18]. Another biological barrier is the fast renal clearance of particles of a certain size. This problem can be solved by creating nanoparticles that range from 10 to 200 nm, as renal clearance occurs for particles smaller than 10 nm [19], while sizes larger than 200 nm favor degradation by macrophages of the reticulo-endothelial system (RES) [20, 21]. Extravasation in the tumor area

is facilitated, as tumor vasculature of many solid tumors is leaky, exhibiting higher permeability than vessels of normal tissue [22]. Once a particle extravasates, it has to pass the extracellular matrix to finally reach its target cell. Upon entry into the cell by endocytosis, which is the preferred mechanism of most carrier systems [23], the siRNA particle has to escape the endosome to reach its final destination, the cytosol (**Figure 2**). Since endosomes exhibit an increasingly acidic pH, endosomal escape should happen early after internalization.

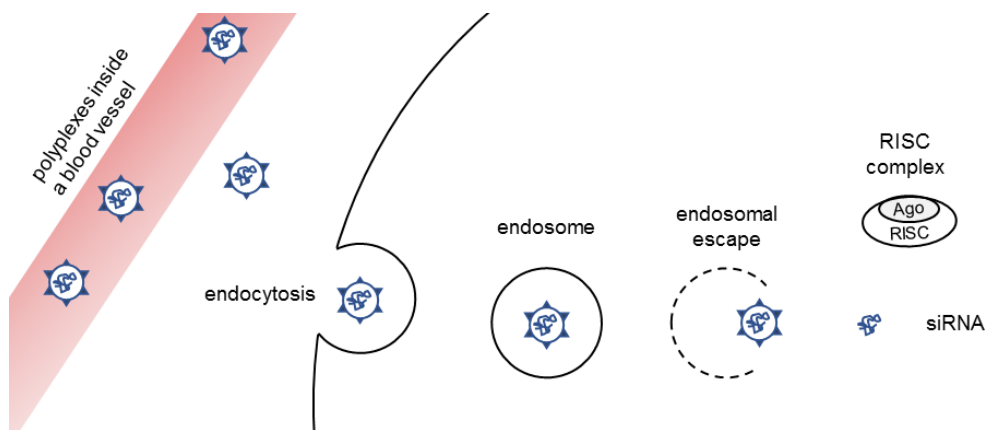


Figure 2: Mechanism of siRNA delivery. After intravenous administration of siRNA polyplexes, particles extravasate in the tumor tissue, since blood vessels in this area are extremely leaky. Polyplexes travel through the extracellular matrix and by endocytosis enter the tumor cell. As the endosome gets increasingly acidic, endosomal escape is mediated by the polyplex to release siRNA to the cytoplasm, where it is incorporated into the RISC complex.

1.2. Carrier systems for siRNA and drug delivery

To deliver siRNA to its site of action and overcome the aforementioned biological barriers, carriers require certain properties. Above all, in order to prevent systemic side effects, they should be both biocompatible and biodegradable [24]. Moreover, they should not provoke immune responses, hence be nonimmunogenic. siRNA should be protected from degradation by serum nucleases and distribution after systemic application should certainly reach the target tissue. Ultimately, endosomal escape should be effectively triggered after entering the cell [25, 26].

When it comes to carrier systems, two major groups can be distinguished:

Viral vectors and non-viral vectors. On the one hand, viral vectors display an excellent transfection efficiency, which is attributed to the ability of viruses to efficiently infect host cells. Although in most cases, the coding regions responsible for replication and toxicity are removed from the virus genome, viral vectors still bear various risks like their immunogenicity, infectious and oncogenic potential [27]. Also, they present very limited loading capacity and their synthesis in high quantities remains challenging [28, 29]. On the other hand, non-viral vectors present very promising alternatives to viruses for the delivery of nucleic acids. As most encouraging carriers of this group, cationic polymers and liposomes have emerged [30]. As the nucleic acid backbone is negatively charged, electrostatic interactions with polymers and liposomes lead to the formation of stable particles, then referred to as polyplex or lipoplex [31]. This process also implies a condensation of the nucleic acid, enabling the internalization into the target cell via endocytosis [32]. Among the polycations, linear polyethylenimine (LPEI) became the gold standard in gene delivery [33]. After endocytosis, in order to deliver their cargo to the cytosol, endosomal release is achieved by the polycations' proton-sponge properties, hence osmotic swelling is induced, followed by rupture of the endosome [34]. However, these nanoparticles are confronted with immunogenicity and degradation by the RES. Moreover, they exhibit poor biodegradability [35], and their cationic charge and molecular weight often provoke unwanted side effects. In order to improve efficiency and increase tolerability, various functional domains can be introduced into these carrier systems and by that mediate surface shielding, active targeting or endosomal escape [36].

Anyway, carriers are not only exploited for nucleic acid delivery. Also, regarding *in vivo* drug delivery, carrier systems provide various advantages as compared to the administration of free drugs. Firstly, they prolong circulation times of small molecule drugs due to their optimized size and surface modifications [37, 38]. Secondly, coming along with the increased size as well as surface shielding, passive targeting is enabled [39]. Thirdly, ligands for active targeting might be introduced to the nanoparticle to facilitate cellular uptake. Ultimately, several drugs with different pharmacokinetic properties can be encapsulated and thereby delivered

simultaneously to the target site [40].

1.2.1. Precise sequence-defined oligomers

Our group has been working on the development of new cationic carrier systems. By solid-phase supported synthesis, we have been creating sequence-defined oligoaminoamides and until today designed more than 1200 oligomers with different functional moieties and various modifications for efficient nucleic acid or drug delivery. These oligomers are small, peptide-like structures with proton-sponge properties [34]. In contrast to conventional polymers, our oligomers are smaller in size while their cationic character is diminished. The combination of both aspects results in a reduced cytotoxicity.

Hartmann *et al.* were the first to design precise, sequence-defined oligomers [41]. Subsequently, these novel carrier systems were further refined by Schaffert *et al.* and Dohmen *et al.* who introduced more building blocks into the carrier systems [42] and included additional substructures into the polymeric backbone [43].

Primarily, an oligomer consists of a linear backbone, which is made from two artificial amino acids: Succinoyl-pentaethylene-hexamine (Sph) and succinoyl-tetraethylene-pentamine (Stp) serving as building blocks. These amino acids are responsible for polyplex formation, as they are positively charged due to their partly protonated state in neutral pH. siRNA however, is negatively charged, hence polymer and nucleic acid can form a polyplex with advantageous properties for siRNA delivery [44]. Further modifications can be introduced into the oligomer. Cysteines are often used as they are able to form disulfide bonds and thereby increase stability. Modification with histidines leads to improved endosomal buffering capacity, whereas tyrosines and fatty acids mediate stabilization through their hydrophobic properties. Various topological subclasses can be distinguished, for example linear, 2-arm, 3-arm, 4-arm or T-shaped oligomers. Topology has a major impact on nucleic acid complexation and polyplex characteristics [45-47]. Regarding siRNA delivery, for example, T-shape oligomers proved to be most suitable. They are characterized by the modification of the cationic backbone with a hydrophobic domain, typically consisting in two

fatty acid units. As aforementioned, fatty acids enhance the polyplex's stability, which is of great importance in the extracellular space. After internalization into the target cell, however, hydrophobic domains and siRNA binding backbone have to disassemble to release siRNA to the cytosol [47, 48]. Disassembly can be facilitated by the introduction of disulfide building blocks (ssbb), which can be located between both domains. ssbb units represent bio-reducible bonds. Hence, siRNA binding polycationic backbone and fatty acid units get cleaved upon entry into the cytosol and siRNA is released for incorporation into the RISC [49].

Another important aspect is the polymer's surface shielding, on the one hand preventing undesired interactions with blood components and on the other hand prolonging circulation time, which finally leads to improved passive targeting by the enhanced permeability and retention (EPR) effect [50]. Ultimately, to direct the polyplex to the desired region and facilitate cellular uptake, active targeting can be provided by introducing a targeting ligand to the polyplex.

1.3. Surface shielding of nanoparticles

To prevent nanoparticles from quick elimination through renal clearance and unspecific interactions with blood components or other nanoparticles, shielding agents can be attached to a particle's surface [50-52]. By protecting the particle from degradation, shielding agents significantly prolong its circulation time in the bloodstream, hence passive targeting through EPR is improved [53, 54].

Up until now, the most widely used shielding agent is polyethylene glycol (PEG). Klibanov *et al.* first demonstrated in 1990 the prolonged circulation time that was achieved by introducing PEG [50]. As uncharged, hydrophilic polymer, it builds a hydrated shell around the nanoparticle, sterically protecting it from undesired interactions [55]. However, more and more reports declare immune responses to PEG, in the worst case leading to a rapid clearance of the so-shielded nanoparticles from circulation [55-61]. One such example was published by Abu Lila *et al.* who demonstrated the production of IgM antibodies against PEG in animals that were injected with PEG repeatedly [62]. Given the mounting evidence that PEG in some

formulations may cause immune responses, the search for alternative shielding agents becomes interesting. Several shielding agents are currently being evaluated, for example natural proteins [63], oligosaccharides [64, 65], hydroxyethyl starch (HES) [66], proline-alanine-serine motif (PAS) [67, 68], hydroxypropylmethacrylamide (HPMA) [65], or poly(2-isoxazoline) [69]. Yet, none of the aforementioned fulfills all criteria collected in the Whiteside's rules for protein resistant surfaces. According to these guidelines, an optimal shielding agent should be a non-charged, hydrophilic polymer that exhibits hydrogen acceptor properties but lacks hydrogen bond donor groups [70]. Polysarcosine (PSar) emerged as one possible alternative to PEG. It belongs to the class of polypeptoides, polymers with a structural resemblance to polypeptides [71], and exhibits all of the advantageous characteristics. Its resistance to proteins was demonstrated on several surfaces [72-74]. Moreover, prolonged circulation times could be shown *in vivo* [75, 76], while in various animal models, no immunogenicity or complement activation was reported [77]. Also, in human serum, aggregation could be prevented successfully [78-81]. Taken together, PSar appears a suitable option for nanoparticle shielding *in vivo*.

1.4. Active and passive targeting of nanoparticles

In order to direct a nanoparticle to its site of action, a formulation can be modified in various ways. The goal of reaching the target tissue can be achieved by either enabling passive targeting or introducing a ligand for active targeting.

Passive targeting exploits the enhanced permeability and retention (EPR) effect, which was first described by Matsumara and Maeda in 1986 [22]. This effect is based on various aspects. The nanoparticle's size and circulation time and two characteristics of tumoral tissue: Its leaky blood vessels and the lack of effective lymphatic drainage. Ideally, macromolecules should have a size in the nanometer range to evade renal filtration [19]. Also, to take advantage of the EPR effect, they should remain not less than 6 h within the blood circulation [82]. This can be accomplished by surface shielding, providing effective protection against opsonization and fast renal clearance [53, 54], which would otherwise occur rapidly after

systemic application [83]. In normal tissues, endothelial cells are separated by tight junctions which only allow small molecules of 2 to 4 nm to pass, whereas they are impermeable for larger nanoparticles. Inside the tumor tissue, however, vessels exhibit a different morphology, which is attributed to the fast tumor growth accompanied by extensive angiogenesis to keep up the supply with oxygen and nutrients. In contrast to normal blood vessels, tumor vessels exhibit gap junctions and pores. Due to this “leakiness”, macromolecules up to a size of 600 nm are able to penetrate the endothelium and extravasate to the tumor tissue [84]. In addition, the lymphatic drainage of tumors is only poorly developed, so removal of nanoparticles from the tumor is impeded [85, 86].

Active targeting, on the other side, promotes attachment at the target tissue and cellular internalization of the formulation through receptor-specific uptake. Unlike most cells of normal tissues, many tumor cell lines overexpress certain surface receptors, which can consequently be targeted by suitable targeting ligands incorporated into the nanoparticle. Some examples for commonly targeted receptors are folate receptor (FR) [87-94], epidermal growth factor receptor (EGFR) [95-98] or transferrin receptor (TfR) [99-101]. These receptors can be addressed by various groups of targeting ligands which can be introduced into the nanoparticle. Some of the most commonly used classes are small molecules [102], peptides [103, 104], glycoproteins [105] or antibodies [106, 107].

In this thesis, the focus lies on the FR and the EGFR targeted delivery. FR is overexpressed in many epithelial tumors [87, 94], while in normal tissues its expression rate is rather low [93, 108]. This can be explained by the high division rate of tumor cells: Folic acid (FolA), the main ligand of the FR, is an essential vitamin. After entering the cell via the FR or the reduced folate carrier (RFC), it is transferred to dihydrofolate and tetrahydrofolate by the enzyme dihydrofolate reductase (DHFR). In this active form, it is required for the *de novo* synthesis of DNA and RNA [109, 110]. Likewise, receptor tyrosine kinase EGFR is overexpressed in many solid tumors [111]. Its expression is associated with poor prognosis [112, 113]. Using the natural ligand epidermal growth factor (EGF) bears a mitogenic risk due to an activation of EGFR, which can successfully be evaded by using GE11

peptide as alternative targeting ligand [114].

2. Combination chemotherapy as therapeutic approach

Besides radiation and surgery, chemotherapy remains the most important pillar in cancer therapy. However, the efficiency of chemotherapy is frequently hampered due to the development of resistances when treatments are administered in a monotherapy approach [115, 116]. There are numerous mechanisms of resistance formation, including DNA damage repair [117, 118], drug inactivation [119] and cell death inhibition [120]. Currently, the best option to reduce this risk, is the combination of two or more therapeutic agents [121-123]. By co-administering various compounds with different mechanisms of action, multiple targets can be addressed and by achieving a synergistic or additive effect, therapeutic efficacy can be increased at lower doses of either drug [124, 125].

Already in 1965, Frei *et al.* reported the successful administration of a combination therapy regimen to pediatric patients suffering from acute lymphocytic leukemia. This approach, formally referred to as POMP regimen led to long-term remission by combining 6-mercaptopurine, vincristine, prednisone and methotrexate (MTX) [126, 127].

However, it is essential to contemplate the pharmacodynamic interactions that occur when multiple drugs are combined [128]. As aforementioned, drugs can enhance each other's efficiency in a synergistic or additive fashion, while synergism is considered stronger than summation. On the other side, different compounds can also act in an antagonistic way, hence they weaken each other's effect and may even lead to unwanted side-effects [129].

2.1. Methotrexate

MTX is the most prominent representative of the class of antifolates. As part of the large group of antimetabolites, these drugs were among the first subjects of research for the treatment of metastatic cancer and -as aforementioned, part of the first successful combination therapy regimen. MTX acts antagonistically to its structural analog Fola (compare **Figure 3**),

using the same mechanisms to enter the cell: It gets internalized by either reduced folate carrier (RFC) or FR [93, 130, 131]. Once in the cytosol, MTX competitively inhibits DHFR, which normally provides elementary components for the *de novo* synthesis of nucleic acids [110].

Notably, MTX is not only used to treat multiple kinds of malignancies, in lower doses, its anti-inflammatory effect predominates [132]. Currently, it is of ubiquitous importance in the treatment of auto-immune diseases and although it was originally not designed to treat rheumatic arthritis, it is today the standard of care for this indication [133]. Despite its extensive use in the clinics, a major drawback, especially in monotherapy approaches, is the incidence of acquired resistance to MTX, which is clearly leading to a reduced applicability [134-136]. Therefore, MTX represents an ideal candidate for combination therapy.

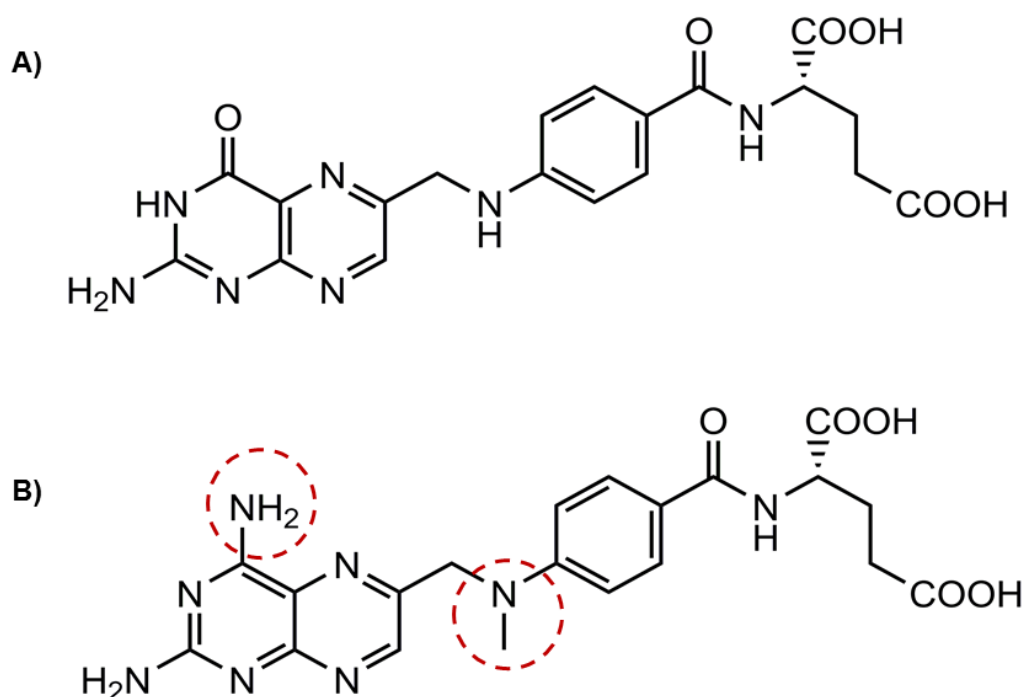


Figure 3: Chemical structures of A) folate and B) MTX as ligands of the folate receptor (FR). Dashed rings indicate structural differences.

2.2. Pretubulysin

Microtubules represent indispensable structures in eukaryotic cells. Their tasks comprise intracellular transport and cell movement. More importantly,

they represent essential components of the mitotic spindle apparatus, which is required to separate the chromosomes during mitosis. Microtubule targeting agents interfere with these processes by either stabilizing or destabilizing microtubule, thus hampering the cell division process, ultimately leading to G2/M arrest [137]. It is not surprising, that this class of therapeutics has been used widely in the clinics for numerous decades. However, they are also commonly facing resistance formation, which for instance is reported frequently for Vinca alkaloids [138, 139]. Therefore, the quest for new compounds of this effective class becomes more and more crucial. The tubulysins are a group of natural compounds, originally obtained from myxobacteria. Despite their great antitumoral efficiency, they are experiencing major drawbacks in regard of sufficient synthesis. Encouragingly, their bio-synthetical precursor pretubulysin (PT) can be synthesized with more convenience as it exhibits less complexity in its chemical structure (**Figure 4**) [140, 141]. Like the tubulysins, it binds to the vinca domain of β -tubulin, effectively inhibiting tubulin polymerization which results in the disruption of the microtubule network and consequently apoptosis [142, 143]. Although its synthesis is facilitated in comparison to the tubulysins, PT exhibits a comparable therapeutic efficiency [140, 144]. PT reduces tumor cell growth of various cell lines [140], mediates inhibitory effects on cancer cell migration *in vitro* [144] and accomplishes promising effects *in vivo*: It shows significant anti-angiogenic effects [144, 145], prevents metastasis [140, 146] and inhibits tumor growth [140, 145, 147, 148].

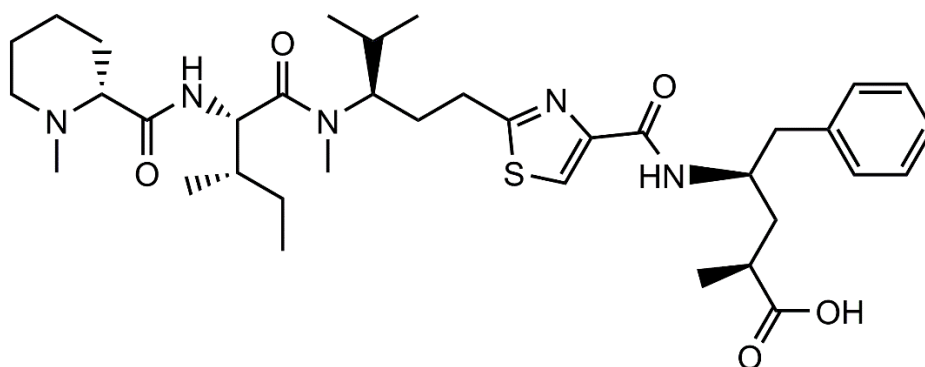


Figure 4: Chemical structure of Pretubulysin

3. Aims of this thesis

3.1. Shielded and targeted nanoparticles for effective siRNA delivery

siRNA is a rather novel, nevertheless powerful tool for the treatment of cancer. However, its delivery faces numerous obstacles, as siRNA by itself exhibits only short blood circulation times and is readily degraded by nucleases. In order to successfully deliver siRNA to its tumor site of action, stable nanoparticles had to be designed, which can be actively and passively targeted to tumor tissues. In this part, siRNA nanoparticles created using click chemistry to add shielding and FR targeting domains should be evaluated in terms of biodistribution and tumor gene silencing efficiency in a tumor mouse model. Furthermore, the aim was to investigate whether the novel shielding agent PSar could act as effective alternative to the well-established agent PEG in a biodistribution experiment. Moreover, antitumoral treatment experiments including the best performing formulation with siEG5 in combination with the natural microtubule inhibitor PT should be performed.

3.2. Combinatorial treatment of PT and MTX

Chemotherapy represents one of the most important elements in the treatment of cancer. Yet, monotherapy approaches are frequently hampered by arising resistances of cancer cells. Therefore, drug combinations are an encouraging alternative to monotherapy. The present work aimed to analyze the potentially beneficial combination effect of the novel antitubulin agent PT with the well-established cytostatic drug MTX in several approaches and tumor models.

II. MICE, MATERIALS AND METHODS

1. Mice

1.1. Mouse strains

1.1.1. NMRI-nude mice

Female Rj: NMRI-Foxn1^{nu}/Foxn1^{nu} mice were obtained from Janvier Labs (Le Genest-St-Isle, France). Due to a defect in the Foxn1^{nu} gene, this mutant outbred strain is characterized by thymic aplasia which leads to a lack of mature T-lymphocytes, while B-lymphocytes and all components of the innate immune system are perfectly functional. Also, the keratinization of hair follicle and epidermis is compromised. Thus, mice are nude, which makes them an ideal model for bioimaging experiments. More importantly, their immunodeficiency in terms of T-lymphocytes enables them as recipients for xenograft tumor models.

1.1.2. BALB/c mice

Female BALB/c mice were purchased from Janvier Labs (Le Genest-St-Isle, France). This inbred albino mouse strain possesses an intact innate and adaptive immune system. Mice are widely used e.g. in the fields of oncology, immunology or in cardiovascular research. They are well appreciated for their calm and gentle manner. Since mice are fully immunocompetent, they are used in our lab as sentinel animals for the quarterly health report.

1.2. Housing conditions

Animals were ordered at the age of 5 weeks and were allowed an acclimatization time of at least 7 days prior to experiments. They were housed in isolated ventilated cages (IVC type II, Tecniplast) under specific pathogen-free conditions, which were controlled quarterly by a complete health analysis of two sentinel animals. A 12 h day / night interval was provided and temperature as well as air humidity were kept constant at 24 - 26°C, respectively 50 - 70% and recorded daily. Also, limits were set concerning light and sound intensities (200 Lux, respectively 40 dB). Stocking density of cages ranged from 2 to 5 mice and animal well-being

was controlled daily. Dust-free bedding was changed weekly and both food and water were provided sterilized and *ad libitum*. Moreover, cages were enriched with cottages, nest building material and wooden tubes. All criteria were in accordance with the official permission based on §11 of the German Animal Welfare Act (Tierschutzgesetz, [149]).

1.3. Health monitoring

In order to ensure specific pathogen-free conditions, quarterly health monitoring of our animal facility was performed. For this purpose, sentinel animals were kept in the same facility and received bedding material and food from all other animal cages once per week. After a period of 12 weeks, two sentinels were sent in for complete health analysis.

2. Materials

2.1. Cell culture

Material	Source
Neuro-2a (N2a) cells (mouse neuroblastoma cells)	American Type Cell Collection (ATCC) (Wesel, Germany)
KB-wt cells (human cervix carcinoma cells)	ATCC (Wesel, Germany)
HUH7-wt cells (human hepatocellular carcinoma cells)	NIBIO (Osaka, Japan)
L1210 cells (mouse lymphocytic leukemia cells)	kindly provided by Prof. Philip S. Low, Department of Chemistry (Purdue University, USA)
RPMI 1640 medium	Invitrogen (Karlsruhe, Germany)
DMEM 1 g/l glucose medium	Invitrogen (Karlsruhe, Germany)
DMEM 4.5 g/l glucose medium	Invitrogen (Karlsruhe, Germany)
Ham's F12 medium	Invitrogen (Karlsruhe, Germany)
FCS (fetal calf serum)	Invitrogen (Karlsruhe, Germany)
PBS (phosphate buffered saline)	Biochrom (Berlin, Germany)
TE (trypsin EDTA) solution	Biochrom (Berlin, Germany)
L-alanyl-L-glutamine	Biochrom (Berlin, Germany)
Cell culture plates and flasks	TPP (Trasadingen, Switzerland)

2.2. *In vivo* experiments

Material	Source
Isoflurane CP®	CP-Pharma (Burgdorf, Germany)
Bepanthen®	Bayer Vital GmbH (Leverkusen, Germany)
Syringes, needles	BD Medical (Heidelberg, Germany)
Multivette (EDTA-coated tubes)	Sarstedt (Nümbrecht, Germany)
HBG (HEPES buffered 5% glucose, pH 7.4)	HEPES: Biomol (Hamburg, Germany) glucose monohydrate: Merck (Darmstadt, Germany)

2.3. Oligomers

Oligomers were synthesized by Dr. Philipp Klein (*postdoc at Pharmaceutical Biotechnology, LMU*) and Ines Truebenbach (*PhD student at Pharmaceutical Biotechnology, LMU*).

Oligomer ID	Sequence	Topology
1073	K(N ₃)-Y ₃ -Stp ₂ -K(G-SSBB-K-CholA ₂)-Stp ₂ -Y ₃	T-shape
1106	K(N ₃)-Y ₃ -Stp ₂ -K(G-K(CholA) ₂ -Stp ₂ -Y ₃	T-shape
1169	K(N ₃)-Y ₃ -Stp ₂ -K(G-K(OleA) ₂ -Stp ₂ -Y ₃	T-shape
1198	K(N ₃)-C-Y ₃ -Stp ₂ -K(K(OleA) ₂ -Stp ₂ -Y ₃ -C	T-shape
951	C-STOTDA-K[K(PEG ₁₂ -E4-MTX) ₂] ₂	4-arm
454	C-Y ₃ -Stp ₂ -K(K-OleA ₂)-Stp ₂ -Y ₃ -C	T-shape

2.4. siRNAs

Material	Source
siCtrl AuGuAuuGGccuGuAuuAG dTsdT CuAAuAcAGGCcAAuAcAU dTsdT	Axolabs (Kulmbach, Germany)
siEG5 ucGAGAAucuAAAcuAAcu dTsdT AGUuAGUUuAGAUUCUCGA dTsdT	Axolabs (Kulmbach, Germany)
siAHA1-Cy7 GGAuGAAGuGGAGAuAGu dTsdT (Cy7)(NHC ₆)ACuAAUCUCcACUUCAUCC dTsdT	Axolabs (Kulmbach, Germany)

* Capital letters: standard RNA ribonucleotides (A: Adenylate, G: Guanylate, C: Cytidylate, U: Uridylate); small letters: 2'methoxy-RNA; dT: DNA building block deoxy-thymidine; s: phosphorothioate linkage

2.5. Compounds

Pretubulysin (PT)	synthesized by Dr. Jan Gorges (Institute for Organic Chemistry, Saarland University, Germany)
Methotrexate (MTX)	Sigma-Aldrich (Munich, Germany)

2.6. Instruments

Caliper DIGI-Met	Preisser (Gammertingen, Germany)
IVIS Lumina	Caliper Life Science (Rüsselsheim, Germany)

2.7. Software

GraphPad Prism 5 software	GraphPad Software (San Diego, USA)
Living Image 3.2	Caliper Life Science (Rüsselsheim, Germany)

3. Methods

3.1. Cell culture

Mouse neuroblastoma cells (Neuro-2a) were grown in Dulbecco's modified Eagle's medium (DMEM 1 g/l glucose), while murine lymphocytic leukemia cells (L1210) and human cervix carcinoma cells (KB) were cultured in RPMI 1640 medium at 37°C in 5% CO₂ humidified atmosphere. Human hepatocellular carcinoma cells (HUH7) were cultured in 1:1 mixture of DMEM and Ham's F12 medium. All media were supplemented with 10% fetal calf serum (FCS) and 4 mM stable glutamine.

3.2. *In vivo* experiments

For animal experiments, tumor cells were suspended in 150 µL PBS and were set subcutaneously into the left flank of 6 to 7-week-old NMRI nude mice using a 27G cannula. Inoculation of tumor cells was performed under

inhalation anesthesia using isoflurane in oxygen (3% for induction and 2.5% for maintenance). Animal well-being was controlled daily and weight was recorded every second day until tumors became measurable and from then on on a daily basis. Tumor sizes were determined by caliper and calculated [$0.5 \times \text{longest diameter} \times \text{shortest diameter}^2$] as stated by Xu *et al.* [150]. Intratumoral injections were carried out under short narcosis, whereas intravenous injections did not require anesthesia and could be performed using a restrainer. For reasons of animal welfare, a maximum of 8 injections in total with 3 treatments per week was not exceeded. Furthermore, tails were thoroughly examined for injection-related lesions before every treatment. Animals were euthanized by cervical dislocation in isoflurane narcosis. Mice of all treatment experiments were sacrificed when previously determined termination criteria were reached. These included a tumor size of 1500 mm³ as well as severely affected well-being (indicated e.g. by continuous weight loss, apathy, visibly enlarged lymph nodes or spleen).

All animal experiments were performed according to the terms stated in the proposal "*Entwicklung von Sequenz-definierten Oligomeren als Träger für die zielgerichtete Einbringung neuer molekularer Therapeutika in Tumore*" (reference number: 55.2-1-54-2532-233-13), that was approved by the local animal ethics committee and the district government of Upper Bavaria on 26 May 2014. All experiments complied with the guidelines contained in the German Animal Welfare Act [149].

3.2.1. Biodistribution study with PSar shielding

Neuro-2a cells (5×10^6) were injected subcutaneously into the left flank of 7-week-old NMRI nude mice. When tumors reached 500 – 1000 mm³, animals were randomly divided into 3 groups (n=2) and injected intravenously with 250 µL of siRNA polyplex solution containing 50 µg of Cy7-labeled siRNA (N/P 10) with either PEG5k or PSar as shielding agent or HBG as buffer control. Mice were anesthetized with 3% isoflurane in oxygen and NIR fluorescence bioimaging was performed with a CCD camera at different time points over 24 h. Color bar scales were equalized and intensity of fluorescence signals was analyzed using the Living Image software 3.2.

3.2.2. Biodistribution of Fola-targeted lipopolyplexes

L1210 cells (1×10^6) were injected subcutaneously into the left flank of 6-week-old NMRI nude mice. When tumors reached 500 mm³, animals were randomly divided into 7 groups (n=3) and injected intravenously with 250 μ L of polyplex solution containing 50 μ g of Cy7-labeled siRNA (N/P 10). Polyplex solution contained oligomers **1106** or **1169** modified with mono- or bis-DBCO, varying lengths of PEG and Fola targeting ligand. Mice were anesthetized with 3% isoflurane in oxygen and NIR fluorescence bioimaging was performed at different time points over 24 h using a CCD camera. Biodistribution was repeated in tumor-free mice, all other conditions remained unaffected.

For the evaluation of acquired images, the efficiency of fluorescence signals was analyzed after color bar scales were equalized using the IVIS Lumina system with Living Image software 3.2 (Caliper Life Sciences, Hopkinton, MA, USA).

3.2.3. Intratumoral *EG5* gene silencing after systemic application

Seven-week-old mice were subcutaneously injected with 1×10^6 L1210 cells and randomly divided into 4 groups (n=5) once their tumors reached 500 mm³. Mice were administered intravenously 250 μ L of **1106**- or **1169**-polyplex solution containing 50 μ g of siCtrl or siEG5 (targeted and untargeted) at N/P 10. Control animals remained untreated but were otherwise handled the same way. The previously described formulations (see II.3.2.2.) were administered twice at daily interval via tail vein injection. Twenty-four hours after the second treatment, animals were sacrificed and tumors were harvested and homogenized. Subsequently, RNA was extracted using Trifast (PepLab, Erlangen, Germany) according to the manufacturer's protocol. Gene silencing efficiency was evaluated by Dr. Dian-Jang Lee (*former PhD student at Pharmaceutical Biotechnology, LMU*) as described in Klein *et al.*: Quantitative real-time polymerase chain reaction (qRT-PCR) was performed to determine the mRNA level of *EG5* in the tumor samples. One milligram of total RNA was used to generate cDNA using qScript cDNA Synthesis Kit (Quanta Biosciences, Beverly, MA, USA). Quantitative RT-PCR was performed on a LightCycler 480 system (Roche, Mannheim, Germany) using UPL Probes (Roche, Mannheim, Germany)

and Probes Master (Roche, Mannheim, Germany) with GAPDH as housekeeping gene. The following probes and primer sequences were used: murine GAPDH (ready-to-use in UPL), and *EG5* (UPL Probe #100) forward: (TTCCCCTG CATCTTTCAATC, reverse: TTCAGGCTTATTCATT ATGTTCTTTG). Results were analyzed by the DCT method. CT values of GAPDH were subtracted from CT values of *EG5*. DCT values of treated animals were calculated as percentage of untreated control animals [147].

3.2.4. Clinical biochemistry after systemic application

Tumor-free animals (n=4-5 mice per group) were either injected with 250 μ L of the best performing formulation (**1106** DBCO₂-ss₂-PEG₂₄-FolA) or remained untreated. At 48 h post injection, all mice were sacrificed by cervical dislocation and final heart puncture was performed to obtain blood for clinical biochemistry analysis. Blood was collected in EDTA-coated tubes and centrifuged instantly at 800 \times g for 7 min to isolate blood plasma. The supernatant was analyzed regarding renal (creatinine, blood urea nitrogen) and liver parameters (alanine aminotransferase, aspartate aminotransferase) in the *Clinic of Small Animal Medicine, Faculty of Veterinary Medicine, LMU Munich*. Untreated control animals served as reference.

3.2.5. Combinatorial treatment with FolA-targeted siEG5 lipopolyplexes and PT

Three days after subcutaneous tumor cell inoculation (0.5×10^6 L1210 cells), mice were randomly distributed into six groups (n=6) and injected intravenously with 250 μ L of siRNA formulations (50 μ g of siEG5 or siCtrl) with or without co-treatment with PT (2 mg/kg) respectively plain PT or HBG. Treatments were repeated 3 times per week (on days 3, 5, 7, 10, 12, 14, 17 and 19) with a maximum of 8 injections. Animals were sacrificed when they reached the previously determined termination criteria and Kaplan Meier survival analysis was compiled.

3.2.6. Treatment with GE11-targeted, PT containing siEG5 lipopolyplexes

Seven-week-old NMR1 nude mice were inoculated with 5×10^6 HUH7 cells. After sufficient tumor growth (200 - 250 mm³), treatments were started

individually. Animals were randomly divided into 6 groups (n=6) and injected via tail vein injection with 250 μ L of siRNA formulations (50 μ g of siEG5 or siCtrl) with or without co-administration with PT (2 mg/kg) respectively plain PT or HBG. Treatments were performed 8 times at most with 3 injections per week. Animals were sacrificed when they reached the previously determined termination criteria and Kaplan Meier survival analysis was carried out.

3.2.7. Intratumoral treatment with E4-MTX-H-PT conjugate

KB cells (5×10^6) were set subcutaneously into the left flank of 7-week-old NMRI nude mice. Two days after tumor cell inoculation, the animals were randomly divided into 4 groups (n=8) and injected intratumorally under general anesthesia with 50 μ L of either E4-MTX (2.7 mg/kg), native PT (PT-COOH, 2 mg/kg) or the analogous conjugate. The untreated group did not receive any injections. Treatments were performed 6 times (on days 2, 5, 7, 9, 12 and 14) for all animals. Animals were sacrificed when they reached the previously determined termination criteria.

3.2.8. Effect of intravenous injections of PT+MTX on L1210 tumor growth

L1210 cells (0.5×10^6) were injected subcutaneously into the left flank of 6-week-old NMRI nude mice. On day three after tumor cell inoculation, the animals were randomly divided into 4 groups (n=4) and injected intravenously with 250 μ L of PT (2 mg/kg), MTX (5 mg/kg), the corresponding combination (PT+MTX) or HBG. Treatments were repeated 3 times per week (on days 5, 7, 10, 12, 14, 17 and 19). When mice reached the previously determined termination criteria, the experiment was ended by cervical dislocation. All MTX-treated animals were sacrificed on day 14, together with the animals of MTX dose finding experiment. Due to its tumor burden, one animal of MTX group had to be sacrificed ahead of schedule on day 13.

3.2.8.1. MTX dose finding

Experiment was performed in two sections under equal conditions. Six-week-old animals were injected subcutaneously with 0.5×10^6 L1210 cells and randomly distributed into 4 respectively 6 groups. In the first

section, low doses of MTX were compared to HBG. Therefore, mice were treated with 2.5, 5, 7, 10 or 20 mg/kg MTX. In the second section, higher doses of 40, 80 and 100 mg/kg MTX were compared to HBG. Injections were performed thrice weekly, starting on day three with a maximum of 7 injections. Mice treated with lower doses of MTX were sacrificed collectively on day 14, whereas animals treated with higher doses were euthanized when termination criteria were reached, respectively.

3.2.9. Effect of intravenous injections of PT+MTX on KB tumor growth

KB cells (5×10^6) were injected subcutaneously into the left flank of 7-week-old NMRI nude mice. When tumors reached 200 – 250 mm³, treatments were started individually. Animals were randomly divided into 4 groups (n=4) and injected intravenously with 250 µL of PT (2 mg/kg), MTX (5 mg/kg), the corresponding combination (PT+MTX) or HBG. Treatments were repeated 3 times per week with a maximum of 8 injections. Animals were euthanized when termination criteria were reached, respectively.

3.2.10. Effect of intravenous injections of PT+MTX on HUH7 tumor growth

Seven-week-old NMRI nude mice were inoculated subcutaneously with HUH7 cells (5×10^6). Animals were divided into 4 groups (n=4) and treatments were started individually once tumors reached 200 – 250 mm³. Systemic applications with 250 µL of PT (2 mg/kg), MTX (5 mg/kg), the combination of both (PT+MTX) or HBG were performed thrice weekly for up to 8 injections. Mice were sacrificed by cervical dislocation after mice reached the previously determined termination criteria, respectively. Kaplan Meier survival analysis was carried out.

3.2.11. Oligomer-based micellar encapsulation of PT+MTX for systemic administration

L1210 cells (0.5×10^6) were implanted subcutaneously into the left flank of 6-week-old NMRI nude mice. On day three after tumor cell implantation, animals were randomly divided into 7 groups (n=6) and injected intravenously with 250 µL of PT (2 mg/kg), PT+MTX (2 mg/kg PT,

2.5 mg/kg MTX), the corresponding groups with **454**, **454** alone, **454** MTX (2.5 mg/kg MTX) or HBG. Treatments were performed 3 times per week (on days 3, 5, 7, 10, 12, 14, 17 and 19). Animals were euthanized by cervical dislocation, as soon as the previously determined termination criteria were reached and Kaplan Meier survival analysis was compiled.

3.3. Statistical analysis

Results are expressed as mean + S.E.M. if not indicated otherwise. Statistical analysis was performed with unpaired students t-test and log-rank test using GraphPad Prism™ and p-values < 0.05 were considered as significant (*p < 0.05; **p < 0.01; ***p < 0.001; ns = not significant).

III. RESULTS

1. Shielded and targeted lipopolyplexes for effective siRNA delivery

For efficient siRNA delivery, a suitable carrier system is required. In previous work, a library containing more than 1200 sequence-defined oligomers was established. This chapter presents the optimization of a siRNA carrier system in terms of stability, body circulation and tissue specific accumulation by functionalization with shielding and targeting agents. Moreover, properties like gene silencing efficiency and therapeutic potential were evaluated.

The PSar biodistribution experiment was performed together with Dr. Eva Kessel (*former veterinary MD student at Pharmaceutical Biotechnology, LMU*). Experiments with oligomers **1106** and **1169** were performed in cooperation with Dr. Dian-Jang Lee (*former PhD student at Pharmaceutical Biotechnology, LMU*). Johannes Schmaus (*veterinary MD student at Pharmaceutical Biotechnology, LMU*) assisted during FoIA + siEG5 + PT treatment experiment. All experiments were carried out in NMRI nude mice.

1.1. Exploiting click chemistry for the modification of lipopolyplexes with functional domains

Previously, a new class of very effective carrier systems was designed by our group. These redox-sensitive lipo-oligomers proved to be very valuable for the delivery of siRNA [49]. The best-performing oligomer of this study, the T-shaped oligomer T-0N₃ (ID number: **992**, see **Figure 5, table top**) was chosen as lead structure for further optimization by surface-functionalization. Therefore, T-0N₃ was further equipped with one (T-1N₃, ID **1073**) or two (T-2N₃, ID **1086**) click-reactive azide groups, serving as anchor points for attaching additional units. The azide function enables the particle for bio-orthogonal click reactions with cyclooctyne derivatives, like dibenzocyclooctyne (DBCO). This reaction between a cyclooctyne and an azide group proceeds effectively without the need for a catalyst, does not produce any side products and - as it works without copper, it does not

cause cytotoxicity [151-153]. The reaction was performed after the formation of siRNA lipopolyplexes. Therefore, surface-functionalization, for instance with shielding domains, could be introduced onto the nanoparticulate siRNA formulation. In addition to the shielding agent polyethylene glycol (PEG), which is the gold standard among shielding agents, polysarcosine (PSar) was investigated as alternative shielding agent. PSar was described to work efficiently while being well tolerated [75-77]. The current work used it C-terminally functionalized with DBCO (DBCO-PSar - **Figure 5, table bottom**). Besides its shielding ability, the DBCO-PSar unit enables the introduction of targeting ligands via its N-terminal amino group. Hence, lipopolyplexes can be further equipped for example with FoIA for active targeting.

Particles were evaluated *in vitro* to choose the most suitable candidate for *in vivo* studies. Gel retardation assays and cell studies revealed a strong reduction of cellular binding and uptake of PSar-shielded particles, which was most pronounced in case of T-1N₃ (**1073**) [154].

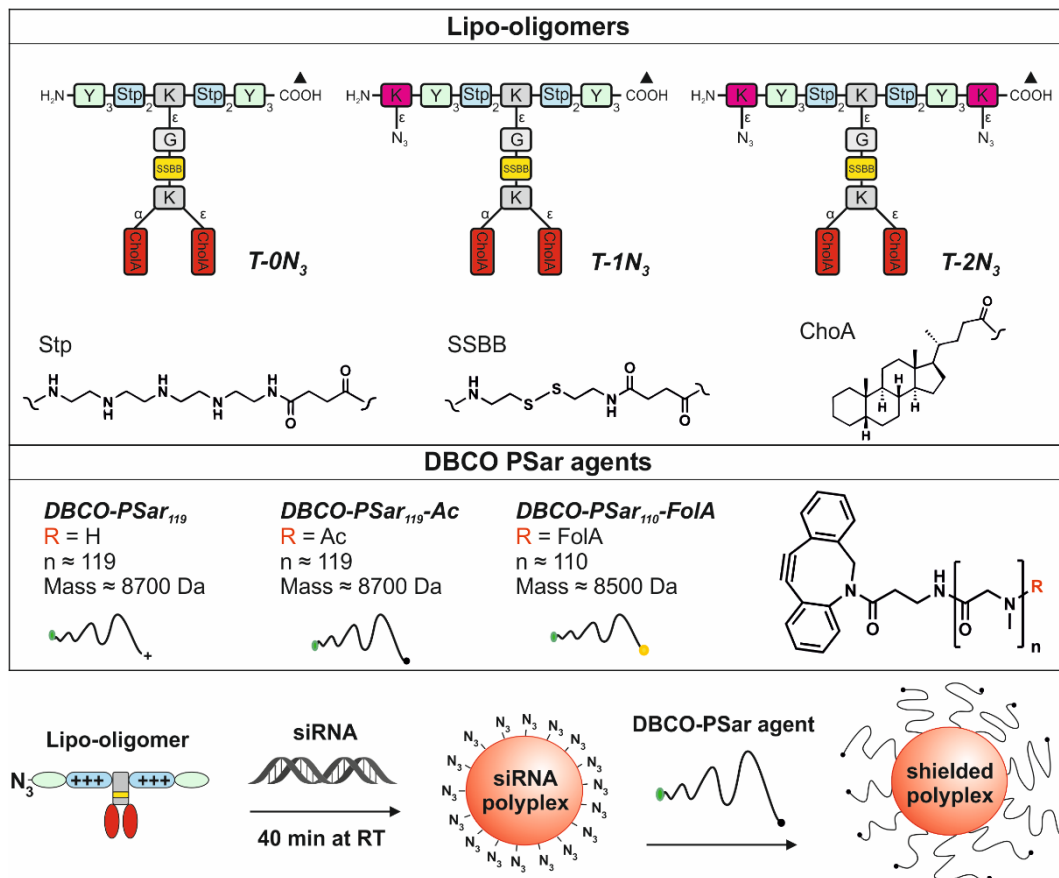


Figure 5: Graphical illustration of compounds for lipoplex formation. **Table top:** Variants of T-shaped oligomers with increasing amounts of terminal azidolysines: T-0N₃ (ID: **992** published in [49]), T-1N₃ (ID: **1073**) and T-2N₃ (ID: **1086**). Further units of the oligomers: Y: tyrosine, K: lysine, G: glycine, Stp: succinoyl-tetraethylene-pentamine, ssbb: succinoyl-cystamine, CholA: 5 β -cholanolic acid, N₃: azide function. **Table bottom:** Chemical structure of different DBCO-PSar shielding domains: DBCO-PSar₁₁₉, acetylated DBCO-PSar₁₁₉-Ac and F α A-targeted DBCO-PSar₁₁₀-F α A. **Scheme:** Simplified illustration of the synthesis of a DBCO-PSar-shielded polyplex. The figure is provided by Klein *et al.* [154].

1.1.1. Comparison of PSar and PEG as shielding agents

The *in vivo* setting aimed for a direct comparison of the shielding capacity of PEG and PSar. For this purpose, the candidate with best shielding properties in the *in vitro* experiments, T-1N₃ (ID: **1073** [154]) was surface-modified with either DBCO-PEG5k or acetylated PSar (DBCO-PSar₁₁₉-Ac). The acetylated PSar agent without terminal cationic charge was chosen for better comparability with the commercial PEG agent.

Biodistribution studies were performed using Neuro-2a tumor bearing mice. Two animals per group were injected intravenously with either the unshielded polyplex, or the formulation shielded with DBCO-PEG5k respectively DBCO-PSar₁₁₉-Ac. Near infrared (NIR) imaging was performed immediately and repeated at various time points until 24 h.

Figure 6 depicts the formulations' biodistribution. At 15 min post injection, the unshielded formulation started accumulating in the liver. However, in case of both shielded formulations, circulation could largely be enhanced, leading to a biodistribution of the whole body which was still visible after 1 h. After 4 h, intensity was notably reduced in all groups. Yet, peripheral body parts like paws still showed strong fluorescence signal. The lack of tumor accumulation after 4 h and the dominant bladder signal at that time point indicate renal clearance, impeding passive targeting via the EPR effect [154].

In sum, direct comparison of PEG and PSar shielding of polyplexes revealed only minor variations in terms of circulation or tumoral retention of the formulation. However, both shielding options clearly increased the formulation's circulation time in comparison to the unshielded control [154].

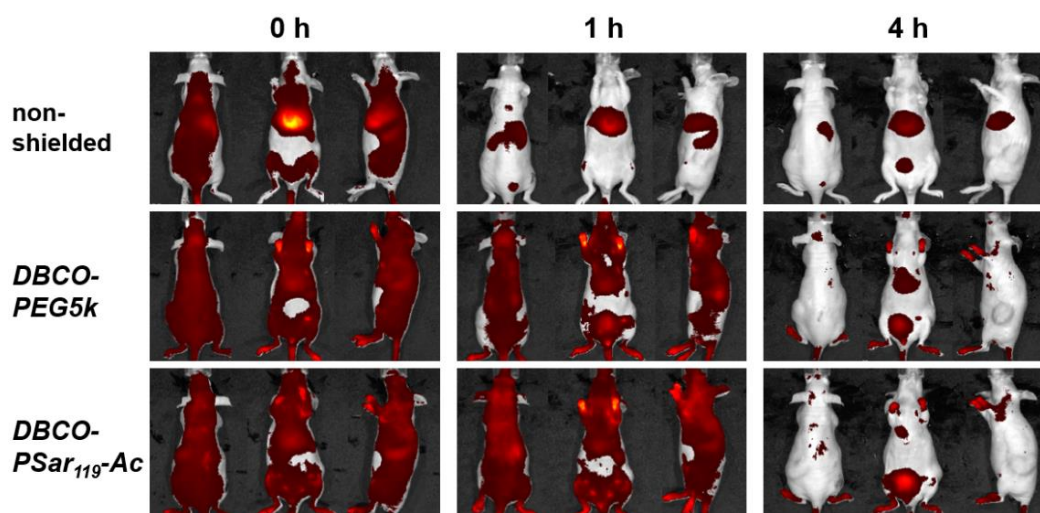


Figure 6: *In vivo* distribution of polyplexes with different forms of shielding in Neuro-2a tumor bearing mice. Unshielded polyplexes (**top**), PEG-shielded (**middle**) or PSar-shielded polyplexes (**bottom**) were injected intravenously and NIR fluorescence bioimaging was performed immediately and repeated at multiple time points until 24 h. Mice are presented in dorsal, ventral and lateral view. Color scale (efficiency) had a minimum of 1.6×10^{-5} and a maximum of 2.2×10^{-4} fluorescent photons/incident excitation photon. Illustration is provided by Klein *et al.* [154].

1.2. FoIA receptor-targeted lipopolyplexes for gene silencing *in vivo*

Besides shielding with PEG or alternatives like PSar, also tumor targeting has a great influence on a formulation's performance after systemic application in tumor bearing mice. Active targeting enables not only the direction of a nanoparticle to its site of action, but also its internalization into the target cell [155]. Therefore, nanoparticles in the following experiments were equipped with FoIA for selective siRNA delivery to FR-overexpressing L1210 cells.

Based on the successful application of lipopolyplexes with click-reactive introduction of functional domains in the previous part (see III.1.1.1., [154]), click chemistry was again exploited for the following experiments. Via solid-phase supported synthesis, a sequence-defined lipo-oligomer was designed. The T-shaped oligomer **991** was chosen to build the particle's core. It comprises two cholanic acid (CholA) chains and tyrosine units promoting polyplex stability, resulting in stable polyplexes with beneficial carrier properties [49]. To enable click-reactive modification with functional

domains, the oligomer was further refined by adding an azido function (new oligomer ID **1106**). Subsequently, mono- and bivalent attachments of DBCO with varying PEG lengths were introduced and particles were equipped with FoIA as targeting ligand (**Figure 7**, [147]).

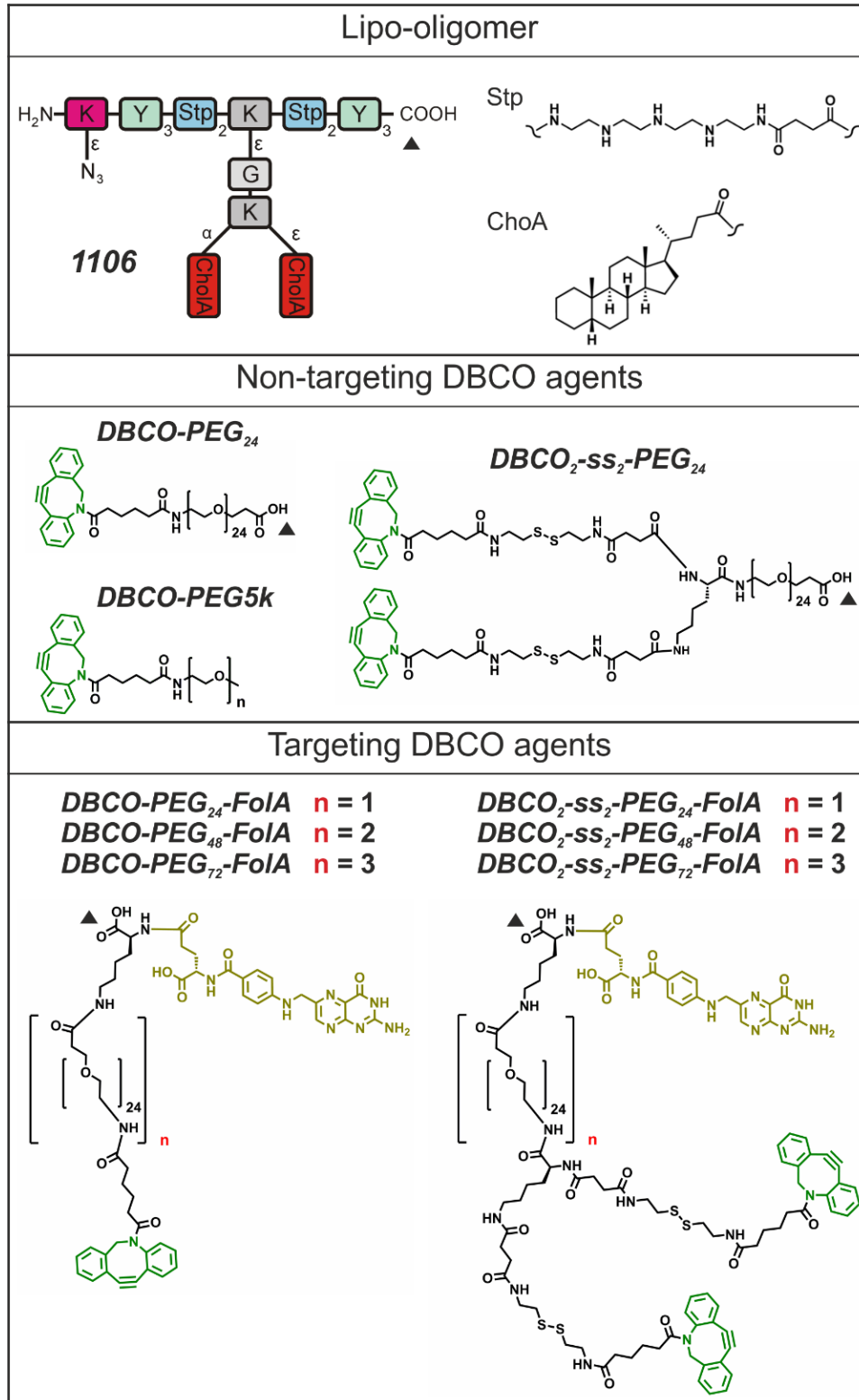


Figure 7: Chemical composition of a PEG-shielded, FoIA-targeted lipo-oligomer. Top: Schematic illustration of the T-shaped oligomer (ID **1106**).

Abbreviations of individual units indicate: Y: tyrosine, K: lysine, G: glycine, Stp: succinoyl-tetraethylene-pentamine, CholA: 5 β -cholanic acid, N₃: azide function. **Middle:** Chemical structure of non-targeting DBCO-PEG units: Shorter DBCO-PEG₂₄, longer DBCO-PEG_{5k} and double-click DBCO₂-SS₂-PEG₂₄. **Bottom:** Chemical structure of F α IA-targeting DBCO-units with mono- or bis-DBCO and varying PEG-lengths. The figure was adapted from Klein *et al.* [147].

1.2.1. Biodistribution study

Biodistribution of lipopolyplexes for effective siRNA delivery depends on various factors. To evaluate the formulation's distribution properties after intravenous injection, fluorescence imaging was performed.

In this experiment, the FR-positive L1210 murine lymphocytic leukemia tumor model was chosen. When tumors reached 500 – 1000 mm³, animals were injected via tail vein with the previously synthesized T-shaped oligomer **1106** modified with mono- or bis-DBCO with varying PEG lengths for surface shielding. Moreover, some formulations were functionalized with the targeting ligand F α IA for selective delivery to L1210 cells.

After the injection of (50% Cy7-labeled) siRNA formulations, the fluorescent dye was monitored using near infrared (NIR) bioimaging. Biodistribution was analyzed at various time points until 24 h after injection.

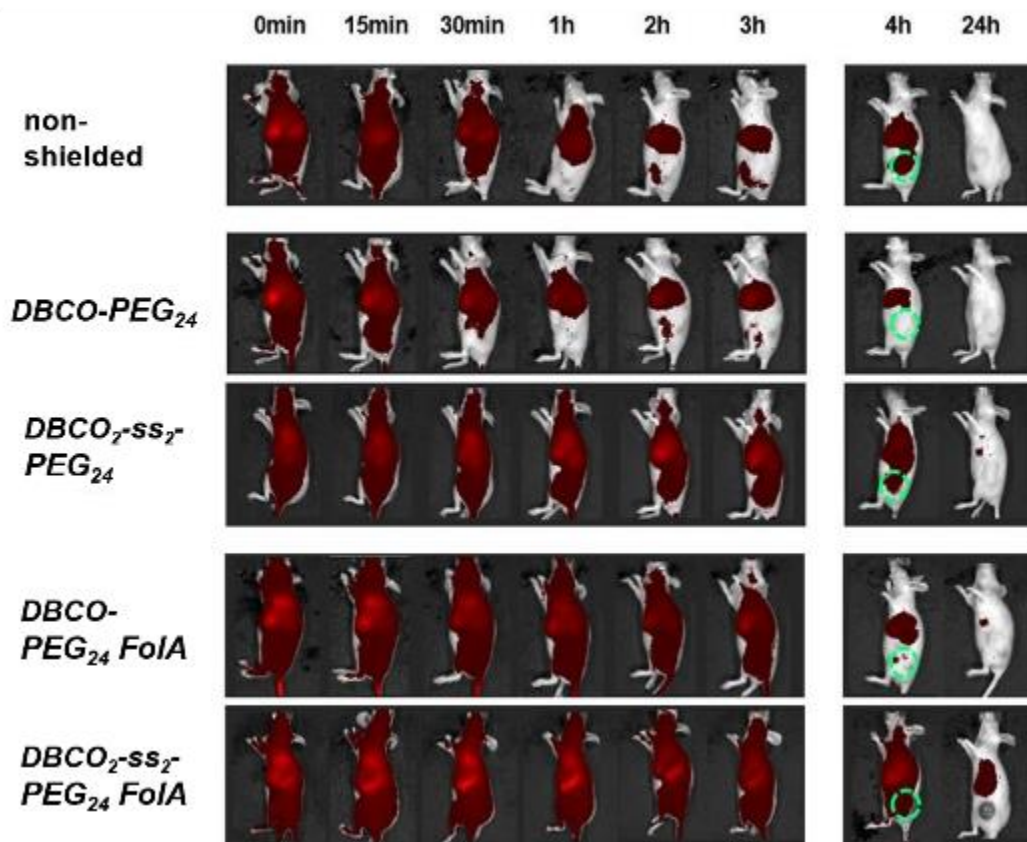
Figure 8 shows the biodistribution of formulations. Unshielded polyplexes accumulated mainly in the liver and blood circulation could not be improved by modification with DBCO-PEG₂₄. However, when mono-DBCO was replaced by bis-DBCO, biodistribution could largely be enhanced. Moreover, the functionalization with F α IA prolonged *in vivo* circulation in both mono- and bis-DBCO formulations. Tumor accumulation could be demonstrated in all F α IA-targeted groups and also in the unshielded group after 4 h. The best all over biodistribution with fluorescence signals in most body parts after 4 h was achieved by DBCO₂-SS₂-PEG₂₄ F α IA formulation.

As shielding can have an impact on blood circulation, clearance and half life time [50-52], different PEG lengths were investigated. For this purpose, 3 animals per group were injected with the same formulations as before, but modified with longer PEG chains: DBCO-PEG_{5k} respectively DBCO-PEG₇₂ F α IA or DBCO₂-SS₂-PEG₇₂ F α IA. The untargeted,

PEG5k-shielded formulation could improve circulation as compared to the unshielded polyplex. Also, strong fluorescence signal was found at superficial peripheral sites like paws after 4 h. Consistent with our findings with mono- and bis-DBCO in PEG₂₄ FoIA groups, bis-DBCO was clearly superior to mono-DBCO in PEG₇₂ FoIA formulations in terms of blood circulation. DBCO-PEG₇₂ FoIA showed weaker biodistribution than the untargeted DBCO-PEG5k formulation. In case of the bis-DBCO containing equivalent, fluorescence signal could first be detected in the lung area and started spreading to the whole body just after 2 h. Subsequently, it was distributed to the whole body, yet lacking tumor accumulation that was shown for the shorter PEG₂₄ analog.

In sum, the superiority of shorter PEG₂₄ chains over longer PEG5k or PEG₇₂ chains regarding tumor accumulation and circulation time was demonstrated.

A)



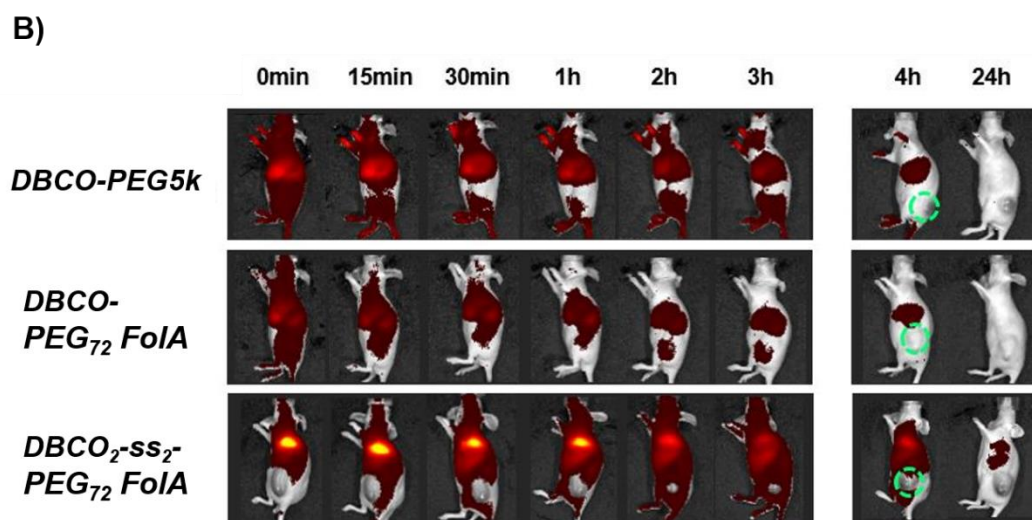


Figure 8: Evaluation of *in vivo* distribution of lipopolyplexes in L1210 tumor bearing mice. Bioimaging of lipopolyplexes (50% Cy7-labeled siRNA) without shielding or modified with mono- or bis-DBCO and varying PEG-lengths in a FoIA-targeted and a non-targeted version, were determined by NIR fluorescence bioimaging. Mice were injected intravenously and imaging was performed immediately and repeated after 15 and 30 min and 1, 2, 3, 4 and 24 h. Experiment was performed with 3 animals per group for time points until 1 h, one animal at 2 and 3 h and two animals at 4 and 24 h. One representative animal per group and time point is shown. Animals are presented in lateral position allowing the observation of the tumor site (indicated by green circles). Color scale (efficiency) had a minimum of 1.2×10^{-5} and a maximum of 3.3×10^{-4} fluorescent photons/incident excitation photon. **A)** Formulations with shorter PEG- (PEG₂₄) chain. **B)** Formulations with longer PEG- (PEG5k / PEG₇₂) chain. Figure is adapted from Klein *et al.* [147].

A formulation's elimination from blood circulation can be evaluated when animals are imaged in ventral position. **Figure 9** shows major accumulation of lipopolyplexes in the liver area starting already after 30 min in case of DBCO-PEG₂₄ and after 1 h in the unshielded group. The only groups with whole body distribution after 4 h are double-click (DBCO₂) FoIA-targeted formulations. Liver signal is eventually decreasing after 24 h in all groups besides DBCO-PEG₂₄ and DBCO-PEG5k in which it has already been cleared before. Elimination from blood circulation occurs through renal clearance which is indicated by a strong fluorescence signal in the bladder area. It appears after 1 h in the unshielded group, also in the DBCO-PEG₂₄ and DBCO-PEG₇₂ FoIA groups, while in most other groups it becomes visible after 4 h. Only in DBCO₂-ss₂-PEG₂₄ FoIA injected animals, no obvious bladder signal is detectable after 4 h, as fluorescence is still

detectable in the whole body.

Summing up all findings, **1106** DBCO₂-ss₂-PEG₂₄ FoIA demonstrated superior biodistribution properties. It exhibited the longest circulation time as well as tumor accumulation and latest clearance of all tested formulations.

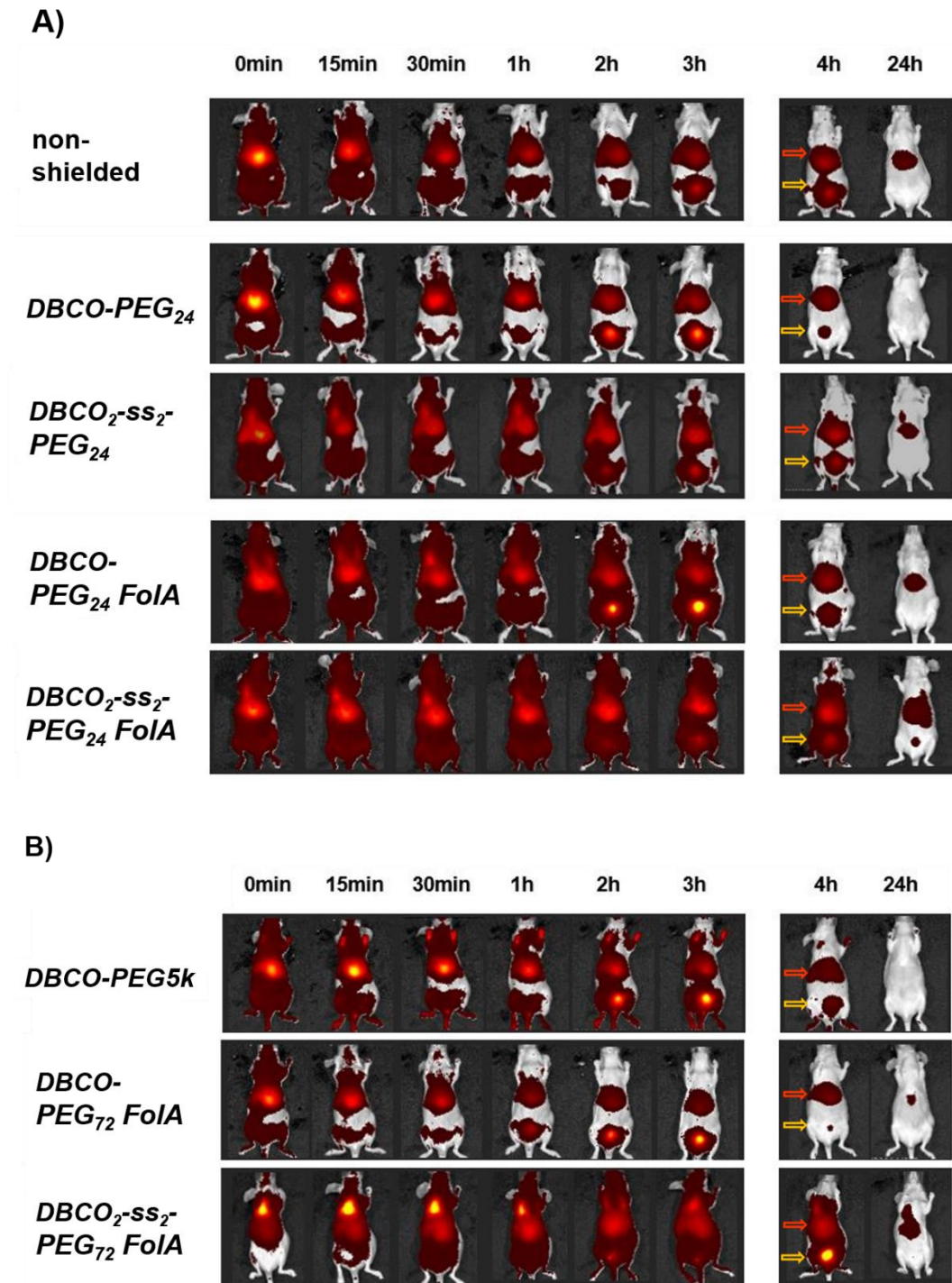


Figure 9: Elimination of lipopolyplexes from the blood circulation after i.v. injection in L1210 tumor bearing mice. Bioimaging of lipopolyplexes (50% Cy7-labeled siRNA) with varying PEG lengths and modified with

mono- or bis-DBCO in a FcA-targeted and a non-targeted version, were determined by NIR fluorescence bioimaging. Mice were injected intravenously and imaging was performed immediately and repeated after 15 and 30 min and 1, 2, 3, 4 and 24 h. Experiment was performed with 3 animals per group for time points until 1 h, one animal at 2 and 3 h and two animals at 4 and 24 h. One representative animal per group and time point is shown. Animals are presented in ventral view allowing the observation of the liver (indicated by orange arrows) and bladder (indicated by yellow arrows) to analyze the formulation's clearance. Color scale (efficiency) had a minimum of 1.2×10^{-5} and a maximum of 3.3×10^{-4} fluorescent photons/incident excitation photon. **A)** Formulations with shorter PEG- (PEG₂₄) chain. **B)** Formulations with longer PEG- (PEG_{5k} / PEG₇₂) chain.

To evaluate the reason behind the obvious improvement of biodistribution through modification with FcA as targeting ligand, the experiment was repeated with the best-performing formulation in tumor-free animals. **Figure 10** depicts a comparison of L1210 tumor bearing mice to tumor-free mice. Biodistribution of DBCO₂-ss₂-PEG₂₄ FcA is not as broad as in L1210 tumor bearing animals. Yet, the detectable fluorescence pattern is comparable to the untargeted DBCO₂-ss₂-PEG₂₄ [147].

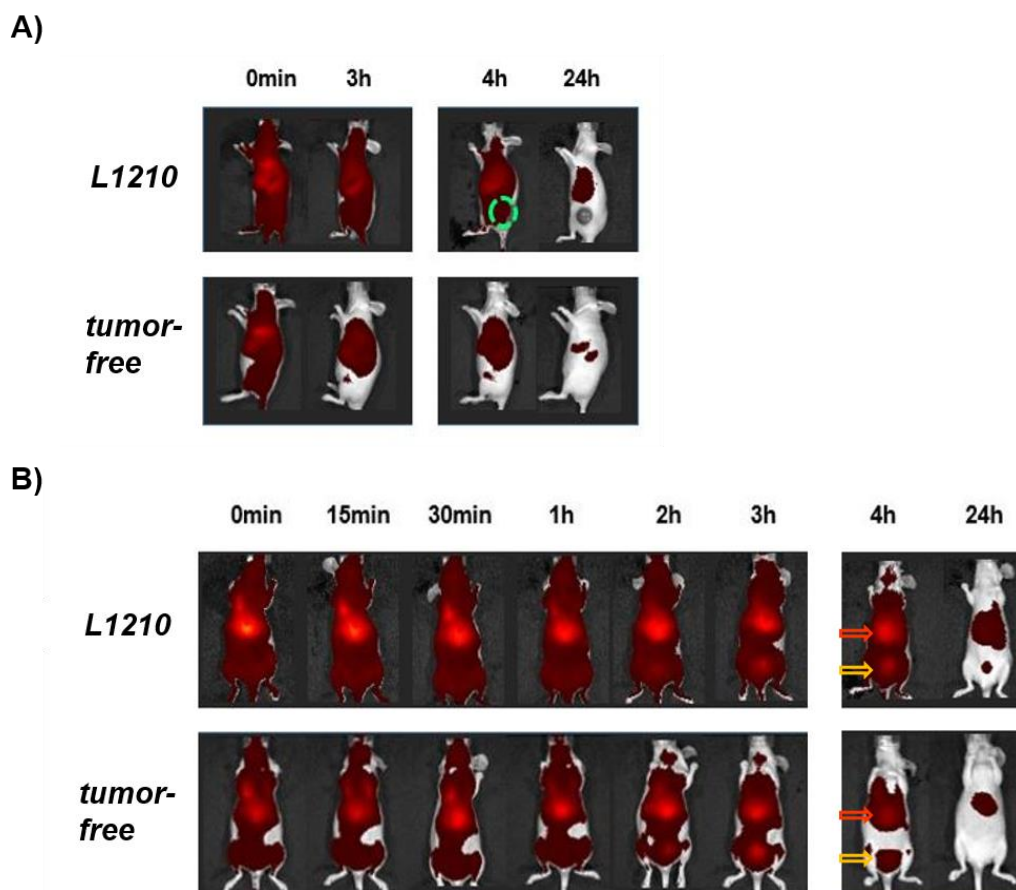


Figure 10: Time-dependent distribution of 1106 DBCO₂-ss₂-PEG₂₄ FoIA in tumor-free mice compared to L1210 tumor bearing mice at different time points after intravenous injection. NIR imaging of 50% Cy7-labeled siRNA polyplexes was performed at 0, 15 and 30 min, 1, 2, 3, 4 and 24 h after systemic administration. The experiment was performed with 3 animals per group for time points until 1 h, one animal at 2 and 3 h and two animals at 4 and 24 h. One representative animal per group and time point is shown. Color scale (efficiency) had a minimum of 1.2×10^{-5} and a maximum of 3.3×10^{-4} fluorescent photons/incident excitation photon. **A)** Comparison of tumor-free animals to L1210 tumor bearing animals in lateral view. **B)** Comparison of tumor-free animals to L1210 tumor bearing animals in ventral view allowing the observation of the liver (indicated by orange arrows) and bladder (indicated by yellow arrows) to analyze the formulation's clearance. Panel **B)** is adapted from Klein *et al.* [147].

Fatty acids or cholic acids are contained in the lipo-oligomer core for hydrophobic stabilization. To evaluate the impact of different acids, cholic acid (CholA) was replaced by oleic acid (OleA), which has been used with FoIA-targeted formulations in previous work [156, 157]. Therefore, an additional experiment with the modified oligomer (new oligomer ID **1169**) was performed. Analog to the first part, L1210 tumor bearing mice were injected with DBCO₂-ss₂-PEG₂₄ FoIA and fluorescence bioimaging was performed at various time points. **Figure 11** shows the biodistribution of injected animals. Although the distribution pattern looks similar to **1106** until 3 h, no advantage of OleA over CholA could be demonstrated.

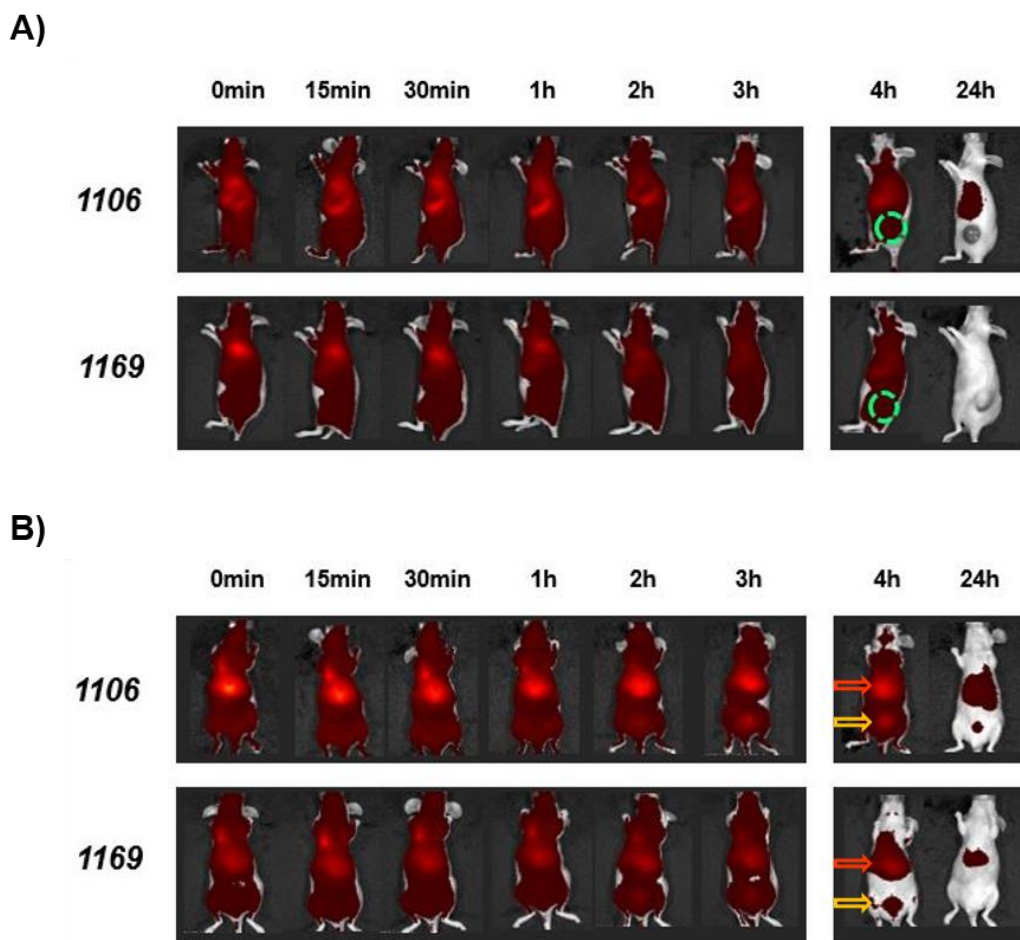


Figure 11: Comparison of time dependent distribution of 1106 and 1169 formulations. The upper panel shows DBCO₂-ss₂-PEG₂₄ FoIA formulation with the CholA-containing oligomer **1106**, whereas the lower panel shows the analog (OleA-containing) **1169** formulation. L1210 tumor bearing mice were injected intravenously and NIR imaging of 50% Cy7-labeled siRNA polyplexes was performed at 0, 15 and 30 min, 1, 2, 3, 4 and 24 h after systemic administration. The experiment was performed with 3 animals per group for time points until 1 h, one animal at 2 and 3 h and two animals at 4 and 24 h. One representative animal per group and time point is shown. Color scale (efficiency) had a minimum of 1.2×10^{-5} and a maximum of 3.3×10^{-4} fluorescent photons/incident excitation photon. **A)** Lateral view of the mice is presented, allowing the observation of the tumor site (indicated by green circles) **B)** Mice are presented in ventral view allowing the observation of the liver (indicated by orange arrows) and bladder (indicated by yellow arrows) to analyze the formulation's clearance. Panel **A)** is adapted from Klein *et al.* [147].

1.2.2. Clinical biochemistry evaluation

Systemic administration of formulations always bears a risk of undesired side effects when non-target tissue is reached. To evaluate whether our lipopolyplex was tolerated well by the animals, clinical biochemistry of blood

samples was analyzed regarding renal and liver parameters which are altered frequently and showed high amounts of fluorescence signal in the biodistribution study. Tumor-free animals were used for this experiment as L1210 tumors tend to metastasize rapidly and by that influence especially liver parameters. Mice were injected intravenously with **1106** DBCO₂-ss₂-PEG₂₄ FoIA. At 24 h later, animals were sacrificed and blood was obtained. Subsequently, plasma was analyzed for renal parameters BUN (blood urea nitrogen) and creatinine and liver parameters AST (aspartate aminotransferase) and ALT (alanine aminotransferase). Comparing the values to untreated tumor-free animals, all parameters were within normal limits, indicating a good tolerance of the formulation (Figure 12).

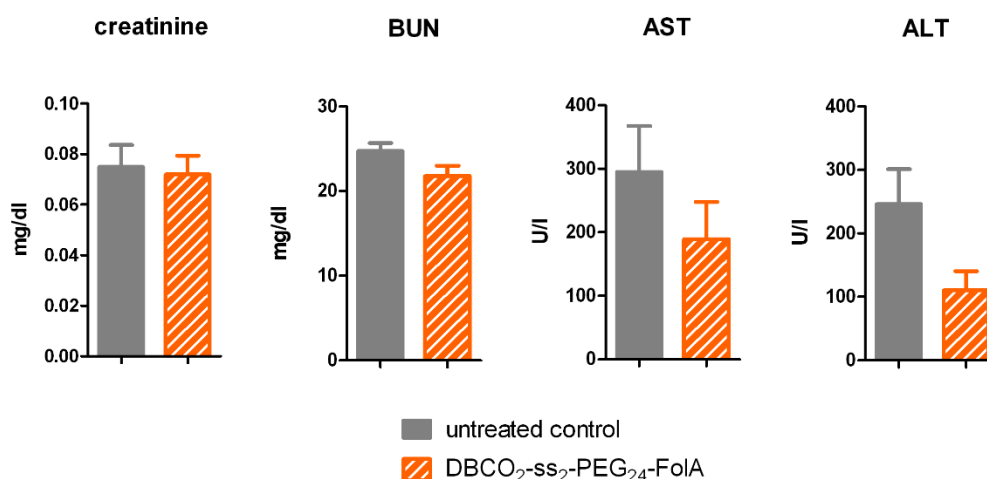


Figure 12: Clinical biochemistry parameters (renal parameters creatinine and BUN, liver parameters ALT and AST). Tumor-free mice injected with **1106** DBCO₂-ss₂-PEG₂₄ FoIA were compared to an internal untreated control group which was otherwise handled in the same way and time schedule. Plasma was obtained when animals were sacrificed and subsequently analyzed in the *Clinic of Small Animal Medicine, Centre for Clinical Veterinary Medicine, Faculty of Veterinary Medicine, LMU Munich*. Represented is the mean + S.E.M. of 4-5 mice per group. Illustration is adapted from Klein *et al.* [147].

1.2.3. Tumoral gene silencing *in vivo*

While fluorescence imaging of Cy7-labeled formulations can only provide information about the distribution pattern, no statement can be made regarding cellular uptake. As siRNA acts in the cytosol, downregulation of a

target gene product implies successful uptake. Hence, an experiment was performed to evaluate gene silencing efficiency of the best performing formulation of our biodistribution experiment. DBCO₂-ss₂-PEG₂₄ FoIA was chosen, since it showed tumor accumulation until 4 h post injection. Lipopolyplexes were prepared with **1106** and siRNA directed against mRNA of the kinesin-related motor protein EG5. By directing EG5, mitosis of cells gets inhibited. As a control, polyplexes were prepared with siCtrl. Also, the untargeted formulation with siEG5 was evaluated for its gene silencing efficacy. Mice bearing L1210 tumors were randomly divided into 4 groups when tumors reached 500 mm³ and intravenous injections were performed twice at 24 h interval. At 48 h after the first treatment, animals were sacrificed and tumors were harvested for RNA extraction and qRT-PCR analysis of mRNA levels of EG5. mRNA levels of treatment groups were eventually compared to untreated animals.

Treatment with **1106** DBCO₂-ss₂-PEG₂₄ FoIA + siEG5 significantly reduced tumoral EG5 mRNA expression (~60%). In case of the siCtrl containing targeted analog, EG5 downregulation was only weak. Also, the untargeted DBCO₂-ss₂-PEG₂₄ + siEG5 formulation mediated only neglectable effects regarding EG5 downregulation (**Figure 13**).

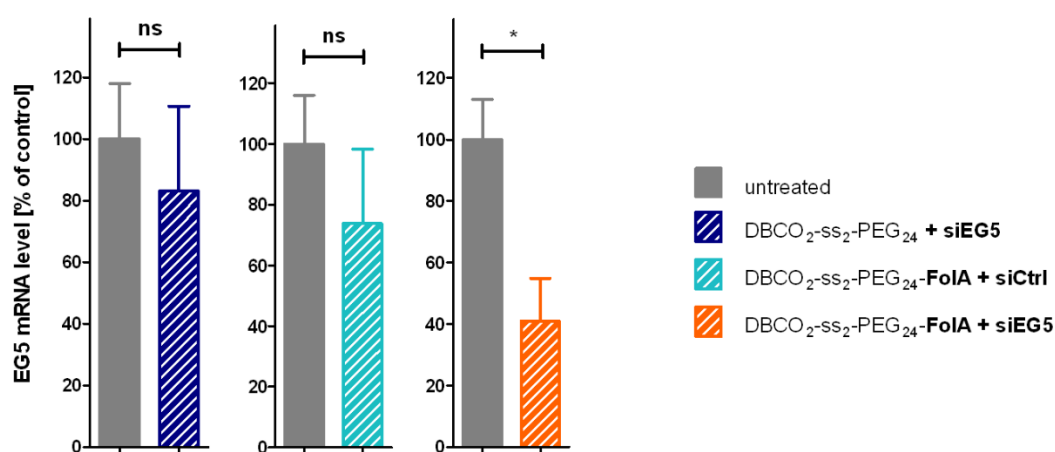


Figure 13: Gene silencing efficiency of 1106 formulations in L1210 tumor bearing mice. Groups (n=5 animals per group) were treated with **1106** DBCO₂-ss₂-PEG₂₄ FoIA with siEG5 or siCtrl or the siEG5 containing untargeted analog. Animals were sacrificed 24 h after twofold intravenous injection and tumors were harvested for qRT-PCR analysis of mRNA levels of EG5 gene. EG5 mRNA levels (mean + S.E.M.) are expressed in % of untreated control. qRT-PCR was performed by Dr. Dian Jang Lee (*former PhD student at Pharmaceutical Biotechnology, LMU*). Figure is adapted

from Klein *et al.* [147].

The evaluation of gene silencing efficiency was repeated with the OleA containing **1169** oligomer to analyze the impact of different fatty or bile acids on gene silencing efficiency. Experimental settings were identical to the first part with **1106** oligomer.

Tendencies between the different formulations were similar to the Chola containing oligomer **1106**. Yet, *EG5* downregulation by **1169** DBCO₂-ss₂-PEG₂₄ FoIA + siEG5 did not reach statistical significance (~40%) (**Figure 14**). This confirmed the superiority of Chola over OleA that was already demonstrated during biodistribution studies (**Figure 11**).

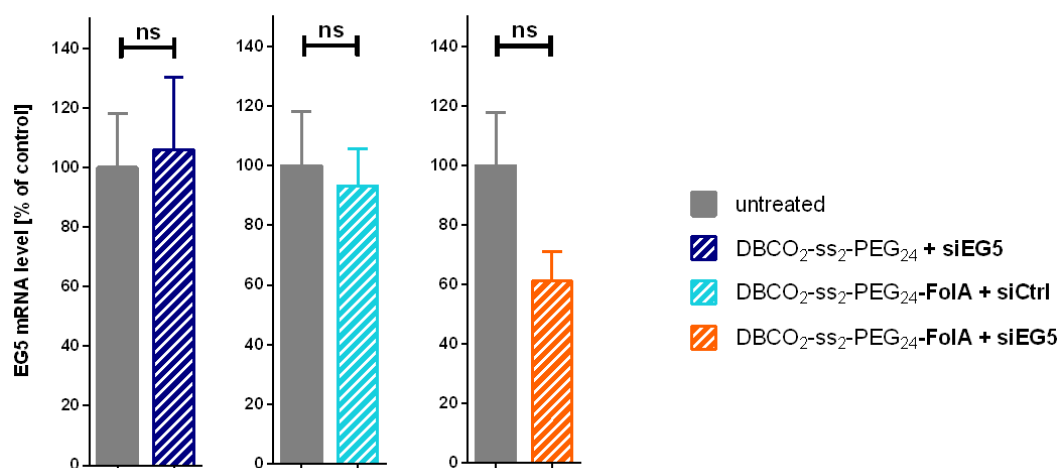


Figure 14: Gene silencing efficiency of 1169 formulations in L1210 tumor bearing mice. Groups (n=5 animals per group) were treated with **1169** DBCO₂-ss₂-PEG₂₄ FoIA with siEG5 or siCtrl or the siEG5 containing untargeted analog. Animals were sacrificed 24 h after twofold intravenous injection and tumors were harvested for qRT-PCR analysis of mRNA levels of *EG5* gene. *EG5* mRNA levels (mean + S.E.M.) are expressed in % of untreated control. qRT-PCR was performed by Dr. Dian Jang Lee (*former PhD student at Pharmaceutical Biotechnology, LMU*). Figure is adapted from Klein *et al.* [147].

During both experimental parts, the animals' weight was recorded to monitor animal well-being especially during treatments. In case of **1106**, no effect of the injections could be observed, while minor weight loss occurred after the first treatment with **1169** formulations (**Figure 15**).

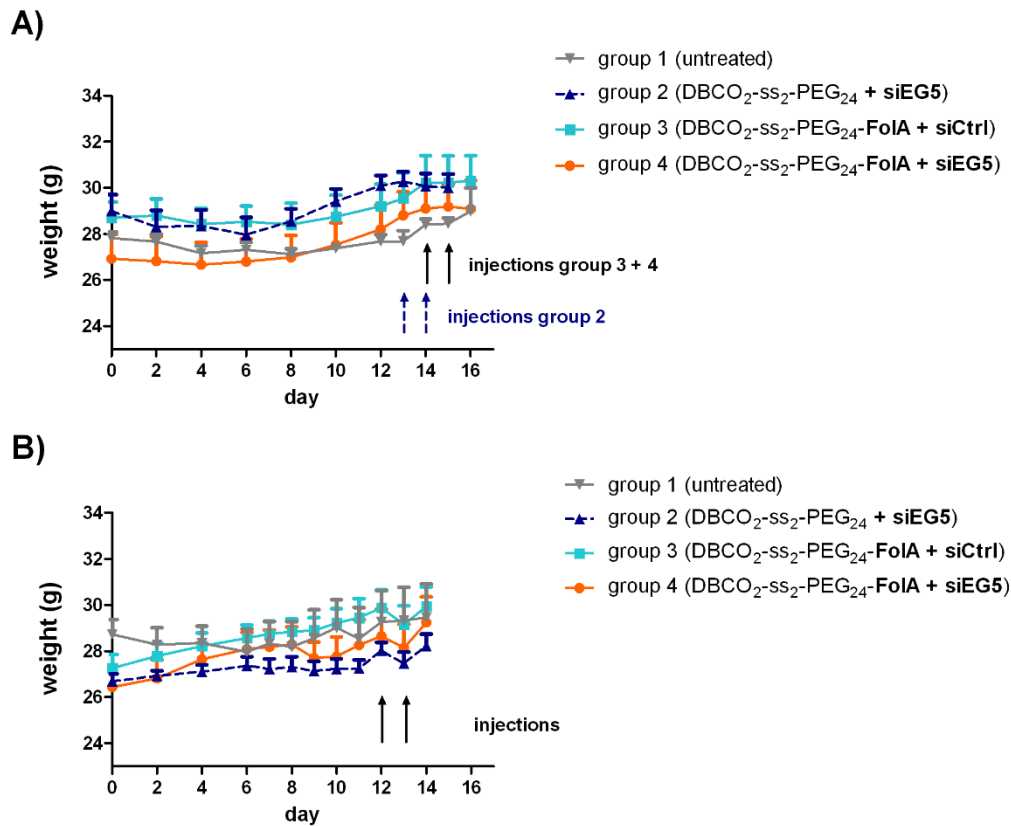


Figure 15: Weight of mice during gene silencing experiments, starting with L1210 tumor cell inoculation (day 0) and ending with euthanasia. Represented is the mean + S.E.M. of 5 mice per group. **A)** Intravenous injections with **1106** formulations are indicated by blue (group 2) and black (group 3 + 4) arrows. **B)** Intravenous injections with **1169** formulations are indicated by black arrows (groups 2, 3, 4). Illustration **A)** is adapted from Klein *et al.* [147].

In sum, **1106** oligomer modified with bis-DBCO, short PEG₂₄ and FolA-targeting proved to be superior in biodistribution studies and blood parameters were unobtrusive in consequence of intravenous treatments. Furthermore, the same formulation in combination with EG5 siRNA mediated significant downregulation of *EG5* mRNA in L1210 tumors. Therefore, it presents an attractive candidate for an *in vivo* treatment experiment.

1.2.4. Combinatorial treatment with FoIA-targeted lipopolyplexes and PT

Building on these encouraging results, a treatment experiment with systemic administration was designed to analyze the therapeutic potential of **1106** DBCO₂-SS₂-PEG₂₄-FoIA with siEG5. Furthermore, the novel microtubule inhibitor pretubulysin (PT) was chosen for a combination therapy approach.

The aforementioned formulation was compared to the corresponding formulation with siCtrl and both groups were further modified with PT, while free PT and HBG served as controls.

The dose of PT was chosen based on previous combination treatment experiments with up to 8 intravenous injections of PT at a dose of 2 mg/kg, in which effective tumor growth inhibition was achieved in absence of any systemic side effects (see III.2.2. and III.2.3.). Therefore, the current study was carried out with the same dose.

L1210 tumor bearing mice were treated intravenously for up to 8 times, starting on day 3. On day 8, tumors of all groups lacking PT became measurable. Subsequently, tumors of HBG and siCtrl group grew rapidly. All PT containing groups revealed distinct tumor growth inhibition. Within these groups, siCtrl + PT mediated a weaker antitumoral effect than free PT, while siEG5 + PT led to the most efficient tumor growth inhibition (**Figure 16**).

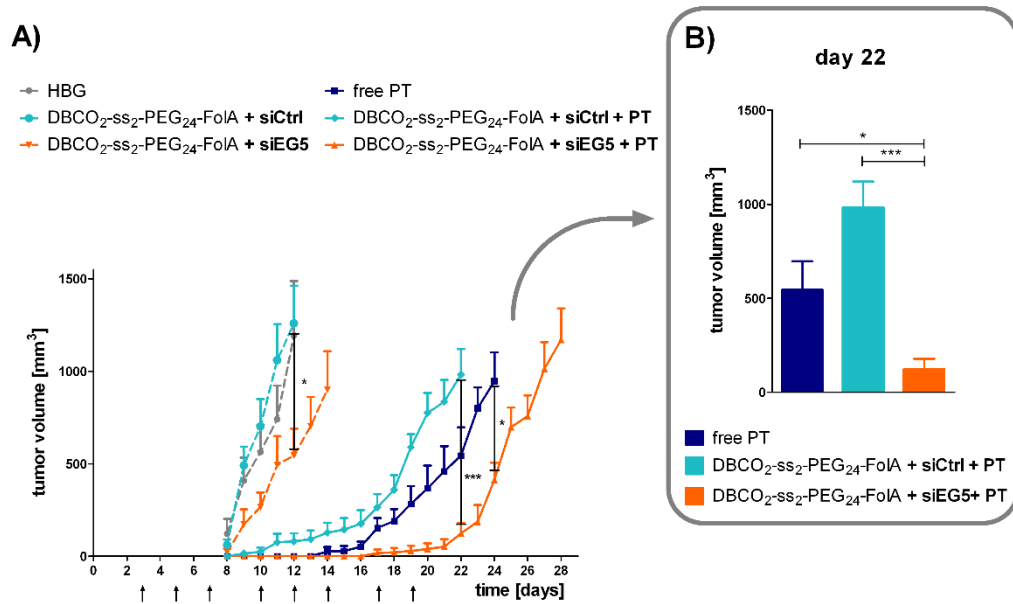
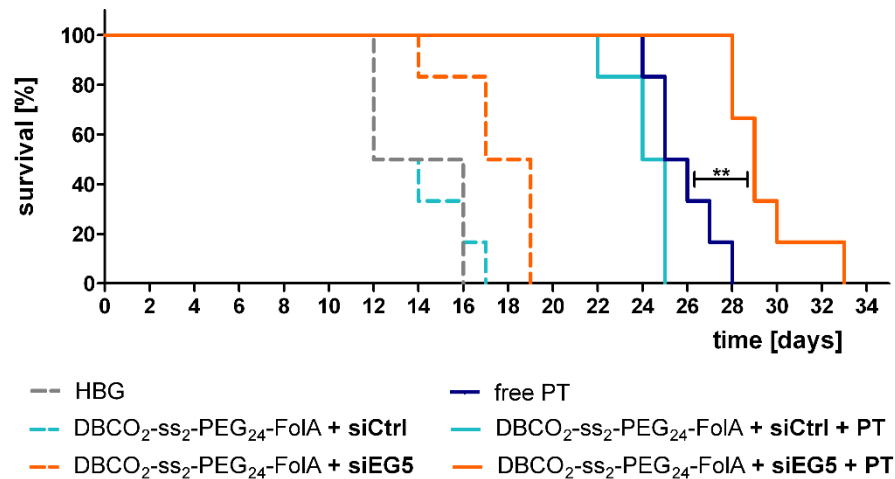


Figure 16: Tumor growth of L1210 tumor bearing mice treated with HBG, free PT or siEG5 respectively siCtrl containing formulations with or without PT. **A)** Tumor growth curve, day 0 represents the day of tumor cell inoculation. Treatments are indicated by black arrows (mean + S.E.M.; n=6; *p < 0.05, **p < 0.01, ***p < 0.001). **B)** Comparison of tumor sizes of PT-containing groups on day 22 (mean + S.E.M.; n=6; *p < 0.05, **p < 0.01, ***p < 0.001). **A)** Illustration is adapted from Klein *et al.* [147].

Animals were sacrificed after they reached the previously determined termination criteria and Kaplan Meier survival analysis was compiled (**Figure 17**, [147]). While the overall survival in PT-free groups ranged from 12 (HBG and siCtrl) to 14 (siEG5) days after rapid tumor progression, all PT-containing groups survived significantly longer. The first animal of siCtrl + PT group was sacrificed on day 22, whereas treatments with free PT resulted in a survival of all animals until day 24. siEG5 + PT group achieved an overall survival until day 28, when all animals of the remaining groups were already sacrificed. This resulted in a significantly prolonged survival of this group (log rank test of Kaplan Meier curve PT vs. siEG5 + PT: 0.0021; Mean survival PT vs. siEG5 + PT: 0.0036).

A)



B)

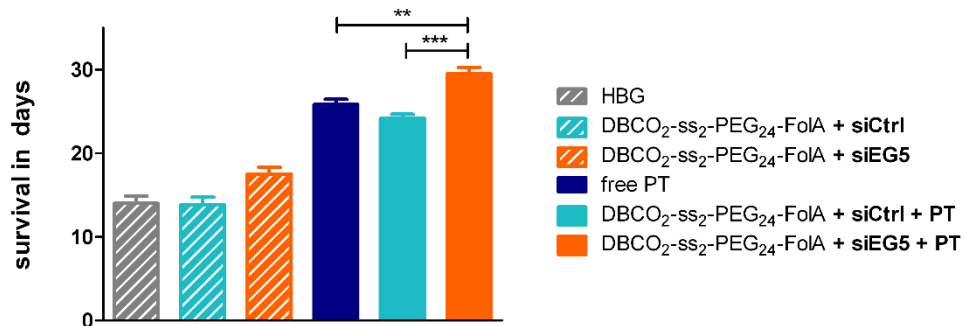


Figure 17: Survival of mice treated with HBG, free PT or **1106** DBCO₂-ss₂-PEG₂₄ FoIA + siEG5 respectively siCtrl formulations with and without combination with PT. **A)** Kaplan Meier survival analysis of indicated groups (n=6; **p < 0.01). **B)** Mean survival of indicated groups (mean + S.E.M.; n=6; **p < 0.01, ***p < 0.001). Panel **A)** is adapted from Klein *et al.* [147].

To ensure animal well-being, mice were controlled daily and weight was recorded. The even weight development of all groups, which is depicted in **Figure 18**, indicates that treatments were tolerated well by the animals.

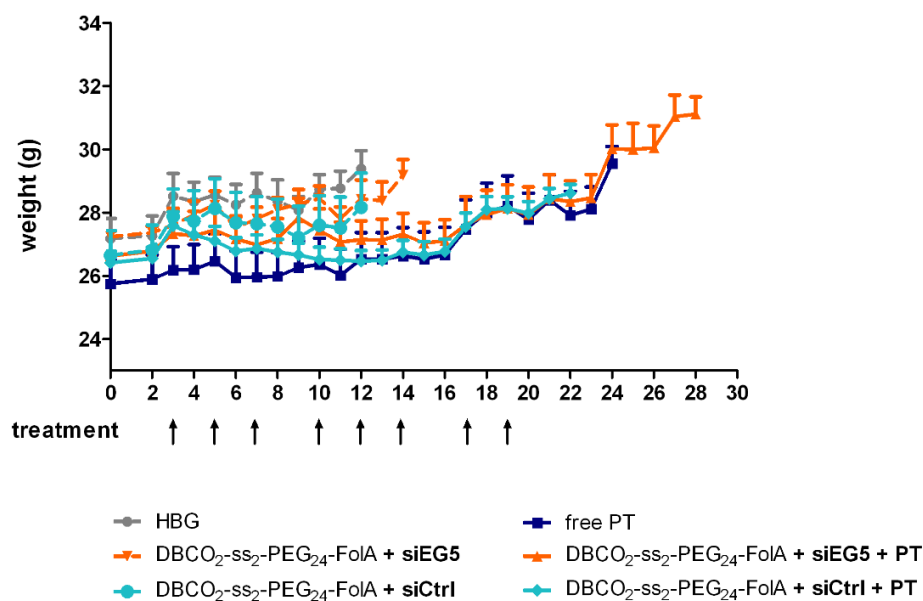


Figure 18: Weight development of L1210 tumor bearing mice treated with HBG, free PT or siEG5 respectively siCtrl containing formulations with or without PT. Day 0 represents the day of tumor cell inoculation. Treatments are indicated by black arrows (mean + S.E.M.; n=6). Graph is adapted from Klein *et al.* [147].

To conclude, significantly inhibited tumor growth and prolonged survival was demonstrated, in absence of any systemic side effects after multiple intravenous injections with the FoIA targeted siEG5 formulation in combination with PT.

1.2.5. Treatment with GE11-targeted, PT containing siEG5 lipopolyplexes

The next aim was to evaluate whether the promising results of siEG5 and PT combination can be reproduced in another tumor model. For this purpose, NMRI-nu/nu mice were inoculated with human HUH7-wt hepatoma cells. HUH7 cells overexpress the EGF receptor. Therefore, a different carrier system was selected, which is targeted to the EGF receptor. Based on its very encouraging transfection efficiency *in vitro*, the T-shaped oligomer **1198** was chosen from our library (**Figure 19**). This lipo-oligomer emerged from oligomer **454**, which was previously used in other animal experiments (see III.2.3.). However, it was additionally equipped with an azide for click chemistry. Thus, siRNA lipopolyplexes of **1198** can be

reacted with DBCO-PEG₂₄-GE11 to introduce PEG as shielding agent and the peptide GE11 as EGFR targeting ligand. The oligomer was formulated together with EG5 or control siRNA and optionally also PT into nanoparticles.

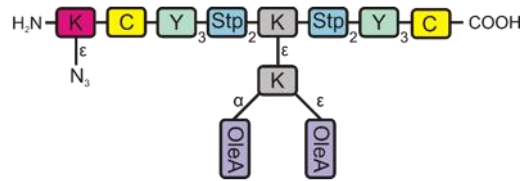


Figure 19: Schematic illustration of T-shaped oligomer 1198. Abbreviations of individual units indicate: K: lysine, C: cysteine, Y: tyrosine, Stp: succinoyl-tetraethylene-pentamine, OleA: oleic acid, N₃: azide function.

When tumors reached a size of 200 to 250 mm³, treatments via tail vein injection were started individually. Mice were injected with GE11-PEG-modified **1198** with siEG5 respectively siCtrl and with or without PT. Free PT and HBG served as controls.

All tumors of HBG and siEG5 respectively siCtrl group without co-formulation with PT exhibited fast tumor progression after the start of injections and neither of the treatments could inhibit tumor growth. This ultimately led to an overall survival until day 5 (siEG5), respectively day 6 (siCtrl) or day 7 (HBG) after treatment start. In all PT-containing groups, however, tumor growth ceased after 3 injections and tumors began to slowly shrink during the treatment period. Various tumors even fell below the measurable size (1 × PT, 1 × siCtrl + PT, 2 × siEG5 + PT). After the end of treatments, tumor growth in all groups eventually proceeded (**Figure 20**), resulting in an overall survival until day 22 (PT), respectively day 23 (siCtrl + PT) and day 26 (siEG5 + PT). Yet, not all tumors of each group had resumed growing by then, which explains the lack of statistical significance. The last animal that had to be sacrificed due to its tumor burden survived until day 40 (PT), 46 (siCtrl + PT) and 58 (siEG5 + PT), respectively (**Figure 21**).

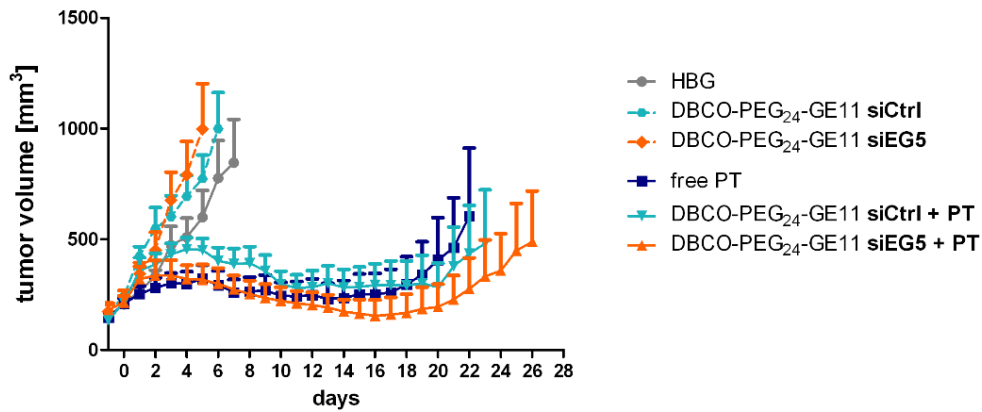


Figure 20: Tumor growth inhibition by systemic administration of HBG, free PT, siEG5 or siCtrl containing GE11-PEG **1198** formulations with or without co-formulation with PT in HUH7 tumor bearing mice. Day 0 represents the day of individual treatment start, treatments were repeated thrice weekly for up to 7 times (mean + S.E.M.; n=6).

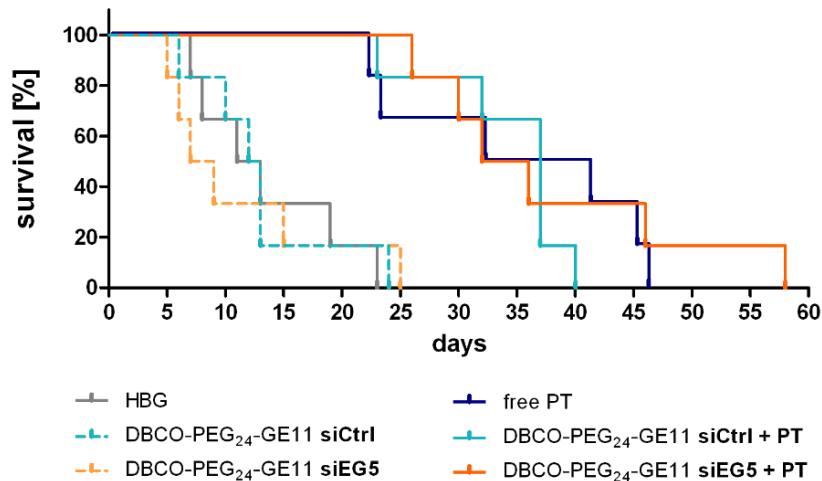


Figure 21: Kaplan Meier survival analysis of HUH7 tumor bearing mice treated intravenously with HBG, free PT, siEG5 or siCtrl containing GE11-PEG **1198** formulations with or without co-formulation with PT (n=6).

To monitor animal well-being and detect any injection-related adverse effects, weight was monitored daily. **Figure 22** depicts the weight development starting on day -1, one day prior to treatment start and ending with euthanasia. The even curve progression of all groups does not indicate any side effects during the treatment period.

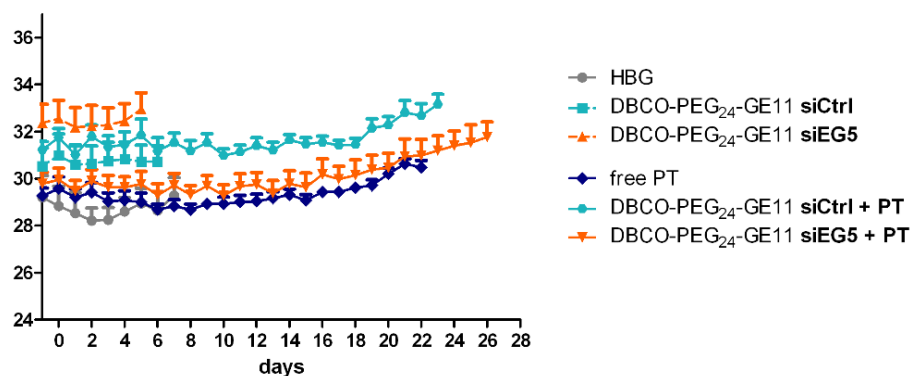


Figure 22: Weight development over time of HUH7 tumor bearing mice treated intravenously with HBG, free PT, siEG5 or siCtrl containing **1198** formulations with or without co-formulation with PT. Day 0 represents the day of individual treatment start, treatments were repeated thrice weekly for up to 7 times (mean + S.E.M.; n=6).

All in all, the GE11-PEG formulation containing siEG5 in combination with PT led to an advantage in tumor growth inhibition and prolonged survival as compared to all other treatment groups.

2. Combinatorial treatment of PT and MTX

In this chapter, a potentially beneficial combination effect of the natural compound pretubulysin (PT), a potent tubulin-binding antitumoral drug, and the well-established antimetabolite methotrexate (MTX) was evaluated in several approaches. First, a conjugate of both components was injected intratumorally into KB tumor bearing mice. Secondly, a combination of the free drugs was analyzed in a treatment experiment with systemic administration in various tumor models. Finally, both drugs were encapsulated and co-delivered in another treatment experiment with intravenous injections in L1210 tumor bearing mice. *In vitro* assays concerning PT+MTX in L1210 and KB tumors were performed by Ines Truebenbach (*PhD student at Pharmaceutical Biotechnology, LMU*). Miriam Höhn (*chemical technician at Pharmaceutical Biotechnology, LMU*) contributed to acquiring CLSM images. Johannes Schmaus (*veterinary MD student at Pharmaceutical Biotechnology, LMU*) assisted during the **454** PT+MTX treatment experiment.

2.1. Intratumoral treatment with E4-MTX-H-PT conjugate

The covalent coupling of compounds enables their simultaneous delivery and, in case that targeting ligands are involved, facilitates receptor-mediated uptake.

Via solid-phase supported synthesis, a conjugate of E4-MTX oligoamide (ID **951**, **Figure 23**) with a thiol-reactive PT derivative was synthesized. The oligomer exhibits a 4-arm topology, as this structure achieved the best results *in vitro* in the FR-overexpressing KB cell line as compared to linear or 2-arm oligomers. In order to determine if this effect also accounted for the situation *in vivo*, mice were inoculated with subcutaneous KB tumors. Intratumoral treatments with the aforementioned co-formulation, free PT-COOH or the 4-arm E4-MTX oligomer alone started on day 2 and were repeated 5 times, while control animals remained untreated (**Figure 24**).

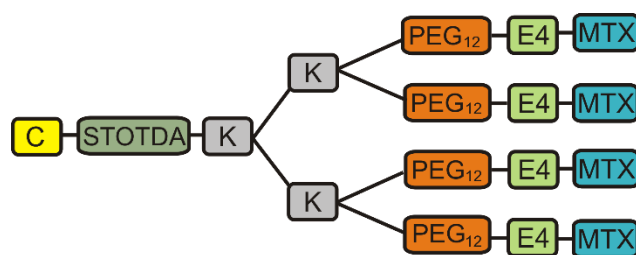


Figure 23: Schematic illustration of 4-arm E4-MTX (ID 951). Abbreviations of individual units indicate: C: cysteine, K: lysine, E4: four glutamic acids; STOTDA: short ethylene glycol linker N-succinyl-4,7,10-trioxa-1,13-tridecanediamine; PEG₁₂: polyethylene glycol unit containing 12 ethylene oxide units; MTX: methotrexate ligands.

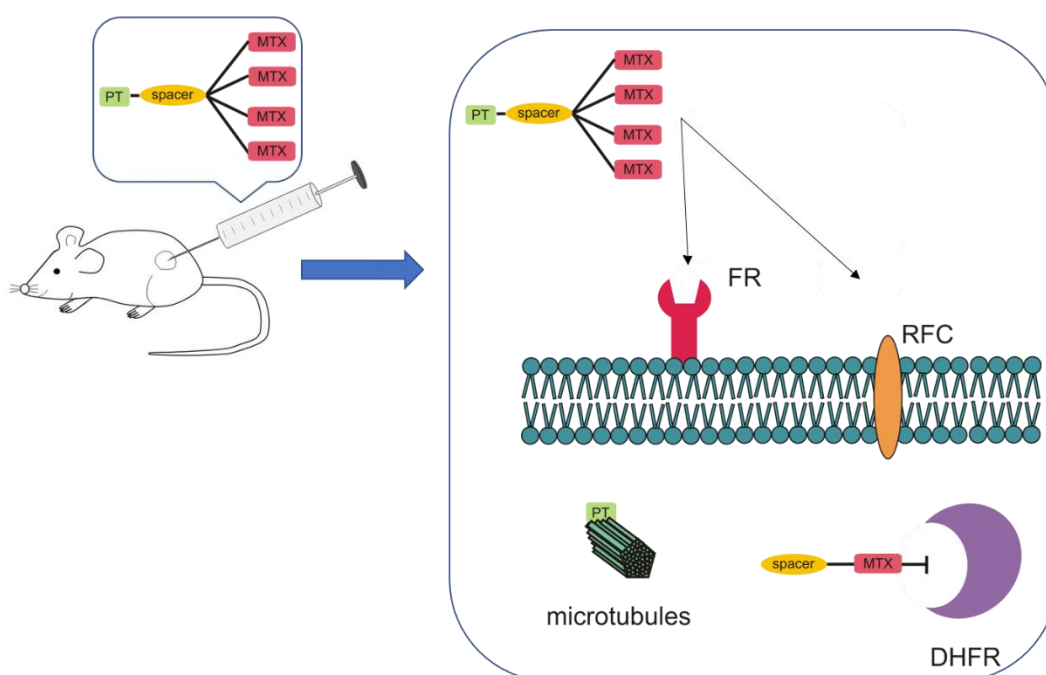


Figure 24: Mechanism of action of E4-MTX-H-PT conjugate. Mice are injected intratumorally with E4-MTX-H-PT conjugate. Particles cross the extracellular matrix and, mediated by the targeting ligand MTX, get internalized into their target cell by FR and RFC. Once inside the cytosol, PT inhibits microtubule, while MTX competitively inhibits DHFR.

The 4-arm E4-MTX oligomer alone did not mediate any antitumoral effect as compared to the untreated control group. Both PT formulations inhibited tumor growth and resulted in noticeably reduced tumor volumes in comparison to the other groups during treatment phase. However, after the last injection tumor growth proceeded in both groups (**Figure 25**). The first animal of E4-MTX group had to be sacrificed on day 22, while all untreated

and PT-treated mice survived until day 23 and injections with E4-MTX-H-PT conjugate led to an overall survival until day 27. During the whole experiment the body weight was monitored. The lack of injection-related weight loss in combination with a good general condition indicates that intratumoral injections and the associated narcosis were tolerated well by the animals (**Figure 26**).

In conclusion, we demonstrated a marked tumor growth retarding effect of PT on KB cells upon intratumoral injections. In addition, we revealed that the E4-MTX-H-PT conjugate mediated comparable antitumoral effects and resulted in the longest survival of all animals.

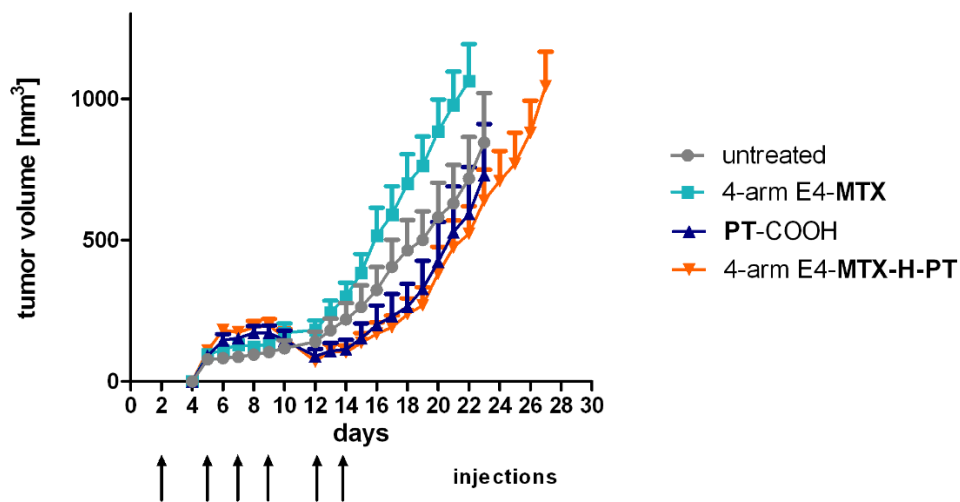


Figure 25: Tumor growth over time starting on day 0 with KB tumor cell inoculation and ending with euthanasia. Intratumoral injections are indicated by black arrows. Represented is the mean + S.E.M. of 8 mice per group. Graph is adapted from Truebenbach *et al.* [148].

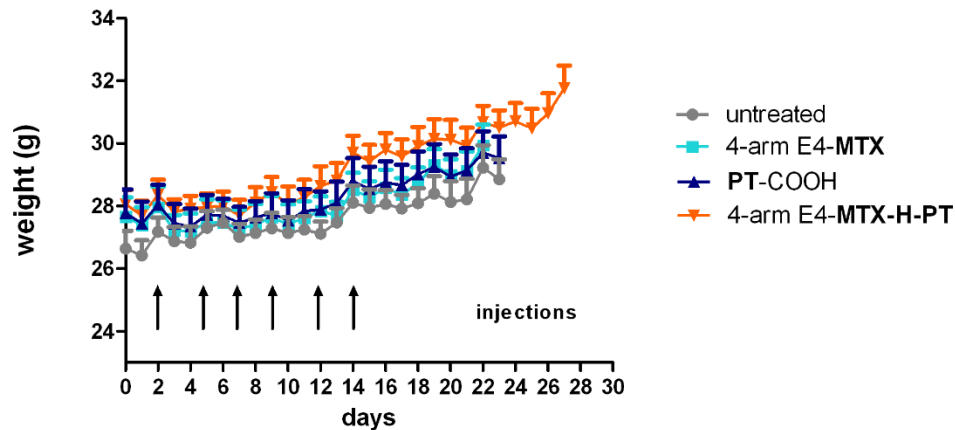


Figure 26: Weight development over time, starting on day 0 with KB tumor cell inoculation and ending with euthanasia. Intratumoral injections are indicated by black arrows. Represented is the mean + S.E.M. of 8 mice per group. Graph is adapted from Truebenbach *et al.* [148].

2.2. Combined antitumoral effects of PT and MTX after systemic application

Research in our lab went on to testing free PT and MTX separately or in combination (PT+MTX) for their antitumoral activity in L1210 leukemia cells and KB cervix carcinoma cells *in vitro* in various assays. Cytotoxicity (MTT) assays revealed strong antitumoral effects of PT and MTX on L1210 cells, while the PT+MTX combination even yielded in a synergistic effect. In cultured KB cells, however, MTX mediated only minor cell killing. Clear antitumoral effects were displayed by PT alone, but could not be enhanced by combination with MTX. Cell cycle analysis confirmed the previously described MTX triggered G1/S-arrest [158, 159] and PT-induced G2/M-arrest in both cell lines [140, 144, 160]. Yet, PT+MTX induced a G2/M-arrest which exceeded the G2/M-arrest caused by PT alone. In an apoptosis assay, no advantage of PT+MTX over the single drugs could be accomplished. Subsequently, confocal laser scanning microscopy (CLSM) was performed and images demonstrated alterations of cell morphology and actin cytoskeleton induced by MTX treatment, especially of KB cells. PT, in turn, caused nuclear fragmentation and microtubule disruption and treatment with PT+MTX resulted in a combination of the effects of the single drugs.

Based on these encouraging results, the next step was to test the efficacy of the combinatorial treatment in an *in vivo* mouse model. Therefore, the abovementioned cell lines L1210 and KB were chosen and an additional experiment in HUH7 hepatocellular carcinoma was compiled.

To determine an optimum dose of PT, we performed an internal dose finding experiment based on doses used in successful *in vivo* experiments published by other groups [140, 144, 145]. KB tumor bearing animals were injected every second day with 0.1, 0.2 or 0.4 mg/kg of PT. However, we did not find any advantageous tumor growth inhibition after these multiple intravenous injections. Subsequently, two single animals were injected with 1.5 mg/kg respectively 3 mg/kg PT, the former dose was well accepted, the mouse injected with the latter dose, however, showed side effects in the form of severe weight loss after the 5th treatment and had to be sacrificed for reasons of animal welfare. Therefore, we chose a dose of 2 mg/kg for the following treatment experiments.

2.2.1. Effect of PT+MTX combination therapy on L1210 tumor growth

First, PT+MTX combination treatment was evaluated in the L1210 tumor model, since *in vitro* cytotoxicity (MTT) data revealed synergistic effects of the combination.

Intravenous treatments with HBG, PT (2 mg/kg), MTX (5 mg/kg) or the combination of both (PT+MTX) were started on day 3 after tumor cell inoculation and were repeated up to 7 times. Animals were sacrificed when termination criteria were reached, respectively on day 13 and 14 in case of MTX treated mice. Animals of this group were euthanized together with all other mice of MTX dose finding experiment (see III.2.2.1.1.) on day 14. Yet, one animal reached the critical tumor size one day earlier and had to be sacrificed ahead of schedule.

Tumors started to grow around day 9 in HBG and MTX group and with a delay of 2 days, also in PT group. In the group treated with PT+MTX, tumor growth could largely be inhibited until day 17, when tumor volume also started to increase (**Figure 27A**). In a comparison of tumor sizes on day 13

(**Figure 27B**), tumors of PT+MTX group were significantly smaller than tumors of all other groups (PT+MTX vs. PT: 0.0132).

Animals of this group also survived significantly longer than animals of HBG group ($p = 0.0062$) and mean survival was 5 days longer than in PT treated animals. Furthermore, weight development was recorded for the duration of the experiment to monitor animal well-being, especially during injections. Although mice of PT+MTX group gained less weight during the first days, all groups showed a constant weight development throughout the experiment (**Figure 28**).

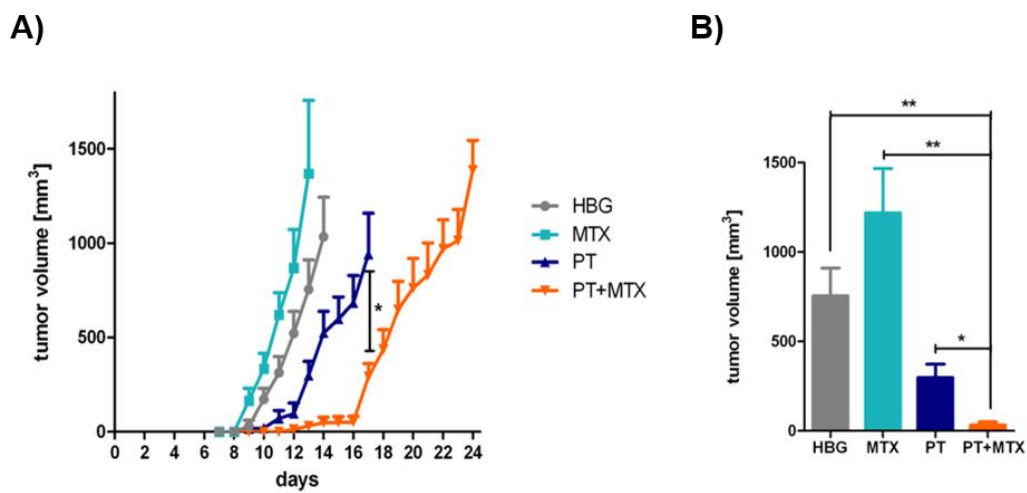


Figure 27: Tumor growth inhibition of subcutaneous L1210 tumors treated intravenously with HBG, MTX, PT or PT+MTX. **A)** Tumor growth of L1210 tumors throughout the experiment. Animals were treated intravenously with 250 μ L of HBG, MTX, PT or PT+MTX combination (mean + S.E.M.; $n=4$; * $p = 0.0293$). **B)** Comparison of tumor sizes on day 13 after tumor cell inoculation (mean + S.E.M.; $n=4$; * $p = 0.0132$, ** $p < 0.01$).

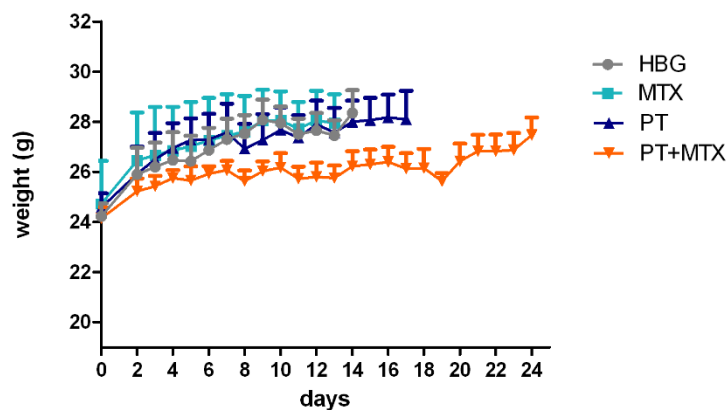


Figure 28: Weight development throughout PT+MTX combination

therapy experiment in L1210 tumor bearing animals, starting on day 0 with tumor cell inoculation. Represented is the mean + S.E.M. of 4 mice per group.

2.2.1.1. Dose finding of MTX

The dose of MTX used in the animal experiments was based on efficacy in cell culture experiments and is lower than used in some other work. Burger *et al.* described 100 mg /kg as the maximum tolerated dose of MTX for NMRI nude mice [161]. Therefore, a new dose finding experiment was conducted.

The experiment was performed in two parts (low dose and high dose MTX) to evaluate the best working dose for tumor growth inhibition *in vivo*. L1210 cells were inoculated and injections of MTX respectively HBG were carried out three times per week. Neither in the first part of the experiment comparing lower doses of 2.5, 5, 7, 10 and 20 mg/kg, nor in the second part comparing 40, 80 and 100 mg/kg we could observe any significant antitumoral effect of MTX as compared to HBG treated animals (**Figure 29A+B**). However, especially in the group treated with the highest dose of 100 mg/kg, side effects in the form of severe weight loss and notably affected well-being occurred (**Figure 29C**). Consequently, 2 out of 4 animals had to be sacrificed before reaching the critical tumor volume for reasons of animal welfare.

In sum, no significant tumor growth inhibition could be shown for any of the tested doses. Yet, tumor growth inhibition was the most pronounced in MTX 100 mg/kg group. Also, given the incidents which occurred in this group, the use of higher doses is inconvenient.

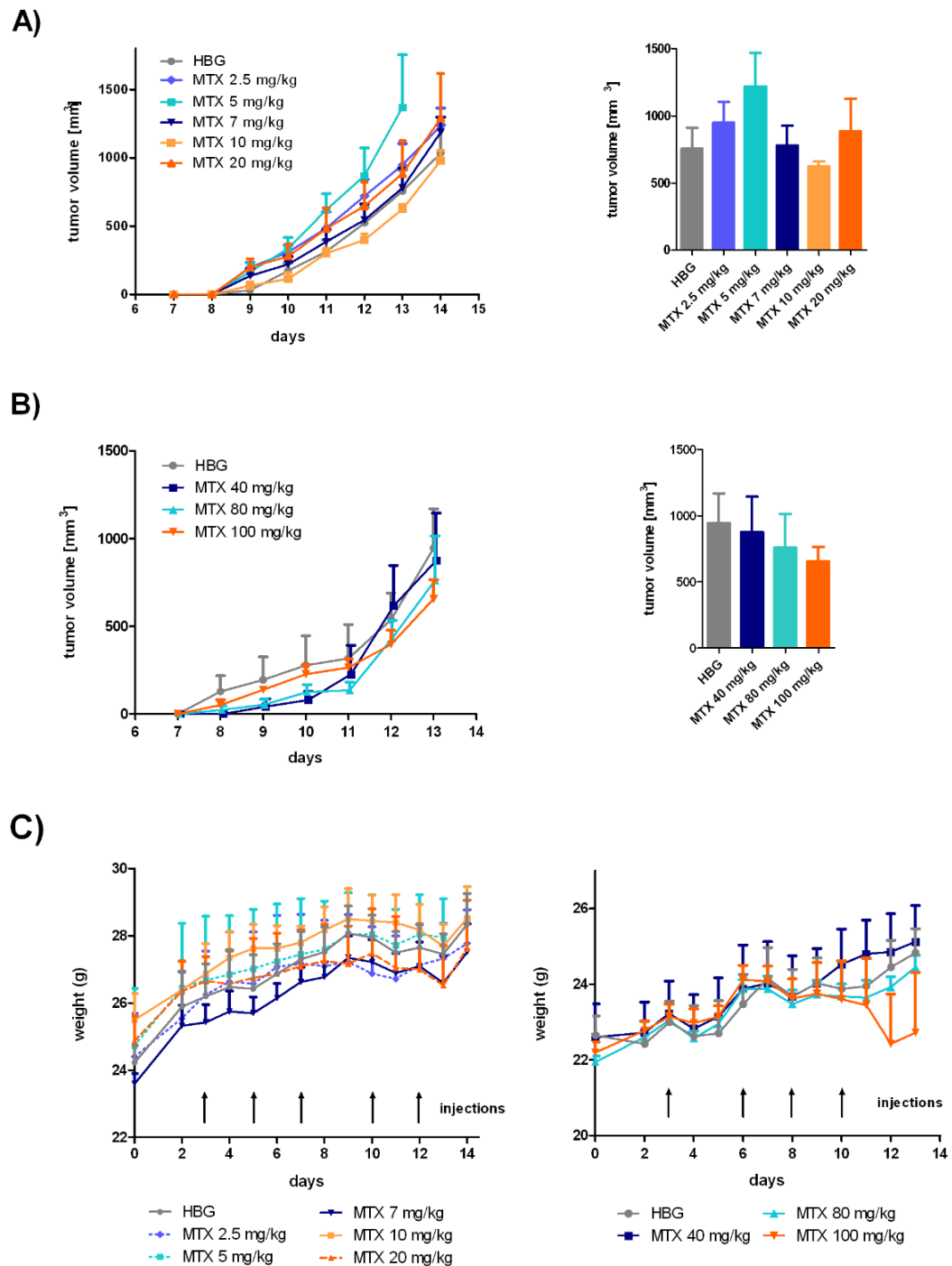


Figure 29: MTX dose finding experiments. A) L1210 tumor growth and comparison of tumor sizes on day 13 of animals treated with doses of 2.5, 5, 7, 10 and 20 mg/kg of MTX. **B)** Tumor growth and comparison of tumor sizes on day 13 of animals treated with 40, 80 and 100 mg/kg of MTX. **C)** Weight development of animals in both experimental parts. Intravenous injections are indicated by black arrows (mean + S.E.M.; n=4).

To evaluate a potential formation of chemoresistance, which could be acquired during multiple treatments, one tumor of 5 mg/kg MTX group and of 80 mg/kg MTX group, respectively, was processed for an MTT assay of

in vivo passaged L1210 cells. Cell viability was analyzed after 72 h of MTX treatment and revealed no resistance of L1210 cells to MTX, even at a high dose of 80 mg/kg.

2.2.2. Effect of PT+MTX combination therapy on KB tumor growth

Subsequently, the combination therapy was evaluated in a xenograft mouse model. Treatments with PT, MTX, PT+MTX or HBG were started individually, when KB tumors reached 200-250 mm³ and repeated 3 times per week. After treatment start, tumor growth in the HBG injected group proceeded rapidly, so the first animal had to be sacrificed after 11 days. Tumor growth in MTX treated animals was slightly slowed down after one week of treatments and the first animal was sacrificed after 12 days. Notably, tumor growth in both PT containing groups was retarded from the first injection on and could be further inhibited in the PT+MTX combination group (**Figure 30A**). While the first animal of PT group was sacrificed on day 15 after treatment start, PT+MTX combination led to an overall survival until day 23. **Figure 30B** depicts a comparison of tumor sizes on day 11, indicating that tumors of PT+MTX group are significantly smaller than in HBG and MTX treated mice (PT+MTX vs. HBG: $p = 0.0052$; PT+MTX vs. MTX: $p = 0.0066$). Also, tumors of PT group are clearly larger in size compared to PT+MTX group. Unfortunately, one of the tumors in the PT treated group showed a slow initial tumor growth, resulting in a high standard error of the mean (S.E.M.). Differences in tumor growth and volume to the PT+MTX group are therefore not statistically significant. Moreover, the animals' weight was monitored regularly, ensuring a continuous monitoring of animal welfare during the experiment. The unobtrusive weight development of all groups indicates that treatments were well tolerated by the animals (**Figure 31**).

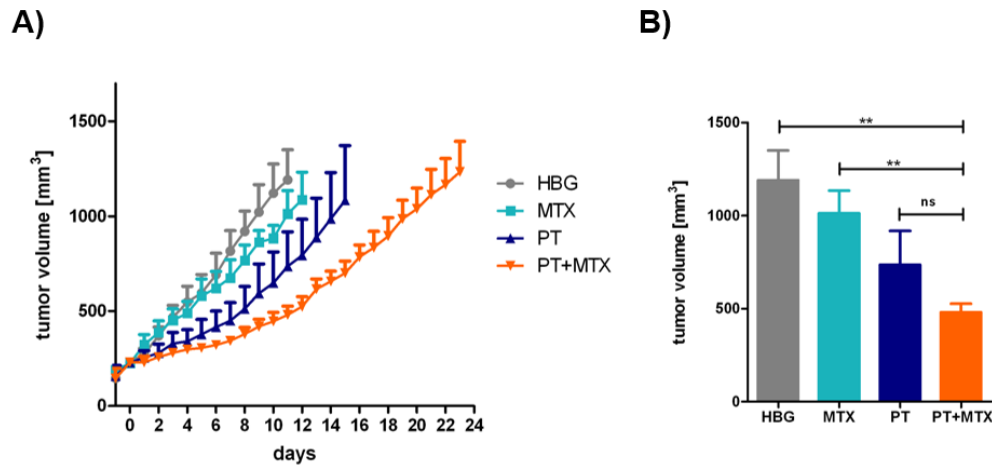


Figure 30: Tumor growth inhibition of subcutaneous KB tumors treated intravenously with HBG, MTX, PT or PT+MTX. **A)** Tumor volume of subcutaneous KB tumors. Intravenous treatments were started individually when tumors reached 200-250 mm³ and were repeated 3 times per week with a maximum of 8 injections. Day -1 represents one day prior to treatment start (mean + S.E.M.; n=4). **B)** Comparison of tumor sizes on day 11 after treatment start (mean + S.E.M.; n=4; *p < 0.05, **p < 0.01, ns: not significant).

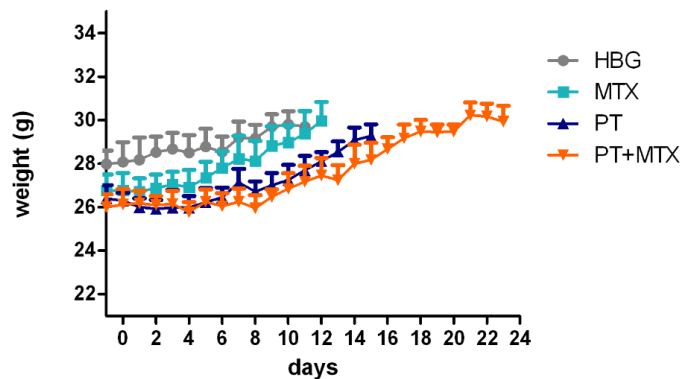


Figure 31: Weight development throughout PT+MTX combination therapy experiment in KB tumor bearing animals, starting on day -1, one day prior to treatment start, and ending with euthanasia. Intravenous treatments with HBG, MTX, PT or PT+MTX were performed thrice weekly with a maximum of 8 injections. Represented is the mean + S.E.M. of 4 mice per group.

2.2.3. Effect of PT+MTX combination therapy on HUH7 tumor growth

As third tumor model, hepatocellular carcinoma HUH7 was chosen for a repetition of PT+MTX combination experiment. This cell line was selected, as its sensitivity to treatments with PT has previously been reported [144]. After sufficient tumor growth (when tumors reached 200-250 mm³),

intravenous injections with HBG, PT, MTX or the combination of both (PT+MTX) were started. Animals were sacrificed after reaching the determined termination criteria and Kaplan Meier survival analysis was compiled.

Similar to treatment of KB tumors, MTX alone showed only minor effect on HUH7 tumor growth. Like in HBG injected mice, the first animal of MTX group had to be sacrificed on day 7 after treatment start due to its tumor burden. In contrast, both PT containing groups exhibited significantly inhibited tumor growth. Tumors ceased to grow after only 2 treatments and even started to shrink during the next injections. Only after the end of treatments, tumors of PT group resumed growth, while in PT+MTX group, the inhibition of tumor growth lasted around 3 days longer (**Figure 32A**). This led to an overall survival of all animals for 22 days in case of PT vs. 25 days in case of PT+MTX. Yet, in both groups not all animals showed resumed tumor growth when the first animal was sacrificed, respectively. In PT group, 2 out of 4 animals exhibited small tumors ($< 300 \text{ mm}^3$) on day 22, whereas in PT+MTX group tumor sizes of even 3 mice were below 300 mm^3 on day 25. Obviously, this had a massive impact on statistics leading to a high standard error of the mean (S.E.M.) and no statistical significance was reached between both groups (**Figure 32B**).

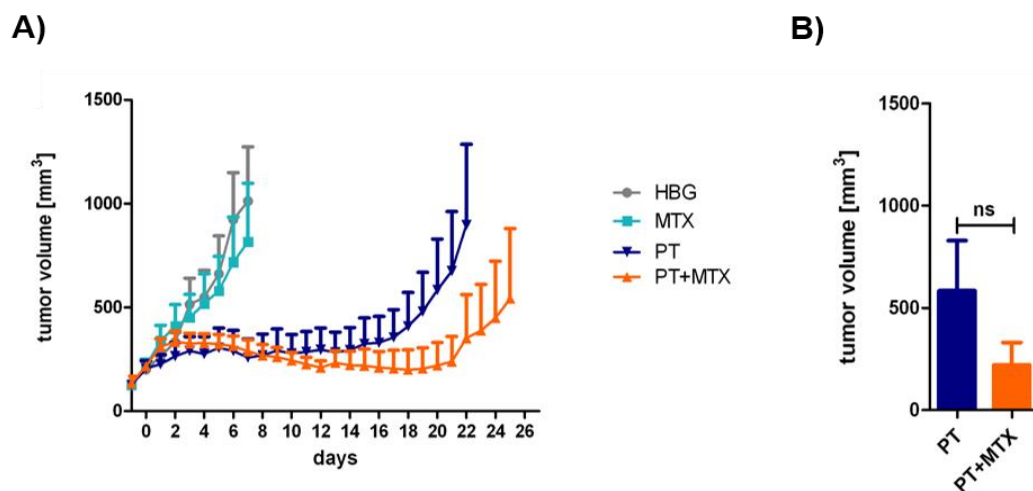


Figure 32: Tumor growth inhibition of subcutaneous HUH7 tumors treated intravenously with HBG, MTX, PT or PT+MTX. **A)** Tumor growth of HUH7 tumors. Treatments were started individually when tumors reached $200\text{-}250 \text{ mm}^3$ and were repeated 3 times per week with a maximum of 8 injections. Day -1 represents one day prior to treatment start (mean + S.E.M.; $n=4$). **B)** Comparison of tumor sizes of PT and PT+MTX

group on day 20 after treatment start (mean + S.E.M.; n=4; ns: not significant).

Figure 33 depicts an analysis of the mouse survival, which clearly could be prolonged by treatment with PT, while combination with MTX resulted in further extended survival.

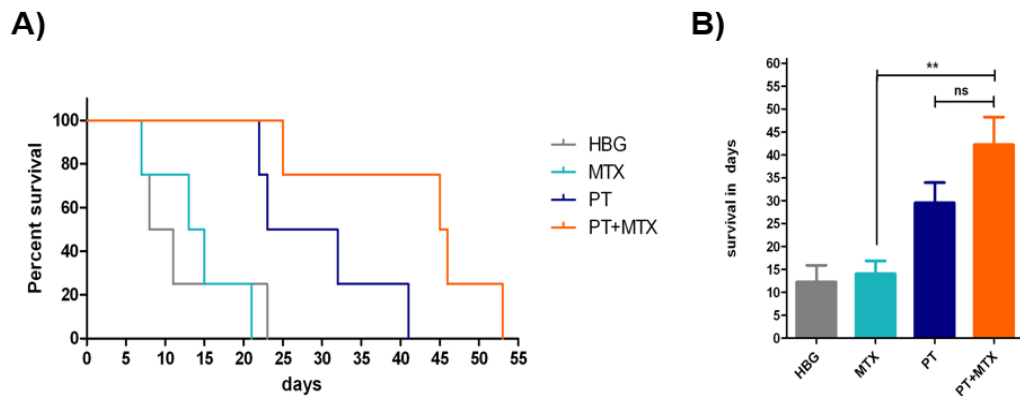


Figure 33: Survival of HUH7 tumor bearing mice. A) Kaplan Meier survival analysis of HBG, MTX, PT or PT+MTX treated groups (n=4 mice per group). **B)** Mean survival of indicated groups (mean + S.E.M.; n=4; **p < 0.01, ns = not significant)

Animals were weighed daily and a weight curve was compiled to monitor the mice's well-being. **Figure 34** demonstrates a very constant weight development throughout treatments in all groups and a steady increase of weight after the end of treatments in both PT containing groups.

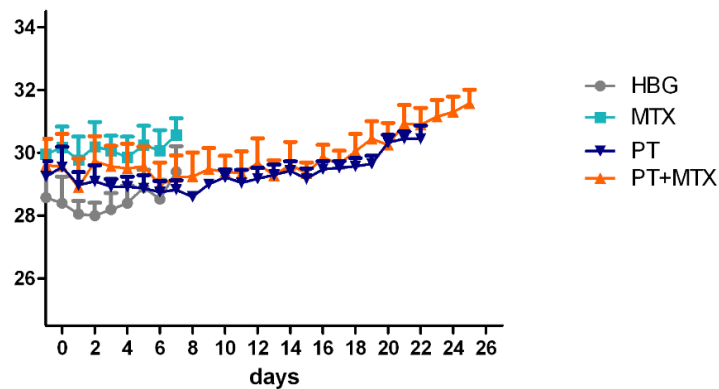


Figure 34: Weight development throughout PT+MTX combination therapy experiment in HUH7 tumor bearing animals, starting on day -1, one day prior to treatment start, and ending with euthanasia. Intravenous treatments were performed thrice weekly with a maximum of 8 injections.

Represented is the mean + S.E.M. of 4 mice per group.

Summing up the results of all experiments, we showed the advantage of PT+MTX combination over the effect of the single drugs in all three cell lines while no injection-related adverse effects were observed.

2.3. Oligomer-based micellar encapsulation of PT+MTX for systemic administration

After the successful treatment experiment with PT+MTX in L1210 tumors (see III.2.2.1.), we aimed for a further optimization of systemically administered PT+MTX. Micellar encapsulation of PT, MTX and PT+MTX with a lipo-oligomer of our library (ID **454**, **Figure 35**) was exploited to ensure simultaneous delivery of the drug combination. The T-shaped lipo-oligomer **454** was chosen for this experiment, since HPLC measurements demonstrated very favorable encapsulation efficiency. Additionally, MTT assays demonstrated the superiority of encapsulated drug over free drug.

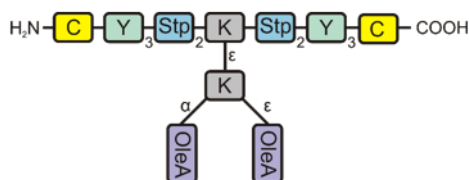


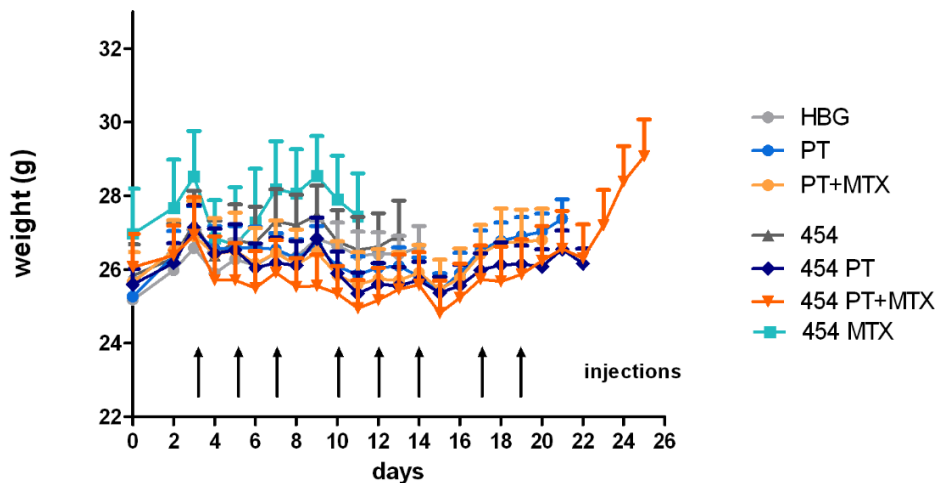
Figure 35: Schematic illustration of T-shaped lipo-oligomer 454. Abbreviations of individual units indicate: C: cysteine, Y: tyrosine, Stp: succinoyl-tetraethylene-pentamine, K: lysine, OleA: oleic acid.

L1210 tumor bearing mice were injected intravenously with plain **454**, **454** PT, **454** MTX, **454** PT+MTX, free PT, free PT+MTX or HBG. An additional group with free MTX was waived with regard to the previous experiment in which MTX alone did not achieve tumor growth inhibition as compared to HBG injected animals. Based on successful previous experiments (see III.2.2. and III.1.2.4. [147]), a dose of 2 mg/kg PT was chosen. In case of MTX, we had to adjust the previously used dose of 5 mg/kg to 2.5 mg/kg, as precipitation occurred when formulations were

prepared with the higher dose. Treatments in this experiment were repeated thrice weekly with a maximum of 8 injections. Animals were sacrificed after reaching the determined termination criteria and Kaplan Meier survival analysis was compiled.

The mice's weight was recorded daily to monitor animal well-being. Two animals of **454** MTX group were found dead in their cages one day after the first injection. Also, distinct weight loss occurred in several animals of **454** MTX and **454** PT+MTX group after the first treatment. However, all further injections were tolerated well by all mice and weight development was unobtrusive throughout the rest of the experiment. During injections, animals displayed a rather constant weight, whereas after the end of treatments, all surviving mice started to steadily gain weight (**Figure 36**).

A)



B)

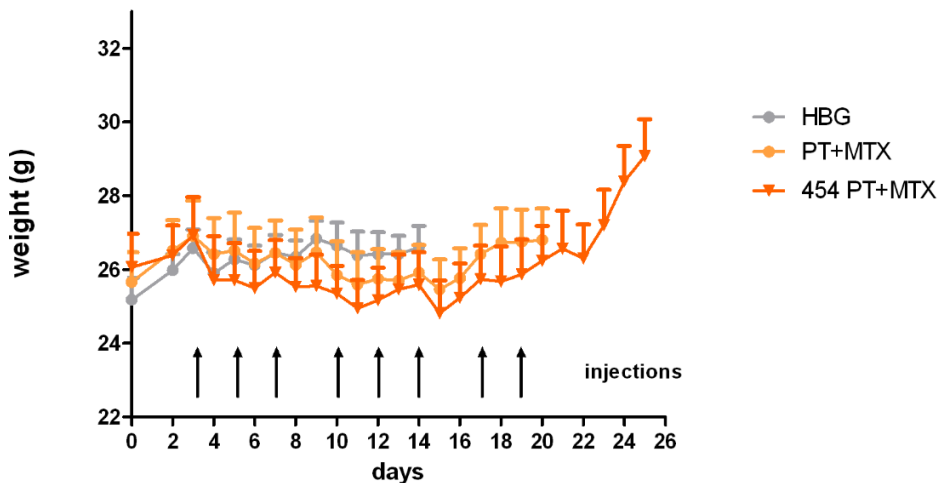
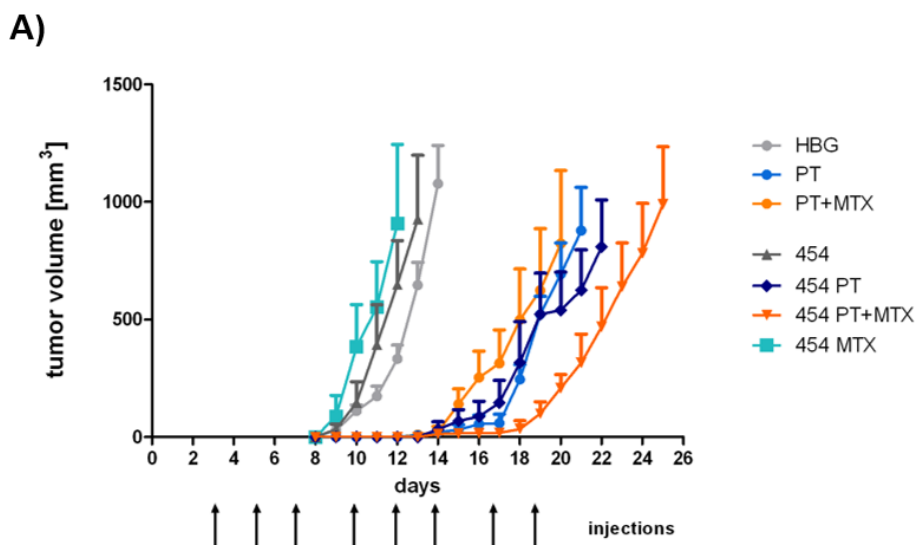


Figure 36: Weight development over time. Weight of mice of **A)** all groups and **B)** HBG, PT+MTX and **454** PT+MTX groups during the experiment, starting on day 0 with L1210 tumor cell inoculation and ending with euthanasia. Intravenous injections are indicated by black arrows. Represented is the mean + S.E.M. of 6 mice per group (**454** MTX: n=4).

Figure 37 depicts tumor growth of indicated groups. Eight days after tumor cell inoculation, tumors of HBG, **454** and **454** MTX groups started to grow and subsequently reached their final volume within another 4 to 5 days. All PT containing groups succeeded in retarding tumor growth for at least 14 days. On day 14, tumors of PT+MTX treated animals started growing, followed by tumors of mice injected with PT and **454** PT. **454** PT+MTX exhibited the strongest tumor growth delay, so tumors did not start to grow before day 18, when treatments were nearly terminated. Also, animals of this group survived longer than mice of all other groups with the last animal being sacrificed on day 38 after tumor cell inoculation. The encapsulation with **454** only slightly improved the antitumoral effect of PT, whereas PT+MTX without **454** demonstrated a poorer performance than all other PT-containing groups. However, this ultimately resulted in a significantly longer survival of **454** PT+MTX treated mice as compared to animals of PT+MTX group (log rank test of Kaplan Meier curve PT+MTX vs. **454** PT+MTX: 0.0131) (**Figure 38**).



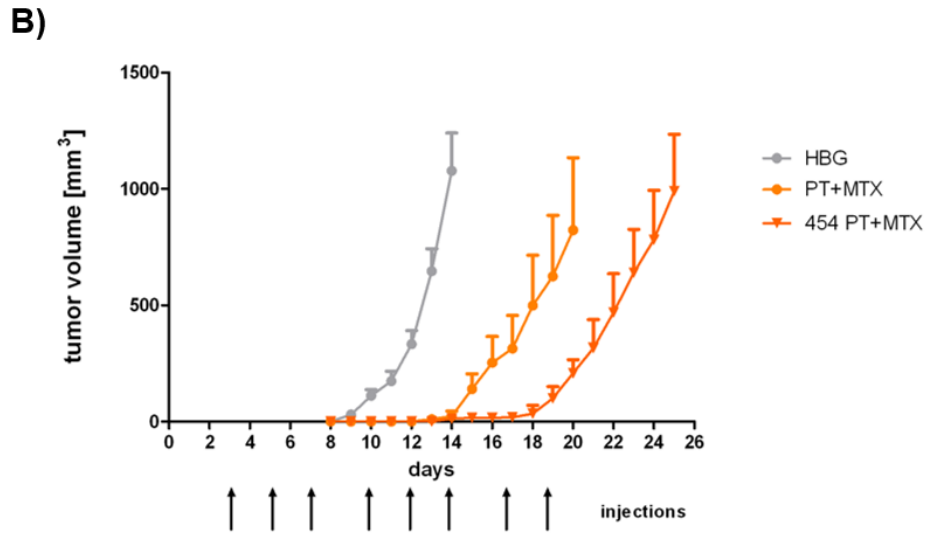


Figure 37: Tumor growth over time in L1210 tumor bearing mice upon intravenous treatments with **454**, **454** PT, **454** MTX, **454** PT+MTX, PT, PT+MTX or HBG. Average tumor volume of **A)** all groups and **B)** HBG, PT+MTX and **454** PT+MTX groups. Intravenous injections are indicated by black arrows. Represented is the mean + S.E.M. of 6 mice per group (**454** MTX: n=4).

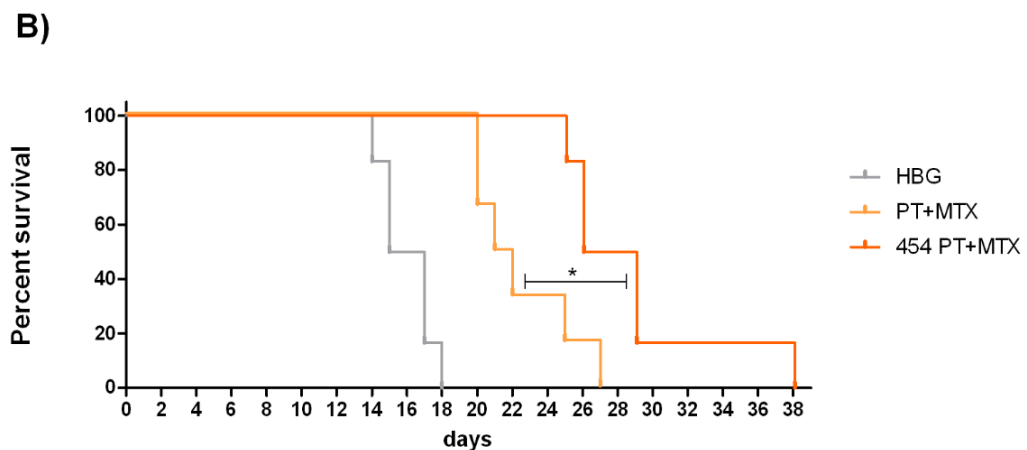
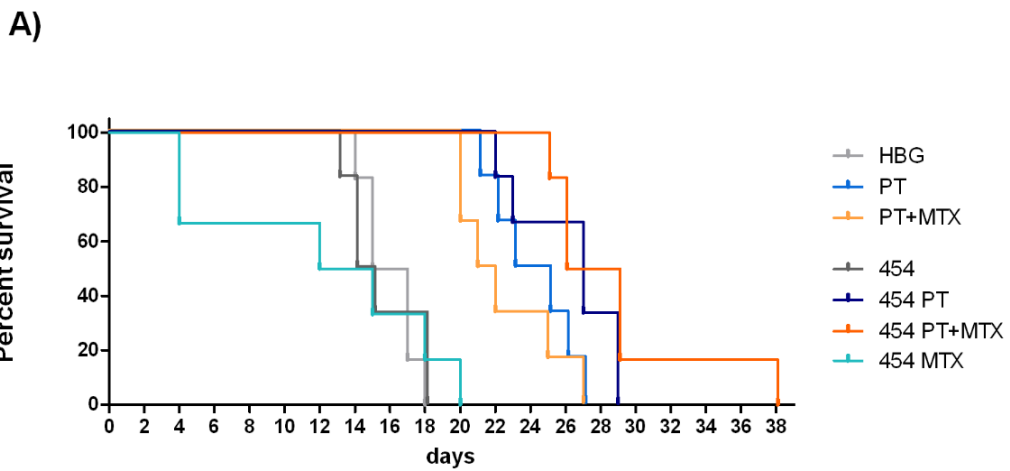


Figure 38: Kaplan Meier survival curve of animals treated with **454**, **454** PT, **454** MTX, **454** PT+MTX, PT, PT+MTX or HBG. Survival analysis of **A)** all groups and **B)** HBG, PT+MTX and **454** PT+MTX treated groups (n=6 mice per group). Significance of the results was evaluated using log-rank test (*p = 0.013).

All in all, we demonstrated the enhanced combination effect of PT+MTX after micellar encapsulation with clearly improved tumor growth inhibition and significantly extended survival of mice.

IV. DISCUSSION

1. Shielded and targeted lipopolyplexes for effective siRNA delivery

Although siRNA emerged as a potent novel tool in the treatment of various diseases, the delivery to its target site remains challenging. siRNA by itself exhibits very poor pharmacokinetics [17]. Hence, efficient carriers are required to prolong circulation times and direct the formulation to its target site. Therefore, suitable carrier systems are under investigation. Researchers of our group have designed a library of more than 1200 sequence-defined oligoaminoamides as carriers for nucleic acid delivery. These oligomers exhibit significantly reduced cytotoxicity as compared to conventional polymers [162, 163], which can be attributed to their smaller size and reduced cationic charge. Recently, our group achieved very promising results in nucleic acid delivery using these polymeric carriers [156, 162, 163]. However, success rates were often hampered by the repeated occurrence of stability issues, rapid renal clearance and reduced efficiency upon systemic administration. To overcome these drawbacks, polymers were modified, resulting in further optimized carrier systems with advantageous properties. For the following experiments, various oligomers of our library were chosen for efficient siRNA delivery to subcutaneous tumors upon systemic administration. Also, we explored PSar as novel shielding agent in comparison to the well-established shielding agent PEG. Moreover, we exploited active targeting for the effective direction of nanoparticles to their site of action.

1.1. PEG and PSar as shielding agents

Shielding of nanoparticles prevents rapid renal clearance, unwanted interactions with blood components or other nanoparticles and thereby enhances their circulation time, which ultimately enables the formulation to reach therapeutic levels at its target site [50-53]. PEG has been used for surface shielding for almost 30 years [50]. However, researchers reported immune responses associated with repeated PEG treatments, potentially hampering its clinical usability [55-62].

In this thesis, the shielding capacity of PSar was evaluated in direct comparison to PEG in a biodistribution experiment. Encouragingly, PSar has already been demonstrated to prolong *in vivo* circulation times [75, 76] and no immunogenicity has been reported until now [77].

In the current approach, an azide functionality was introduced into T-shaped oligomers of our library [49]. Azide groups enable copper-free click reactions with cyclooctyne derivatives and by that an alternative method for the introduction of functional domains to the lipoplex [151, 152]. In former work, functional groups of oligomers, for example thiols, were exploited for this purpose [157, 164-166]. Although promising results regarding gene silencing and biophysical properties were achieved *in vitro*, *in vivo* delivery of siRNA was frequently compromised by stability issues. Bio-orthogonal click chemistry offers some valuable benefits: It proceeds effectively without the requirement of a catalyst. Moreover, no potentially harmful side products are produced and no cytotoxicity is caused [151-153].

In the thesis, unshielded lipopolyplexes were compared to lipopolyplexes covalently linked to PEG (DBCO-PEG5k) or PSar (DBCO-PSar₁₁₉-Ac) with regard to their distribution upon systemic application. In accordance with previous findings of our group [48, 165], the unshielded T-shape lipopolyplexes demonstrated a preferred accumulation in the liver [154]. The underlying mechanism behind this might be the unspecific interaction of unprotected nanoparticles with cell surfaces and serum proteins, which consequently affects tissue specificity [167-169].

As expected, shielding with PEG yielded in significantly prolonged circulation time and improved tumor accumulation of our nanoparticles. Modification with PSar likewise enhanced biodistribution properties, thus surface shielding turned out to be as effective as with PEG. An unexpected finding was the strong fluorescence signal in the mice's paws that lasted until 24 h post injection, whereas in most body parts, the signal had largely decreased by then. This might possibly be due to anesthesia-induced hypotension leading to peripheral vasoconstriction [170-172], hence particles of a certain size can get stuck.

In summary, we provide evidence that shielding with PSar is as effective as

with PEG [154]. In future research, carrier systems might require further *in vivo* stabilization to prolong circulation time and enable passive targeting [82].

1.2. Targeted lipopolyplexes for gene silencing *in vivo*

In the previous part, we demonstrated the impact of surface shielding on biodistribution upon systemic application. Another important aspect that contributes to the successful delivery of nanoparticles is targeting to the site of action. Concerning targeting, an active and a passive form can be distinguished. Passive targeting occurs due to the EPR effect, a combination of suitable particle size, adequate circulation time and leaky blood vessels, as well as impaired lymphatic drainage in the tumor area [22, 39, 82, 173, 174]. Thereby a formulation can effectively be directed to its site of action. However, to enable not only the localization, but also the actual internalization into the target cell, active targeting might be required. Here, receptor-mediated endocytosis is facilitated by the modification of nanoparticles with specific ligands. These mediate a high selectivity in cellular binding caused by their ability to target specific receptors overexpressed by many solid tumors [53, 155]. In the following experiments, we mainly focused on the FR. FR is overexpressed by many carcinoma cell lines [87, 94], which require high amounts of folate for the synthesis of nucleic acids due to their increased division rate.

An azido function was incorporated into a T-shape oligomer with promising carrier properties [49] to enable the introduction of functional domains using bio-orthogonal click chemistry. Subsequently, the obtained core polymer **1106** was modified with DBCO-PEG for surface shielding. Furthermore, the targeting ligand folate was incorporated into this domain, yielding in particles with optimized properties in terms of successful siRNA delivery. To analyze different variants of this carrier system, both mono- and (double-click) bis-DBCO, as well as different PEG lengths and modification with folate as targeting ligand, were investigated [147].

First, biodistribution of our formulations was evaluated upon systemic administration. Similar to the previous part, unshielded polyplexes mainly accumulated in the liver tissue, which is a common finding for unshielded

T-shape oligomers [48, 165]. No improvement of circulation time or tumor accumulation was achieved by incorporating mono-DBCO with either length of PEG. Yet, modification with bis-DBCO clearly prolonged blood circulation [147]. This might be explained by an enhanced stability mediated by the crosslinking with a second lipo-oligomer. Surprisingly, the introduction of the targeting ligand Folate led to a broader distribution with prolonged blood circulation. Based on an internal experiment, in which we found L1210 tumors to metastasize at an early stage (unpublished data), we assumed that the enhanced circulation of Folate-targeted formulations is attributed to tumor cells that have spread from the primary tumor to distant body parts. As anticipated, when administered into tumor-free mice, the best-performing formulation DBCO₂-ss₂-PEG₂₄ Folate displayed weaker biodistribution properties than in L1210 tumor bearing mice [147].

We further investigated whether the replacement of cholanic acid (CholA) by oleic acid (OleA) in the lipo-oligomer core resulted in beneficial biodistribution properties since transfection efficiency *in vitro* was similar for both oligomers (unpublished data). Fatty acids are incorporated for their hydrophobic character which enhances polyplex stability. In former *in vivo* experiments of our group, OleA was successfully used with Folate-targeted formulations [156, 157]. Yet, in the current approach the OleA analog **1169** did not exhibit any advantageous effect as compared to **1106** [147]. Also in different previous work, the saturated C24 bile acid derivative CholA was chosen over the unsaturated C18 fatty acid OleA, as it exhibits higher stability both during synthesis and storage [49].

Moreover, the same formulation was evaluated in terms of gene silencing efficiency using siRNA against mRNA of the *EG5* gene. EG5, also referred to as eglin 5 or kinesin spindle protein (KSP), is a member of the kinesin family. It is actively involved in the assembly of the spindle apparatus during cell division [175]. Therefore, it represents a powerful target for anti-cancer therapeutics. Through the inhibition of protein translation of *EG5*, mitosis is hampered, cells accumulate in the G2/M phase and ultimately die [176, 177]. By directing **1106** DBCO₂-ss₂-PEG₂₄ Folate towards *EG5*, we reached ~60% of gene silencing, whereas the untargeted analog showed negligible effects on *EG5* expression [147]. This demonstrates the pronounced

advantage of folate targeting. Also, unspecific effects of the polyplexes themselves on *EG5* could be excluded, since only minor decrease of the mRNA level was achieved by the targeted siCtrl formulation. The experiment was repeated with the OleA containing analog **1169**. In this case, the FolaA targeted siEG5 formulation only led to ~40% of gene silencing. Hereby, we could confirm the superiority of CholaA containing **1106** over **1169**, which was already observed during biodistribution experiments. While biodistribution only provides information about *in vivo* circulation and tumor accumulation, the significant downregulation of *EG5* expression by **1106** formulation proves the successful internalization of the polyplexes and cytosolic siRNA release [147].

Based on these encouraging findings, a treatment experiment was performed to evaluate the antitumoral potency of **1106** DBCO₂-ss2-PEG₂₄ FolaA siEG5 in combination with the potent microtubule inhibitor pretubulysin (PT). PT has emerged as promising candidate of the group of microtubule-targeting agents. As precursor of the tubulysins, which have recently been evaluated in several clinical trials [178], it is almost as effective but in the same time easier to synthesize due to its simplified chemical structure [140, 141, 144]. PT was chosen as it exhibits very favorable antitumoral effects *in vivo* [140, 144, 145, 148] and promotes cell accumulation in the G2/M phase, like siEG5 [137]. However, this natural compound is directed at a different mechanism, namely the vinca domain of β -tubulin. After binding to its target site, it inhibits tubulin polymerization, which consequently leads to an inhibition of mitosis and cell death [142, 143].

Encouragingly, intravenous treatments of L1210 tumor bearing mice with the siEG5 + PT containing formulation resulted in significant tumor growth inhibition and extended survival [147]. While tissue specificity and enhanced circulation time are provided by the optimized carrier system with FolaA targeting and PEG shielding, both siEG5 and PT interfere with the mitotic spindle apparatus but in a different manner. This provides a coherent explanation for the encouraging effect of this combination.

Given the successful treatment of FR-overexpressing L1210 tumors [147], the experimental setup was taken up in a new *in vivo* experiment aiming at

a different target. Therefore, the human hepatocellular carcinoma cell line HUH7 was chosen, since these tumors –like many other solid tumors, are known to overexpress epidermal growth factor receptor (EGFR) [111]. EGFR, in turn, can be targeted by the targeting ligand GE11, a short artificial peptide which - in contrast to the natural ligand EGF - lacks mitogenic activity [114]. Hence, GE11 was included in our formulation. Analogous to the previous experiment with L1210 tumors, it further contained siEG5 and PT.

Notably, intravenous treatments with this formulation achieved remarkable tumor growth inhibition. Tumor progression could be stopped during treatments with all PT containing formulations, leading to major differences in tumor sizes between PT containing and PT free groups, but less pronounced differences within these groups, respectively. This indicates a predominant PT effect. The great sensitivity of HUH7 tumors to treatment with PT has previously been demonstrated by Rath *et al.* [144]. Moreover, the authors could show the significantly reduced vessel density of HUH7 tumors upon PT treatment, confirming the anti-angiogenic effect that was described earlier by Kaur *et al.* for tubulysin A [179]. Thereupon, a reduced vascularization deprives the tissue of nutrients and oxygen, urgently needed by the growing tumor [180, 181]. After the end of treatments however, tumors of all groups eventually resumed progression. Yet, animals treated with PT in combination with siEG5 displayed strongest tumor growth inhibition and longest survival of all groups. Presumably, this can be attributed to the additional mitosis inhibition mediated by siEG5. Lee *et al.* reported the recurrence-free survival of 50% of mice treated intratumorally with a combination of siEG5 and MTX-conjugated polyplexes, while the same formulation without siEG5 did not inhibit KB tumor growth [182]. Given the predominant PT effect, we need to conclude that the combination effect of siEG5 and PT in the current study was not as pronounced as in the previous experiment with Fola targeting.

Taking together the promising results of both treatment experiments, the combination of eglin 5 siRNA with PT, both aiming at the same intracellular target but affecting it in different manners, represents a promising approach in the treatment of various forms of cancer. However, further experiments

should be conducted, investigating the effect of this combination in more cell lines and with further improved oligomeric carrier systems for effective delivery and improved circulation times. Moreover, an interesting aspect would be the histologic evaluation of tumor tissue during treatments for a precise evaluation of the PT and siEG5 combination effect.

2. Combinatorial treatment of PT and MTX

The use of drug combinations becomes increasingly important as standard therapy setting for the treatment of cancer. While monotherapy approaches often fail to control this medical condition successfully [122, 123, 183, 184], combination therapy settings represent a promising strategy as they can address the disease from different angles [185-187]. According to Zimmermann *et al.*, multi-target therapeutics can be divided into three groups: (i) two components aiming at two separate targets, (ii) one component enabling the second to attack its target or (iii) two components binding to separate sites of one target [188].

In the following studies, we aimed for a possibly beneficial combinatorial effect of PT and the well-established chemotherapeutic drug methotrexate (MTX).

2.1. Intratumoral treatment with E4-MTX-H-PT conjugate

In the first attempt, MTX was exploited, on the one hand, for its inhibitory effect on DHFR, an enzyme that transforms folic acid to dihydrofolic acid and finally tetrahydrofolic acid which is required for the *de novo* synthesis of DNA and RNA [109, 110]. On the other hand, we also took advantage of its function as targeting ligand, enabling a formulation to precisely address cells overexpressing the folate receptor [131, 189], which accounts for many carcinoma cell lines [87, 94].

In this experiment, co-delivery of PT and MTX was achieved by the covalent attachment of thiol-reactive PT derivatives to cysteine residues of MTX-oligoamides [148]. By administering both compounds as a conjugate, we aimed at improved cell internalization through receptor-specific uptake, as well as a combination effect of PT and MTX.

For the *in vivo* treatment study, a 4-arm E4-MTX oligoamide was chosen. E4-MTX refers to the bioactive (tetraglutamylated) form of MTX, which usually is generated by the folyl-polyglutamate synthase after internalization into the target cell [126, 190]. During treatments of mice bearing subcutaneous FR-overexpressing KB tumors, E4-MTX alone was found to

have no tumor growth retarding effect as compared to the untreated controls [148], which is in accordance with previous findings of our group [182]. The antitumoral effect mediated by the conjugate was similar to native PT-COOH. However, as PT in the conjugate was used in the form of its hydrazide derivative, which *in vitro* was inferior to native PT-COOH, our finding can be regarded as a valuable result [148]. Moreover, we could show for the first time the antitumoral effect of PT in the KB tumor model [148].

Yet, with regard to clinical relevance, local application of drugs in most cases is inconvenient or insufficient. Therefore, future experiments should focus on the systemic delivery of these conjugates. For this purpose, renal clearance has to be overcome and circulation time should be prolonged to reach therapeutic levels in the tumor tissue.

2.2. Combined antitumoral effects of PT and MTX

Subsequently, we evaluated the potential combination effect of free PT and MTX after systemic administration *in vivo*.

We first chose the L1210 murine leukemia tumor model, since *in vitro* cytotoxicity studies demonstrated that PT and MTX acted synergistically on L1210 cells, exceeding the effect of both compounds alone. In contrast to the *in vitro* cytotoxicity (MTT) assay, MTX did not achieve an inhibition of L1210 tumor growth *in vivo*. However, this finding is supported by previous studies in which free MTX could neither cause tumor growth inhibition [148, 182]. PT on the other hand, exhibited a strong antitumoral effect on L1210 tumors during multiple intravenous injections which is in accordance with previous experiments in MDA-MB-231 [140], HUH7 [144] and L1210 tumors [147]. Encouragingly, this favorable effect could be further enhanced by co-administering PT with MTX, resulting in a significantly retarded tumor growth in the combination group.

Notably, the doses of PT and MTX used in these animal experiments were chosen based on *in vitro* experiments and an internal dose-finding experiment with PT. Subsequently, a dose-finding experiment was performed to evaluate the best working dose of MTX. Considering the comparison of tumor growth curves after multiple intravenous injections with

different doses of MTX, it becomes obvious that the dosage of MTX used in the animal experiments was inferior to higher doses of MTX. Burger *et al.* described 100 mg/kg as the maximum tolerated dose (MTD) for NMRI nude mice [161]. This could be confirmed by our group since 2 out of 4 animals suffered from severe side effects and consequently had to be sacrificed for reasons of animal welfare. However, even after multiple injections with the highest doses of 80 mg/kg and 100 mg/kg, we did not achieve a significant tumor growth inhibition. A reason for the lack of an MTX effect *in vivo* could be an acquired resistance that formed during the *in vivo* experiment due to multiple treatments. *In vivo* passaged tumors were investigated towards such a resistance in cell culture. However, they were still sensitive to MTX. Yet, the differences in tumor growth inhibition indicate that the combination effect achieved with the suboptimal dose of 5 mg/kg MTX is even more remarkable and could be further enhanced by adjusting the dose of MTX.

Subsequently, the experiment was repeated in the KB human cervix carcinoma model and in the HUH7 hepatocellular carcinoma. In both tumor models, PT had already previously demonstrated advantageous antitumoral effects [144, 148]. In our current study, we confirmed antitumoral activity of 2 mg/kg PT upon multiple intravenous injections. MTX slightly but not significantly inhibited KB tumor growth after multiple 5 mg/kg i.v. injections. This is consistent with the known *in vitro* partial chemoresistance of KB cells to MTX [190] and our previous *in vivo* studies [148, 182]. Importantly, also in this carcinoma model the co-administration of 5 mg/kg MTX resulted in an increased antitumoral effect of PT. Thereby, we could show for the first time a beneficial effect of PT after systemic administration in the KB tumor model. In the HUH7 tumor model, PT mediated significant tumor growth inhibition, whereas MTX displayed only minor effects as compared to HBG buffer. Yet, the PT+MTX combination resulted in enhanced retardation of tumor progression and prolonged survival as compared to PT. We thereby confirm the strong antitumoral effect of PT on HUH7 cells, previously reported by Rath *et al.* [144] and demonstrate the advantage of the PT+MTX combination approach in a third cell line.

To conclude, we showed clear antitumoral effects of 2 mg/kg PT in all three cell lines *in vivo*, whereas tumor treatment with 5 mg/kg MTX (or even

100 mg/kg in case of L1210 tumors) failed under *in vivo* conditions. Surprisingly, a combination of PT with this low dose of MTX boosted the *in vivo* tumor growth inhibition and prolonged the survival of animals. As revealed by CLSM, this effect could be explained by the impairment of the actin cytoskeleton of the cell by MTX, which was previously reported by Otricka *et al.* [191] and Mazur *et al.* [192]. An unimpaired cytoskeleton is required for the formation of actin stress fibers as a cellular survival response after treatment with the microtubule inhibitor PT, since several studies have shown that microtubule inhibitors likewise influence the actin cytoskeleton [193-195]. Hence, treatment with PT+MTX results in an enhanced cell killing due to a combined loss in microtubule as well as actin cytoskeleton function.

The promising therapeutic PT+MTX combination effect provides an interesting starting point for further biological research and therapeutic translation. However, in case of KB and HUH7 tumors, group sizes should be adapted to reach statistical significance and increase validity of the obtained results.

2.3. Oligomer-based micellar encapsulation of PT+MTX for systemic administration

Encapsulation of PT+MTX in nanoparticulate micelles was an approach to facilitate simultaneous delivery of the two drugs. Therefore, a suitable carrier system was required. Lipo-oligomer **454** was chosen from our library, as it exhibited great encapsulation efficiency *in vitro*. PT, MTX and PT+MTX were incorporated into a nano-micellar formulation based on oligomer **454**. Subsequently, mice bearing L1210 tumors were treated with the abovementioned formulations or the respective compounds without **454**, whereby a group receiving plain MTX was waived considering the lack of therapeutic efficiency observed during previous experiments.

Unexpectedly, distinct weight loss and two cases of death were observed after the first injection of **454** MTX and **454** PT+MTX. However, we could not identify the cause of these adverse effects, especially since the unobtrusive weight development and well-being during all further treatments

indicate that formulations were tolerated well by the animals.

As expected, tumor growth could successfully be inhibited in all PT-containing groups. Within these groups, free PT+MTX mediated the weakest antitumoral effect, which may be explained by the adjusted dose of MTX in comparison to previous experiments. Hence, we hypothesize that the aforementioned inhibition of the actin rescue effect by MTX is less pronounced and the combined loss in microtubule and actin cytoskeleton function mediated by PT+MTX is reduced. In case of PT, nanoparticulate incorporation did not lead to a superior growth retardation, whereas the effect of PT+MTX combination could largely be enhanced in **454** PT+MTX group. One advantage of the co-formulation of two drugs within the same nanoparticle is their simultaneous delivery, which is not achieved by the mere combination of two compounds. Thus, after the injection of PT+MTX, both drugs exhibit completely different pharmacokinetics and biodistribution occurs in an unspecific manner. Another benefit is the prevention of encapsulated drugs from interactions with blood components and by that early renal clearance [37, 39]. The likelihood of resistance formation can be decreased and previously acquired resistances can even be reversed [196]. Moreover, nanoparticle formation of drugs results in improved pharmacokinetic behavior and controlled delivery to their site of action [197].

In sum, this work showed the successful co-delivery of nanoparticulate encapsulated PT+MTX in a systemic treatment experiment, leading to effective tumor growth retardation and extended survival of so treated mice. In future experiments, nanoparticles should be further optimized by shielding and targeting domains for enhanced passive and active targeting.

V. SUMMARY

These days, cancer represents one of the leading causes of death worldwide. In the near future, the number of newly diagnosed patients will continue to rise, since the proportion of elderly people is increasing. Thereby also the economic burden associated with the elaborate treatment will further increase. Despite intensive research in this area, current treatment options only lead to unsatisfying cure rates. Hence, new treatment modalities are urgently required. The recent emergence of siRNA as novel therapeutic tool holds great promise, with the first FDA approved drug Patisiran (Onpattro™, a PEGylated liposomal siRNA formulation) on the medical market. However, siRNA delivery into tumors remains challenging.

Accordingly, the first part of this thesis aimed at the investigation of polymeric nanocarriers for efficient siRNA delivery. Lipopolyplexes click-modified with DBCO-containing surface shielding and targeting agents were tolerated well upon systemic administration in NMRI-nu/nu mice. In Neuro-2a murine neuroblastoma bearing animals, both PEG as the most commonly used shielding agent and the novel polysarcosine (PSar) in direct comparison demonstrated a comparable *in vivo* efficiency. In the next part, the *in vivo* delivery of folate (FolA) containing DBCO-PEG polyplexes was analyzed in the folate-receptor overexpressing L1210 murine leukemia model. A biodistribution study demonstrated the superiority of a formulation containing bis-DBCO, PEG₂₄ and FolA with tumor accumulation until 4 h. In a gene silencing experiment with intravenous administration, the same formulation combined with siRNA against the mitosis-related *EG5* gene product resulted in significant downregulation of the respective mRNA in the subcutaneous L1210 tumor. Subsequently, the formulation was evaluated in a systemic treatment experiment in combination with the novel microtubule inhibitor pretubulysin (PT). Encouragingly, it accomplished significantly inhibited L1210 tumor growth and extended survival. In continuation, GE11-containing siEG5 polyplexes were used for treatment targeting epidermal growth factor (EGF) receptor-overexpressing human HUH7 hepatocellular carcinoma in the xenograft model. A formulation with GE11 targeting ligand, siEG5 and PT led to longest survival and

pronounced tumor growth inhibition. Yet, the superiority of the combination over PT alone did not reach the level of statistical significance due to the high antitumoral activity of free PT against HUH7 tumors.

The use of chemotherapy is frequently impaired by the acquisition of resistances, which is commonly associated with monotherapy approaches. Currently, the most promising strategy to narrow this risk is combination therapy. The second part of this thesis evaluated the combination of PT with the antifolate methotrexate (MTX). Firstly, both compounds were covalently linked and injected intratumorally into NMRI-nu/nu mice, exploiting MTX on the one hand concerning its ability to inhibit DHFR, and on the other hand for its ligand qualities associated with the high affinity to the FR. Thereby, a retardation of KB tumor growth was achieved similar to treatments with native PT. Subsequently, a combination of the free drugs was injected intravenously into L1210, KB and HUH7 tumor bearing NMRI-nu/nu mice. In all three tumors models, PT+MTX proved to be superior over the effect of each drug alone, reaching levels of significance in the L1210 model. Finally, PT+MTX was incorporated into a lipo-oligomer nanomicelle to provide simultaneous delivery upon systemic administration. Encouragingly, L1210 tumor progression could be successfully retarded and resulted in significantly prolonged survival as compared to free PT+MTX.

In conclusion, a shielded and targeted carrier nanosystem was validated for effective EG5 siRNA delivery, successfully inhibiting tumor growth in combination with PT. Moreover, the promising combination effect of PT with MTX was described in several tumor models and the enhancement by nanoformulation demonstrated.

VI. ZUSAMMENFASSUNG

Antitumorale polymerische siRNA Nanoformulierungen und Pretubulysin-basierte Kombinationstherapien

Krebs stellt in der heutigen Zeit weltweit eine der häufigsten Todesursachen dar. Aufgrund des steigenden Anteils an älteren Menschen in unserer Bevölkerung, wird die Zahl an neudiagnostizierten Krebspatienten innerhalb der nächsten Jahre weiter zunehmen. Damit nimmt auch die wirtschaftliche Belastung zu, die mit der aufwendigen Behandlung einhergeht. Trotz intensiver Forschung auf diesem Gebiet, können mit den derzeit verfügbaren Therapiemöglichkeiten nur unzufriedenstellende Heilungsraten erzielt werden. Daher ist die Entwicklung neuer Therapieformen von großer Dringlichkeit. Die Verwendung von siRNA als therapeutisches Werkzeug stellt einen vielversprechenden neuen Ansatz dar, der bereits zur Zulassung eines ersten medizinischen Produktes (Patisiran, Onpattro™, einer PEGylierten liposomalen siRNA Formulierung) geführt hat. Die klinische Anwendung von siRNA im Tumorbereich wird allerdings derzeit noch beeinträchtigt durch die Schwierigkeiten ihres Transports in die Zielzelle. Daher war das Ziel des ersten Teiles dieser Dissertation, optimierte polymerische Trägersysteme für den effizienten Transport von siRNA zu ihrer Zielzelle zu untersuchen.

Die vorliegende Arbeit zeigt, dass Lipopolyplexe, die über neuartige Click-Chemie mit DBCO-enthaltenden Abschirmungs- und Targeting-Domänen ausgestattet wurden, nach systemischer Verabreichung in der NMRI-nu/nu Maus sehr gut toleriert werden. Sowohl PEG (als das am häufigsten zur Oberflächen-Abschirmung eingesetzte Polymer), als auch das im direkten Vergleich eingesetzte Polymer Polysarcosine (PSar) zeigten eine vorteilhafte Biodistribution im Neuro-2a murinen Neuroblastom Mausmodell. Der nächste Teil dieser Arbeit strebte den effizienten Transport von DBCO-PEG Fola Polyplexen in die Zielzelle an. Ein Bioimaging-Experiment zeigt die Überlegenheit einer Formulierung mit bis-DBCO, PEG₂₄ und Fola, die eine Anreicherung im Folatrezeptor-überexprimierenden L1210 Tumorgewebe bis nach 4 Stunden aufwies. In

einem weiteren Versuch wurde die Hemmung der Expression eines Genproduktes auf mRNA-Ebene durch die systemische Verabreichung einer siRNA in Kombination mit der zuvor beschriebenen Formulierung untersucht. Ziel war in diesem Fall die mRNA des an der Mitose beteiligten Gens *EG5*. Hierbei ergab sich eine signifikante Herabregulierung des entsprechenden Genproduktes. Anschließend wurde die selbe Formulierung in einem Behandlungsversuch in Kombination mit dem neuen Mikrotubuli-Hemmer Pretubulysin (PT) getestet. Erfreulicherweise führte eine intravenöse Behandlung mit dieser Kombination zu einem deutlich gehemmten L1210 Tumorstadium und verlängerte das Überleben der Gruppe. Darauf aufbauend wurde ein weiterer Behandlungsversuch mit GE11-Targeting von EGF Rezeptor-überexprimierenden HUH7 hepatozellulären Karzinomen durchgeführt. Eine Formulierung mit GE11 Targeting Ligand, siEG5 und PT führte zum längsten Überleben und am deutlichsten gehemmten HUH7 Tumorstadium. Allerdings sind die Ergebnisse aufgrund der starken antitumoralen Wirkung von PT auf HUH7 Tumore statistisch nicht signifikant.

Der Einsatz von Chemotherapie wird oft durch die Entwicklung von Resistenzen erschwert, welche häufig im Zusammenhang mit Monotherapie Ansätzen auftreten. Zurzeit stellt der Einsatz von Kombinationstherapie die vielversprechendste Strategie dar, um dieses Risiko zu minimieren. Der zweite Teil dieser Dissertation untersucht die Kombination von PT mit dem Antifolat Methotrexat (MTX). Zuerst wurden beide Wirkstoffe kovalent verbunden und intratumoral in NMRI-nu/nu Mäuse injiziert, um gleich zwei Eigenschaften von MTX auszunutzen, einerseits seine Fähigkeit, das Enzym DHFR zu hemmen und andererseits seine Ligandenqualität, welche durch die hohe Affinität zum Folatrezeptor bedingt wird. Hierdurch wurde ein verlangsamtes KB Tumorstadium erreicht, ähnlich wie durch die Behandlung mit freiem PT. Anschließend wurde eine Kombination der freien Komponenten in L1210, KB und HUH7 Tumor tragende Tiere intravenös injiziert. In allen drei Tumormodellen zeigte sich ein Vorteil von PT+MTX im Vergleich zur Behandlung mit den jeweiligen Wirkstoffen allein, im L1210 Tumormodell erreichte diese Überlegenheit sogar statistische Signifikanz. Zuletzt wurde PT+MTX in eine

nanopartikuläre Mizelle integriert, um einen gleichzeitigen Transport der Wirkstoffe in die Zielzelle zu gewährleisten. Erfreulicherweise konnte das L1210 Tumorwachstum während der intravenösen Behandlungen erfolgreich gehemmt werden. Der Einbau in eine mizellare Struktur führte zu einem signifikant längeren Überleben der Gruppe, verglichen mit Tieren der Gruppe freies PT+MTX.

Zusammenfassend stellt die Dissertation ein polymerisches Trägersystem für den Transport von siRNA zur Zielzelle mittels Targeting und Oberflächen-Abschirmung vor, das in Kombination mit siEG5 und PT erfolgreich das Tumorwachstum hemmen konnte. Weiterhin wird ein vielversprechender Kombinationseffekt von PT mit MTX in mehreren Tumormodellen beschrieben und die Verstärkung dieses Effekts durch Integration der Komponenten in eine Nanoformulierung gezeigt.

VII. REFERENCES

1. World Health Organization. *Cancer*. 2018 [cited 2018 24 july]; Available from: <http://www.who.int/cancer/en/>.
2. International Agency for Research on Cancer. *GLOBOCAN 2012: Estimated Cancer Incidence, Mortality and Prevalence Worldwide in 2012*. 2012 [cited 2018 August 10]; Available from: http://globocan.iarc.fr/Pages/fact_sheets_cancer.aspx.
3. World Cancer Research Fund International. *Cancer trends*. 2018 [cited 2018 24 july]; Available from: <https://www.wcrf.org/int/cancer-facts-and-figures>.
4. Zentrum für Krebsregisterdaten, *Bericht zum Krebsgeschehen in Deutschland 2016*. 2017. [cited 2018 24 july]; Available from: https://www.krebsdaten.de/Krebs/DE/Content/Publikationen/Krebsgeschehen/Krebsgeschehen_download.pdf?__blob=publicationFile
5. Zhang, G., Budker, V., and Wolff, J.A., *High levels of foreign gene expression in hepatocytes after tail vein injections of naked plasmid DNA*. *Hum Gene Ther*, 1999. **10**(10): p. 1735-7.
6. Bartlett, D.W., and Davis, M.E., *Insights into the kinetics of siRNA-mediated gene silencing from live-cell and live-animal bioluminescent imaging*. *Nucleic Acids Res*, 2006. **34**(1): p. 322-33.
7. Tabernero, J., Shapiro, G.I., LoRusso, P.M., Cervantes, A., Schwartz, G.K., Weiss, G.J., Paz-Ares, L., Cho, D.C., Infante, J.R., Alsina, M., Gounder, M.M., Falzone, R., Harrop, J., White, A.C.S., Toudjarska, I., Bumcrot, D., Meyers, R.E., Hinkle, G., Svrzikapa, N., Hutabarat, R.M., Clausen, V.A., Cehelsky, J., Nochur, S.V., Gamba-Vitalo, C., Vaishnav, A.K., Sah, D.W.Y., Gollob, J.A., and Burris, H.A., *First-in-Humans Trial of an RNA Interference Therapeutic Targeting VEGF and KSP in Cancer Patients with Liver Involvement*. *Cancer Discovery*, 2013. **3**(4): p. 406-417.
8. Haussecker, D., *Current issues of RNAi therapeutics delivery and development*. *Journal of Controlled Release*, 2014. **195**: p. 49-54.
9. Davis, M.E., Zuckerman, J.E., Choi, C.H.J., Seligson, D., Tolcher, A., Alabi, C.A., Yen, Y., Heidel, J.D., and Ribas, A., *Evidence of RNAi in humans from systemically administered siRNA via targeted nanoparticles*. *Nature*, 2010. **464**(7291): p. 1067-1070.
10. Chou, S.-T., and Mixson, A.J., *siRNA nanoparticles: the future of RNAi therapeutics for oncology?* *Nanomedicine* (London, England), 2014. **9**(15): p. 2251-2254.
11. Kacsinta, A.D., and Dowdy, S.F., *Current views on inducing synthetic lethal RNAi responses in the treatment of cancer*. *Expert Opinion on Biological Therapy*, 2016. **16**(2): p. 161-172.

12. Ameres, S.L., Martinez, J., and Schroeder, R., *Molecular basis for target RNA recognition and cleavage by human RISC*. Cell, 2007. **130**(1): p. 101-12.
13. Matranga, C., Tomari, Y., Shin, C., Bartel, D.P., and Zamore, P.D., *Passenger-strand cleavage facilitates assembly of siRNA into Ago2-containing RNAi enzyme complexes*. Cell, 2005. **123**(4): p. 607-20.
14. Chakraborty, C., Sharma, A.R., Sharma, G., Doss, C.G.P., and Lee, S.-S., *Therapeutic miRNA and siRNA: Moving from Bench to Clinic as Next Generation Medicine*. Molecular Therapy. Nucleic Acids, 2017. **8**: p. 132-143.
15. U.S. Food and Drug Administration. *FDA approves first-of-its kind targeted RNA-based therapy to treat a rare disease*. 2018 [cited 2018 14 september]; Available from: <https://www.fda.gov/NewsEvents/Newsroom/PressAnnouncements/UCM616518.htm>.
16. Ledford, H. *Investors flee as firm scraps RNA-interference drug candidate -Struggling RNAi field faces another blow as its first treatments near the clinic*. 2016 [cited 2018 August 14]; Available from: <https://www.nature.com/news/investors-flee-as-firm-scraps-rna-interference-drug-candidate-1.20769>.
17. van de Water, F.M., Boerman, O.C., Wouterse, A.C., Peters, J.G., Russel, F.G., and Masereeuw, R., *Intravenously administered short interfering RNA accumulates in the kidney and selectively suppresses gene function in renal proximal tubules*. Drug Metab Dispos, 2006. **34**(8): p. 1393-7.
18. Alexis, F., Pridgen, E., Molnar, L.K., and Farokhzad, O.C., *Factors affecting the clearance and biodistribution of polymeric nanoparticles*. Mol Pharm, 2008. **5**(4): p. 505-15.
19. Zuckerman, J.E., Choi, C.H., Han, H., and Davis, M.E., *Polycation-siRNA nanoparticles can disassemble at the kidney glomerular basement membrane*. Proc Natl Acad Sci U S A, 2012. **109**(8): p. 3137-42.
20. Kulkarni, S.A., and Feng, S.S., *Effects of particle size and surface modification on cellular uptake and biodistribution of polymeric nanoparticles for drug delivery*. Pharm Res, 2013. **30**(10): p. 2512-22.
21. Faraji, A.H., and Wipf, P., *Nanoparticles in cellular drug delivery*. Bioorg Med Chem, 2009. **17**(8): p. 2950-62.
22. Matsumura, Y., and Maeda, H., *A new concept for macromolecular therapeutics in cancer chemotherapy: mechanism of tumoritropic accumulation of proteins and the antitumor agent smancs*. Cancer Res, 1986. **46**(12 Pt 1): p. 6387-92.
23. Wang, J., Lu, Z., Wientjes, M.G., and Au, J.L.S., *Delivery of siRNA Therapeutics: Barriers and Carriers*. The AAPS Journal, 2010. **12**(4): p. 492-503.

24. Lin, G., Chen, C.-K., Yin, F., Yang, C., Tian, J., Chen, T., Xu, G., He, C., Lin, M.C.-M., Wang, J., Lu, F., Wang, X., and Yong, K.-T., *Biodegradable nanoparticles as siRNA carriers for in vivo gene silencing and pancreatic cancer therapy*. *Journal of Materials Chemistry B*, 2017. **5**(18): p. 3327-3337.
25. Pack, D.W., Hoffman, A.S., Pun, S., and Stayton, P.S., *Design and development of polymers for gene delivery*. *Nat Rev Drug Discov*, 2005. **4**(7): p. 581-93.
26. Mokhtarzadeh, A., Alibakhshi, A., Yaghoobi, H., Hashemi, M., Hejazi, M., and Ramezani, M., *Recent advances on biocompatible and biodegradable nanoparticles as gene carriers*. *Expert Opin Biol Ther*, 2016. **16**(6): p. 771-85.
27. Baldo, A., van den Akker, E., Bergmans, H.E., Lim, F., and Pauwels, K., *General Considerations on the Biosafety of Virus-derived Vectors Used in Gene Therapy and Vaccination*. *Current Gene Therapy*, 2013. **13**(6): p. 385-394.
28. Gao, K., and Huang, L., *Non-viral Methods for siRNA Delivery*. *Molecular pharmaceutics*, 2009. **6**(3): p. 651-658.
29. Seow, Y., and Wood, M.J., *Biological Gene Delivery Vehicles: Beyond Viral Vectors*. *Molecular Therapy: the Journal of the American Society of Gene Therapy*, 2009. **17**(5): p. 767-777.
30. Lorenzer, C., Dirin, M., Winkler, A.M., Baumann, V., and Winkler, J., *Going beyond the liver: progress and challenges of targeted delivery of siRNA therapeutics*. *J Control Release*, 2015. **203**: p. 1-15.
31. Felgner, P.L., Barenholz, Y., Behr, J.P., Cheng, S.H., Cullis, P., Huang, L., Jessee, J.A., Seymour, L., Szoka, F., Thierry, A.R., Wagner, E., and Wu, G., *Nomenclature for synthetic gene delivery systems*. *Hum Gene Ther*, 1997. **8**(5): p. 511-2.
32. Spagnou, S., Miller, A.D., and Keller, M., *Lipidic carriers of siRNA: differences in the formulation, cellular uptake, and delivery with plasmid DNA*. *Biochemistry*, 2004. **43**(42): p. 13348-56.
33. Ogris, M., Steinlein, P., Carotta, S., Brunner, S., and Wagner, E., *DNA/polyethylenimine transfection particles: Influence of ligands, polymer size, and PEGylation on internalization and gene expression*. *AAPS PharmSci*, 2001. **3**(3): p. 43-53.
34. Behr, J.-P., *The Proton Sponge: a Trick to Enter Cells the Viruses Did Not Exploit*. *CHIMIA International Journal for Chemistry*, 1997. **51**(1-2): p. 34-36.
35. Fischer, D., Li, Y., Ahlemeyer, B., Kriegelstein, J., and Kissel, T., *In vitro cytotoxicity testing of polycations: influence of polymer structure on cell viability and hemolysis*. *Biomaterials*, 2003. **24**(7): p. 1121-31.

36. Wagner, E., *Polymers for siRNA Delivery: Inspired by Viruses to be Targeted, Dynamic, and Precise*. Accounts of Chemical Research, 2012. **45**(7): p. 1005-1013.
37. Zhang, L., Gu, F.X., Chan, J.M., Wang, A.Z., Langer, R.S., and Farokhzad, O.C., *Nanoparticles in medicine: therapeutic applications and developments*. Clin Pharmacol Ther, 2008. **83**(5): p. 761-9.
38. Mayer, L.D., and St.-Onge, G., *Determination of Free and Liposome-Associated Doxorubicin and Vincristine Levels in Plasma under Equilibrium Conditions Employing Ultrafiltration Techniques*. Analytical Biochemistry, 1995. **232**(2): p. 149-157.
39. Iyer, A.K., Khaled, G., Fang, J., and Maeda, H., *Exploiting the enhanced permeability and retention effect for tumor targeting*. Drug Discov Today, 2006. **11**(17-18): p. 812-8.
40. P. Mendes, L., Pedroso Nogueira Gaeti, M., Henrique Marcelino de Ávila, P., de Sousa Vieira, M., dos Santos Rodrigues, B., Ávila, R., Cristina Rosa Dos Santos, L., Campos Valadares, M., and Lima, E., *Multicompartmental Nanoparticles for Co-Encapsulation and Multimodal Drug Delivery to Tumor Cells and Neovasculature*. Vol. 31. 2013.
41. Hartmann, L., Hafele, S., Peschka-Suss, R., Antonietti, M., and Borner, H.G., *Tailor-made poly(amidoamine)s for controlled complexation and condensation of DNA*. Chemistry, 2008. **14**(7): p. 2025-33.
42. Schaffert, D., Badgujar, N., and Wagner, E., *Novel Fmoc-polyamino acids for solid-phase synthesis of defined polyamidoamines*. Org Lett, 2011. **13**(7): p. 1586-9.
43. Dohmen, C., Edinger, D., Fröhlich, T., Schreiner, L., Lächelt, U., Troiber, C., Rädler, J., Hadwiger, P., Vornlocher, H.-P., and Wagner, E., *Nanosized Multifunctional Polyplexes for Receptor-Mediated siRNA Delivery*. ACS Nano, 2012. **6**(6): p. 5198-5208.
44. Salcher, E.E., Kos, P., Fröhlich, T., Badgujar, N., Scheible, M., and Wagner, E., *Sequence-defined four-arm oligo(ethanamino)amides for pDNA and siRNA delivery: Impact of building blocks on efficacy*. J Control Release, 2012. **164**(3): p. 380-6.
45. Lee, E.R., Marshall, J., Siegel, C.S., Jiang, C., Yew, N.S., Nichols, M.R., Nietupski, J.B., Ziegler, R.J., Lane, M.B., Wang, K.X., Wan, N.C., Scheule, R.K., Harris, D.J., Smith, A.E., and Cheng, S.H., *Detailed Analysis of Structures and Formulations of Cationic Lipids for Efficient Gene Transfer to the Lung*. Human Gene Therapy, 1996. **7**(14): p. 1701-1717.
46. Wightman, L., Kircheis, R., Rössler, V., Carotta, S., Ruzicka, R., Kursá, M., and Wagner, E., *Different behavior of branched and linear polyethylenimine for gene delivery in vitro and in vivo*. J Gene Med, 2001. **3**(4): p. 362-72.
47. Schaffert, D., Troiber, C., Salcher, E.E., Fröhlich, T., Martin, I.,

- Badgular, N., Dohmen, C., Edinger, D., Kläger, R., Maiwald, G., Farkasova, K., Seeber, S., Jahn-Hofmann, K., Hadwiger, P., and Wagner, E., *Solid-phase synthesis of sequence-defined T-, i-, and U-shape polymers for pDNA and siRNA delivery*. *Angew Chem Int Ed Engl*, 2011. **50**(38): p. 8986-9.
48. Troiber, C., Edinger, D., Kos, P., Schreiner, L., Kläger, R., Herrmann, A., and Wagner, E., *Stabilizing effect of tyrosine trimers on pDNA and siRNA polyplexes*. *Biomaterials*, 2013. **34**(5): p. 1624-33.
49. Klein, P.M., Reinhard, S., Lee, D.J., Müller, K., Ponader, D., Hartmann, L., and Wagner, E., *Precise redox-sensitive cleavage sites for improved bioactivity of siRNA lipopolyplexes*. *Nanoscale*, 2016. **8**(42): p. 18098-18104.
50. Klibanov, A.L., Maruyama, K., Torchilin, V.P., and Huang, L., *Amphipathic polyethyleneglycols effectively prolong the circulation time of liposomes*. *FEBS Lett*, 1990. **268**(1): p. 235-7.
51. Senior, J., Delgado, C., Fisher, D., Tilcock, C., and Gregoriadis, G., *Influence of surface hydrophilicity of liposomes on their interaction with plasma protein and clearance from the circulation: Studies with poly(ethylene glycol)-coated vesicles*. *Biochimica et Biophysica Acta (BBA) - Biomembranes*, 1991. **1062**(1): p. 77-82.
52. Mori, A., Klibanov, A.L., Torchilin, V.P., and Huang, L., *Influence of the steric barrier activity of amphipathic poly(ethyleneglycol) and ganglioside GM1 on the circulation time of liposomes and on the target binding of immunoliposomes in vivo*. *FEBS Letters*, 1991. **284**(2): p. 263-266.
53. Huynh, N.T., Roger, E., Lautram, N., Benoit, J.P., and Passirani, C., *The rise and rise of stealth nanocarriers for cancer therapy: passive versus active targeting*. *Nanomedicine (Lond)*, 2010. **5**(9): p. 1415-33.
54. Singh, R., and Lillard, J.W., Jr., *Nanoparticle-based targeted drug delivery*. *Exp Mol Pathol*, 2009. **86**(3): p. 215-23.
55. Yang, Q., and Lai, S.K., *Anti-PEG immunity: emergence, characteristics, and unaddressed questions*. *Wiley interdisciplinary reviews. Nanomedicine and nanobiotechnology*, 2015. **7**(5): p. 655-677.
56. Moghimi, S.M., Hunter, A.C., Dadswell, C.M., Savay, S., Alving, C.R., and Szebeni, J., *Causative factors behind poloxamer 188 (Pluronic F68, Flocor™)-induced complement activation in human sera: A protective role against poloxamer-mediated complement activation by elevated serum lipoprotein levels*. *Biochimica et Biophysica Acta (BBA) - Molecular Basis of Disease*, 2004. **1689**(2): p. 103-113.
57. Wenande, E., and Garvey, L.H., *Immediate-type hypersensitivity to polyethylene glycols: a review*. *Clinical & Experimental Allergy*, 2016. **46**(7): p. 907-922.

58. Knop, K., Hoogenboom, R., Fischer, D., and Schubert, U.S., *Poly(ethylene glycol) in drug delivery: pros and cons as well as potential alternatives*. *Angew Chem Int Ed Engl*, 2010. **49**(36): p. 6288-308.
59. Hamad, I., Hunter, A.C., Szebeni, J., and Moghimi, S.M., *Poly(ethylene glycol)s generate complement activation products in human serum through increased alternative pathway turnover and a MASP-2-dependent process*. *Molecular Immunology*, 2008. **46**(2): p. 225-232.
60. Dewachter, P., and Mouton-Faivre, C., *Anaphylaxis to macrogol 4000 after a parenteral corticoid injection*. *Allergy*, 2005. **60**(5): p. 705-706.
61. Garay, R.P., El-Gewely, R., Armstrong, J.K., Garratty, G., and Richette, P., *Antibodies against polyethylene glycol in healthy subjects and in patients treated with PEG-conjugated agents*. *Expert Opin Drug Deliv*, 2012. **9**(11): p. 1319-23.
62. Abu Lila, A.S., Kiwada, H., and Ishida, T., *The accelerated blood clearance (ABC) phenomenon: clinical challenge and approaches to manage*. *J Control Release*, 2013. **172**(1): p. 38-47.
63. Ralf, K., Wightman, L., Schreiber, A., Robitza, B., Rössler, V., Kursa, M., and Wagner, E., *Polyethylenimine/DNA complexes shielded by transferrin target gene expression to tumors after systemic application*. *Gene Ther* 8: 28-40. Vol. 8. 2001. 28-40.
64. Wang, W., Tetley, L., and Uchegbu, I.F., *The Level of Hydrophobic Substitution and the Molecular Weight of Amphiphilic Poly-L-lysine-Based Polymers Strongly Affects Their Assembly into Polymeric Bilayer Vesicles*. *Journal of Colloid and Interface Science*, 2001. **237**(2): p. 200-207.
65. Toncheva, V., Wolfert, M.A., Dash, P.R., Oupicky, D., Ulbrich, K., Seymour, L.W., and Schacht, E.H., *Novel vectors for gene delivery formed by self-assembly of DNA with poly(l-lysine) grafted with hydrophilic polymers*. *Biochimica et Biophysica Acta (BBA) - General Subjects*, 1998. **1380**(3): p. 354-368.
66. Noga, M., Edinger, D., Kläger, R., Wegner, S.V., Spatz, J.P., Wagner, E., Winter, G., and Besheer, A., *The effect of molar mass and degree of hydroxyethylation on the controlled shielding and deshielding of hydroxyethyl starch-coated polyplexes*. *Biomaterials*, 2013. **34**(10): p. 2530-2538.
67. Schlapschy, M., Binder, U., Börger, C., Theobald, I., Wachinger, K., Kisling, S., Haller, D., and Skerra, A., *PASylation: a biological alternative to PEGylation for extending the plasma half-life of pharmaceutically active proteins*. *Protein Engineering, Design and Selection*, 2013. **26**(8): p. 489-501.
68. Mendler, C.T., Friedrich, L., Laitinen, I., Schlapschy, M., Schwaiger, M., Wester, H.-J., and Skerra, A., *High contrast tumor imaging with radio-labeled antibody Fab fragments tailored for optimized pharmacokinetics via PASylation*. *mAbs*, 2015. **7**(1): p. 96-109.

69. Bludau, H., Czapar, A.E., Pitek, A.S., Shukla, S., Jordan, R., and Steinmetz, N.F., *POxylation as an alternative stealth coating for biomedical applications*. Eur Polym J, 2017. **88**: p. 679-688.
70. Wei, Q., Becherer, T., Angioletti-Uberti, S., Dzubiella, J., Wischke, C., Neffe, A.T., Lendlein, A., Ballauff, M., and Haag, R., *Protein interactions with polymer coatings and biomaterials*. Angew Chem Int Ed Engl, 2014. **53**(31): p. 8004-31.
71. Chan, B.A., Xuan, S., Li, A., Simpson, J.M., Sternhagen, G.L., Yu, T., Darvish, O.A., Jiang, N., and Zhang, D., *Polypeptoid polymers: Synthesis, characterization, and properties*. Biopolymers, 2018. **109**(1).
72. Yoo, J., Birke, A., Kim, J., Jang, Y., Song, S.Y., Ryu, S., Kim, B.S., Kim, B.G., Barz, M., and Char, K., *Cooperative Catechol-Functionalized Polypept(o)ide Brushes and Ag Nanoparticles for Combination of Protein Resistance and Antimicrobial Activity on Metal Oxide Surfaces*. Biomacromolecules, 2018. **19**(5): p. 1602-1613.
73. Schneider, M., Tang, Z., Richter, M., Marschelke, C., Förster, P., Wegener, E., Amin, I., Zimmermann, H., Scharnweber, D., Braun, H.G., Luxenhofer, R., and Jordan, R., *Patterned Polypeptoid Brushes*. Macromol Biosci, 2016. **16**(1): p. 75-81.
74. Schneider, M., Fetsch, C., Amin, I., Jordan, R., and Luxenhofer, R., *Polypeptoid brushes by surface-initiated polymerization of N-substituted glycine N-carboxyanhydrides*. Langmuir, 2013. **29**(23): p. 6983-8.
75. Lau, K.H.A., Sileika, T.S., Park, S.H., Sousa, A.M.L., Burch, P., Szleifer, I., and Messersmith, P.B., *Molecular Design of Antifouling Polymer Brushes Using Sequence-Specific Peptoids*. Advanced Materials Interfaces, 2015. **2**(1): p. 1400225.
76. Makino, A., Kizaka-Kondoh, S., Yamahara, R., Hara, I., Kanzaki, T., Ozeki, E., Hiraoka, M., and Kimura, S., *Near-infrared fluorescence tumor imaging using nanocarrier composed of poly(L-lactic acid)-block-poly(sarcosine) amphiphilic polydepsipeptide*. Biomaterials, 2009. **30**(28): p. 5156-60.
77. Hara, E., Ueda, M., Kim, C.J., Makino, A., Hara, I., Ozeki, E., and Kimura, S., *Suppressive immune response of poly-(sarcosine) chains in peptide-nanosheets in contrast to polymeric micelles*. J Pept Sci, 2014. **20**(7): p. 570-7.
78. Birke, A., Huesmann, D., Kelsch, A., Weilbacher, M., Xie, J., Bros, M., Bopp, T., Becker, C., Landfester, K., and Barz, M., *Polypeptoid-block-polypeptide copolymers: synthesis, characterization, and application of amphiphilic block Copolypept(o)ides in drug formulations and miniemulsion techniques*. Biomacromolecules, 2014. **15**(2): p. 548-57.
79. Otter, R., Klinker, K., Spitzer, D., Schinnerer, M., Barz, M., and Besenius, P., *Folding induced supramolecular assembly into pH-responsive nanorods with a protein repellent shell*. Chem Commun (Camb), 2018.

54(4): p. 401-404.

80. Heller, P., Hobernik, D., Lächelt, U., Schinnerer, M., Weber, B., Schmidt, M., Wagner, E., Bros, M., and Barz, M., *Combining reactive triblock copolymers with functional cross-linkers: A versatile pathway to disulfide stabilized-polyplex libraries and their application as pDNA vaccines*. J Control Release, 2017. **258**: p. 146-160.

81. Klinker, K., Schäfer, O., Huesmann, D., Bauer, T., Capeloa, L., Braun, L., Stergiou, N., Schinnerer, M., Dirisala, A., Miyata, K., Osada, K., Cabral, H., Kataoka, K., and Barz, M., *Secondary-Structure-Driven Self-Assembly of Reactive Polypept(o)ides: Controlling Size, Shape, and Function of Core Cross-Linked Nanostructures*. Angew Chem Int Ed Engl, 2017. **56**(32): p. 9608-9613.

82. Maeda, H., *The enhanced permeability and retention (EPR) effect in tumor vasculature: the key role of tumor-selective macromolecular drug targeting*. Adv Enzyme Regul, 2001. **41**: p. 189-207.

83. Grislain, L., Couvreur, P., Lenaerts, V., Roland, M., Deprez-Decampeneere, D., and Speiser, P., *Pharmacokinetics and distribution of a biodegradable drug-carrier*. International Journal of Pharmaceutics, 1983. **15**(3): p. 335-345.

84. Yuan, F., Dellian, M., Fukumura, D., Leunig, M., Berk, D.A., Torchilin, V.P., and Jain, R.K., *Vascular permeability in a human tumor xenograft: molecular size dependence and cutoff size*. Cancer Res, 1995. **55**(17): p. 3752-6.

85. Cho, K., Wang, X., Nie, S., Chen, Z.G., and Shin, D.M., *Therapeutic nanoparticles for drug delivery in cancer*. Clin Cancer Res, 2008. **14**(5): p. 1310-6.

86. Talekar, M., Kendall, J., Denny, W., and Garg, S., *Targeting of nanoparticles in cancer: drug delivery and diagnostics*. Anticancer Drugs, 2011. **22**(10): p. 949-62.

87. Parker, N., Turk, M.J., Westrick, E., Lewis, J.D., Low, P.S., and Leamon, C.P., *Folate receptor expression in carcinomas and normal tissues determined by a quantitative radioligand binding assay*. Anal Biochem, 2005. **338**(2): p. 284-93.

88. Jackman, A.L., Theti, D.S., and Gibbs, D.D., *Antifolates targeted specifically to the folate receptor*. Adv Drug Deliv Rev, 2004. **56**(8): p. 1111-25.

89. Leamon, C.P., and Low, P.S., *Folate-mediated targeting: from diagnostics to drug and gene delivery*. Drug Discov Today, 2001. **6**(1): p. 44-51.

90. Sudimack, J., and Lee, R.J., *Targeted drug delivery via the folate receptor*. Adv Drug Deliv Rev, 2000. **41**(2): p. 147-62.

91. Leamon, C.P., DePrince, R.B., and Hendren, R.W., *Folate-mediated drug delivery: effect of alternative conjugation chemistry*. *J Drug Target*, 1999. **7**(3): p. 157-69.
92. Toffoli, G., Cernigoi, C., Russo, A., Gallo, A., Bagnoli, M., and Boiocchi, M., *Overexpression of folate binding protein in ovarian cancers*. *International Journal of Cancer*, 1998. **74**(2): p. 193-198.
93. Ross, J.F., Chaudhuri, P.K., and Ratnam, M., *Differential regulation of folate receptor isoforms in normal and malignant tissues in vivo and in established cell lines. Physiologic and clinical implications*. *Cancer*, 1994. **73**(9): p. 2432-43.
94. Weitman, S.D., Lark, R.H., Coney, L.R., Fort, D.W., Frasca, V., Zurawski, V.R., Jr., and Kamen, B.A., *Distribution of the folate receptor GP38 in normal and malignant cell lines and tissues*. *Cancer Res*, 1992. **52**(12): p. 3396-401.
95. Shir, A., Ogris, M., Wagner, E., and Levitzki, A., *EGF Receptor-Targeted Synthetic Double-Stranded RNA Eliminates Glioblastoma, Breast Cancer, and Adenocarcinoma Tumors in Mice*. *PLOS Medicine*, 2005. **3**(1): p. e6.
96. Li, Z., Zhao, R., Wu, X., Sun, Y., Yao, M., Li, J., Xu, Y., and Gu, J., *Identification and characterization of a novel peptide ligand of epidermal growth factor receptor for targeted delivery of therapeutics*. *The FASEB Journal*, 2005. **19**(14): p. 1978-1985.
97. Blessing, T., Kursa, M., Holzhauser, R., Kircheis, R., and Wagner, E., *Different strategies for formation of pegylated EGF-conjugated PEI/DNA complexes for targeted gene delivery*. *Bioconjug Chem*, 2001. **12**(4): p. 529-37.
98. Mickler, F.M., Möckl, L., Ruthardt, N., Ogris, M., Wagner, E., and Bräuchle, C., *Tuning nanoparticle uptake: live-cell imaging reveals two distinct endocytosis mechanisms mediated by natural and artificial EGFR targeting ligand*. *Nano Lett*, 2012. **12**(7): p. 3417-23.
99. Wagner, E., Cotten, M., Foisner, R., and Birnstiel, M.L., *Transferrin-polycation-DNA complexes: the effect of polycations on the structure of the complex and DNA delivery to cells*. *Proc Natl Acad Sci U S A*, 1991. **88**(10): p. 4255-9.
100. Huang, R.Q., Qu, Y.H., Ke, W.L., Zhu, J.H., Pei, Y.Y., and Jiang, C., *Efficient gene delivery targeted to the brain using a transferrin-conjugated polyethyleneglycol-modified polyamidoamine dendrimer*. *Faseb j*, 2007. **21**(4): p. 1117-25.
101. Liang, K.W., Hoffman, E.P., and Huang, L., *Targeted Delivery of Plasmid DNA to Myogenic Cells via Transferrin-Conjugated Peptide Nucleic Acid*. *Molecular Therapy*, 2000. **1**(3): p. 236-243.
102. Weissleder, R., Kelly, K., Sun, E.Y., Shtatland, T., and Josephson,

L., *Cell-specific targeting of nanoparticles by multivalent attachment of small molecules*. Nat Biotechnol, 2005. **23**(11): p. 1418-23.

103. Lee, T.Y., Lin, C.T., Kuo, S.Y., Chang, D.K., and Wu, H.C., *Peptide-mediated targeting to tumor blood vessels of lung cancer for drug delivery*. Cancer Res, 2007. **67**(22): p. 10958-65.

104. Martin, I., Dohmen, C., Mas-Moruno, C., Troiber, C., Kos, P., Schaffert, D., Lächelt, U., Teixido, M., Günther, M., Kessler, H., Giral, E., and Wagner, E., *Solid-phase-assisted synthesis of targeting peptide-PEG-oligo(ethane amino)amides for receptor-mediated gene delivery*. Org Biomol Chem, 2012. **10**(16): p. 3258-68.

105. Yang, J., Hirata, T., Croce, K., Merrill-Skoloff, G., Tchernychev, B., Williams, E., Flaumenhaft, R., Furie, B.C., and Furie, B., *Targeted gene disruption demonstrates that P-selectin glycoprotein ligand 1 (PSGL-1) is required for P-selectin-mediated but not E-selectin-mediated neutrophil rolling and migration*. J Exp Med, 1999. **190**(12): p. 1769-82.

106. Merdan, T., Callahan, J., Petersen, H., Kunath, K., Bakowsky, U., Kopeckova, P., Kissel, T., and Kopecek, J., *Pegylated polyethylenimine-Fab' antibody fragment conjugates for targeted gene delivery to human ovarian carcinoma cells*. Bioconjug Chem, 2003. **14**(5): p. 989-96.

107. Wang, L., Su, W., Liu, Z., Zhou, M., Chen, S., Chen, Y., Lu, D., Liu, Y., Fan, Y., Zheng, Y., Han, Z., Kong, D., Wu, J.C., Xiang, R., and Li, Z., *CD44 antibody-targeted liposomal nanoparticles for molecular imaging and therapy of hepatocellular carcinoma*. Biomaterials, 2012. **33**(20): p. 5107-14.

108. Low, P.S., Henne, W.A., and Doorneweerd, D.D., *Discovery and Development of Folic-Acid-Based Receptor Targeting for Imaging and Therapy of Cancer and Inflammatory Diseases*. Accounts of Chemical Research, 2008. **41**(1): p. 120-129.

109. Rajagopalan, P.T.R., Zhang, Z., McCourt, L., Dwyer, M., Benkovic, S.J., and Hammes, G.G., *Interaction of dihydrofolate reductase with methotrexate: Ensemble and single-molecule kinetics*. Proceedings of the National Academy of Sciences, 2002. **99**(21): p. 13481-13486.

110. Kremer, J.M., *Toward a better understanding of methotrexate*. Arthritis Rheum, 2004. **50**(5): p. 1370-82.

111. Salomon, D.S., Brandt, R., Ciardiello, F., and Normanno, N., *Epidermal growth factor-related peptides and their receptors in human malignancies*. Critical Reviews in Oncology/Hematology, 1995. **19**(3): p. 183-232.

112. Yarden, Y., *The EGFR family and its ligands in human cancer. signalling mechanisms and therapeutic opportunities*. Eur J Cancer, 2001. **37 Suppl 4**: p. S3-8.

113. Nicholson, R.I., Gee, J.M., and Harper, M.E., *EGFR and cancer*

prognosis. Eur J Cancer, 2001. **37 Suppl 4**: p. S9-15.

114. Schäfer, A., Pahnke, A., Schaffert, D., van Weerden, W.M., de Ridder, C.M., Rödl, W., Vetter, A., Spitzweg, C., Kraaij, R., Wagner, E., and Ogris, M., *Disconnecting the yin and yang relation of epidermal growth factor receptor (EGFR)-mediated delivery: a fully synthetic, EGFR-targeted gene transfer system avoiding receptor activation*. Hum Gene Ther, 2011. **22**(12): p. 1463-73.

115. Khdair, A., Chen, D., Patil, Y., Ma, L., Dou, Q.P., Shekhar, M.P., and Panyam, J., *Nanoparticle-mediated combination chemotherapy and photodynamic therapy overcomes tumor drug resistance*. J Control Release, 2010. **141**(2): p. 137-44.

116. Gottesman, M.M., Fojo, T., and Bates, S.E., *Multidrug resistance in cancer: role of ATP-dependent transporters*. Nat Rev Cancer, 2002. **2**(1): p. 48-58.

117. Nikolaev, A., and Yang, E.S., *The Impact of DNA Repair Pathways in Cancer Biology and Therapy*. Cancers, 2017. **9**(9): p. 126.

118. Salehan, M., and Morse, R., *DNA damage repair and tolerance: A role in chemotherapeutic drug resistance*. Vol. 70. 2013. 31-40.

119. Murray, G.I., *The role of cytochrome P450 in tumour development and progression and its potential in therapy*. J Pathol, 2000. **192**(4): p. 419-26.

120. Safa, A.R., *Resistance to Cell Death and Its Modulation in Cancer Stem Cells*. Critical reviews in oncogenesis, 2016. **21**(3-4): p. 203-219.

121. Housman, G., Byler, S., Heerboth, S., Lapinska, K., Longacre, M., Snyder, N., and Sarkar, S., *Drug Resistance in Cancer: An Overview*. Cancers, 2014. **6**(3): p. 1769-1792.

122. Blagosklonny, M.V., *Analysis of FDA approved anticancer drugs reveals the future of cancer therapy*. Cell Cycle, 2004. **3**(8): p. 1035-42.

123. W. Humphrey, R., M. Brockway-Lunardi, L., T. Bonk, D., Dohoney, K.M., Doroshov, J.H., Meech, S.J., Ratain, M.J., Topalian, S.L., and M. Pardoll, D., *Opportunities and Challenges in the Development of Experimental Drug Combinations for Cancer*. JNCI: Journal of the National Cancer Institute, 2011. **103**(16): p. 1222-1226.

124. Bayat Mokhtari, R., Homayouni, T.S., Baluch, N., Morgatskaya, E., Kumar, S., Das, B., and Yeger, H., *Combination therapy in combating cancer*. Oncotarget, 2017. **8**(23): p. 38022-38043.

125. Chou, T.C., *Theoretical basis, experimental design, and computerized simulation of synergism and antagonism in drug combination studies*. Pharmacol Rev, 2006. **58**(3): p. 621-81.

126. Chabner, B.A., and Roberts, T.G., Jr., *Timeline: Chemotherapy and the war on cancer*. Nat Rev Cancer, 2005. **5**(1): p. 65-72.

127. Frei, E., 3rd, Karon, M., Levin, R.H., Freireich, E.J., Taylor, R.J., Hananian, J., Selawry, O., Holland, J.F., Hoogstraten, B., Wolman, I.J., Abir, E., Sawitsky, A., Lee, S., Mills, S.D., Burgert, E.O., Jr., Spurr, C.L., Patterson, R.B., Ebaugh, F.G., James, G.W., 3rd, and Moon, J.H., *The effectiveness of combinations of antileukemic agents in inducing and maintaining remission in children with acute leukemia*. *Blood*, 1965. **26**(5): p. 642-56.
128. Riechelmann, R.P., Tannock, I.F., Wang, L., Saad, E.D., Taback, N.A., and Krzyzanowska, M.K., *Potential drug interactions and duplicate prescriptions among cancer patients*. *J Natl Cancer Inst*, 2007. **99**(8): p. 592-600.
129. Delbaldo, C., Michiels, S., Syz, N., Soria, J.C., Le Chevalier, T., and Pignon, J.P., *Benefits of adding a drug to a single-agent or a 2-agent chemotherapy regimen in advanced non-small-cell lung cancer: a meta-analysis*. *Jama*, 2004. **292**(4): p. 470-84.
130. Zhao, R., Diop-Bove, N., Visentin, M., and Goldman, I.D., *Mechanisms of Membrane Transport of Folates into Cells and Across Epithelia*. *Annual Review of Nutrition*, 2011. **31**(1): p. 177-201.
131. Visentin, M., Zhao, R., and Goldman, I.D., *The antifolates*. *Hematol Oncol Clin North Am*, 2012. **26**(3): p. 629-48, ix.
132. Cutolo, M., Sulli, A., Pizzorni, C., Serio, B., and Straub, R., *Anti-inflammatory mechanisms of methotrexate in rheumatoid arthritis*. *Annals of the Rheumatic Diseases*, 2001. **60**(8): p. 729-735.
133. Weinblatt, M.E., *Methotrexate: who would have predicted its importance in rheumatoid arthritis?* *Arthritis Research & Therapy*, 2018. **20**: p. 103.
134. Bertino, J.R., Goker, E., Gorlick, R., Li, W.W., and Banerjee, D., *Resistance Mechanisms to Methotrexate in Tumors*. *Oncologist*, 1996. **1**(4): p. 223-226.
135. Zhao, R., and Goldman, I.D., *Resistance to antifolates*. *Oncogene*, 2003. **22**(47): p. 7431-57.
136. Gorlick, R., Goker, E., Trippett, T., Steinherz, P., Elisseyeff, Y., Mazumdar, M., Flintoff, W.F., and Bertino, J.R., *Defective transport is a common mechanism of acquired methotrexate resistance in acute lymphocytic leukemia and is associated with decreased reduced folate carrier expression*. *Blood*, 1997. **89**(3): p. 1013-8.
137. Mukhtar, E., Adhami, V.M., and Mukhtar, H., *Targeting microtubules by natural agents for cancer therapy*. *Mol Cancer Ther*, 2014. **13**(2): p. 275-84.
138. Bessho, Y., Oguri, T., Ozasa, H., Uemura, T., Sakamoto, H., Miyazaki, M., Maeno, K., Sato, S., and Ueda, R., *ABCC10/MRP7 is associated with vinorelbine resistance in non-small cell lung cancer*. *Oncol*

Rep, 2009. **21**(1): p. 263-8.

139. Mozzetti, S., Ferlini, C., Concolino, P., Filippetti, F., Raspaglio, G., Prislei, S., Gallo, D., Martinelli, E., Ranelletti, F.O., Ferrandina, G., and Scambia, G., *Class III beta-tubulin overexpression is a prominent mechanism of paclitaxel resistance in ovarian cancer patients*. Clin Cancer Res, 2005. **11**(1): p. 298-305.

140. Braig, S., Wiedmann, R.M., Liebl, J., Singer, M., Kubisch, R., Schreiner, L., Abhari, B.A., Wagner, E., Kazmaier, U., Fulda, S., and Vollmar, A.M., *Pretubulysin: a new option for the treatment of metastatic cancer*. Cell Death Dis, 2014. **5**: p. e1001.

141. Ullrich, A., Chai, Y., Pistorius, D., Elnakady, Y.A., Herrmann, J.E., Weissman, K.J., Kazmaier, U., and Müller, R., *Pretubulysin, a potent and chemically accessible tubulysin precursor from Angiococcus disciformis*. Angew Chem Int Ed Engl, 2009. **48**(24): p. 4422-5.

142. Khalil, M.W., Sasse, F., Lunsdorf, H., Elnakady, Y.A., and Reichenbach, H., *Mechanism of action of tubulysin, an antimitotic peptide from myxobacteria*. Chembiochem, 2006. **7**(4): p. 678-83.

143. Sasse, F., Steinmetz, H., Heil, J., Höfle, G., and Reichenbach, H., *Tubulysins, new cytostatic peptides from myxobacteria acting on microtubuli. Production, isolation, physico-chemical and biological properties*. J Antibiot (Tokyo), 2000. **53**(9): p. 879-85.

144. Rath, S., Liebl, J., Fürst, R., Ullrich, A., Burkhart, J.L., Kazmaier, U., Herrmann, J., Müller, R., Günther, M., Schreiner, L., Wagner, E., Vollmar, A.M., and Zahler, S., *Anti-angiogenic effects of the tubulysin precursor pretubulysin and of simplified pretubulysin derivatives*. Br J Pharmacol, 2012. **167**(5): p. 1048-61.

145. Kretzschmann, V.K., Gellrich, D., Ullrich, A., Zahler, S., Vollmar, A.M., Kazmaier, U., and Fürst, R., *Novel tubulin antagonist pretubulysin displays antivascular properties in vitro and in vivo*. Arterioscler Thromb Vasc Biol, 2014. **34**(2): p. 294-303.

146. Schwenk, R., Stehning, T., Bischoff, I., Ullrich, A., Kazmaier, U., and Fürst, R., *The pretubulysin-induced exposure of collagen is caused by endothelial cell retraction that results in an increased adhesion and decreased transmigration of tumor cells*. Oncotarget, 2017. **8**(44): p. 77622-77633.

147. Klein, P.M., Kern, S., Lee, D.J., Schmaus, J., Höhn, M., Gorges, J., Kazmaier, U., and Wagner, E., *Folate receptor-directed orthogonal click-functionalization of siRNA lipopolyplexes for tumor cell killing in vivo*. Biomaterials, 2018. **178**, 630-642.

148. Truebenbach, I., Gorges, J., Kuhn, J., Kern, S., Baratti, E., Kazmaier, U., Wagner, E., and Lächelt, U., *Sequence-Defined Oligoamide Drug Conjugates of Pretubulysin and Methotrexate for Folate Receptor Targeted Cancer Therapy*. Macromol Biosci, 2017. **17**, 1600520.

149. Bundesministerium der Justiz und für Verbraucherschutz. *Tierschutzgesetz (TierSchG)*. 2017 [cited 2018 23 august]; Available from: <https://www.gesetze-im-internet.de/tierschg/>.
150. Xu, X.M., Chen, Y., Chen, J., Yang, S., Gao, F., Underhill, C.B., Creswell, K., and Zhang, L., *A peptide with three hyaluronan binding motifs inhibits tumor growth and induces apoptosis*. *Cancer Res*, 2003. **63**(18): p. 5685-90.
151. Baskin, J.M., Prescher, J.A., Laughlin, S.T., Agard, N.J., Chang, P.V., Miller, I.A., Lo, A., Codelli, J.A., and Bertozzi, C.R., *Copper-free click chemistry for dynamic in vivo imaging*. *Proc Natl Acad Sci U S A*, 2007. **104**(43): p. 16793-7.
152. Chang, P.V., Prescher, J.A., Sletten, E.M., Baskin, J.M., Miller, I.A., Agard, N.J., Lo, A., and Bertozzi, C.R., *Copper-free click chemistry in living animals*. *Proc Natl Acad Sci U S A*, 2010. **107**(5): p. 1821-6.
153. Rostovtsev, V.V., Green, L.G., Fokin, V.V., and Sharpless, K.B., *A Stepwise Huisgen Cycloaddition Process: Copper(I)-Catalyzed Regioselective "Ligation" of Azides and Terminal Alkynes*. *Angewandte Chemie*, 2002. **114**(14): p. 2708-2711.
154. Klein, P., Klinker, K., Zhang, W., Kern, S., Kessel, E., Wagner, E., and Barz, M., *Efficient Shielding of Polyplexes Using Heterotelechelic Polysarcosines*. *Polymers*, 2018. **10**(6).
155. Bazak, R., Houry, M., El Achy, S., Kamel, S., and Refaat, T., *Cancer active targeting by nanoparticles: a comprehensive review of literature*. *J Cancer Res Clin Oncol*, 2015. **141**(5): p. 769-84.
156. Lee, D.J., Kessel, E., Lehto, T., Liu, X., Yoshinaga, N., Padari, K., Chen, Y.C., Kempster, S., Uchida, S., Rädler, J.O., Pooga, M., Sheu, M.T., Kataoka, K., and Wagner, E., *Systemic Delivery of Folate-PEG siRNA Lipopolyplexes with Enhanced Intracellular Stability for In Vivo Gene Silencing in Leukemia*. *Bioconjug Chem*, 2017. **28**(9): p. 2393-2409.
157. Müller, K., Kessel, E., Klein, P.M., Höhn, M., and Wagner, E., *Post-PEGylation of siRNA Lipo-oligoamino Amide Polyplexes Using Tetra-glutamylated Folic Acid as Ligand for Receptor-Targeted Delivery*. *Molecular Pharmaceutics*, 2016. **13**(7): p. 2332-2345.
158. Linke, S.P., Clarkin, K.C., Di Leonardo, A., Tsou, A., and Wahl, G., *A reversible, p53-dependent G0/G1 cell cycle arrest induced by ribonucleotide depletion in the absence of detectable DNA damage*. Vol. 10. 1996. 934-47.
159. Fairchild, C.R., Maybaum, J., and Straw, J.A., *Enhanced cytotoxicity with methotrexate in conjunction with hypoxanthine in L1210 cells in culture*. *Cancer Chemother Pharmacol*, 1988. **22**(1): p. 26-32.
160. Herrmann, J., Elnakady, Y.A., Wiedmann, R.M., Ullrich, A., Rohde, M., Kazmaier, U., Vollmar, A.M., and Müller, R., *Pretubulysin: from*

hypothetical biosynthetic intermediate to potential lead in tumor therapy. PLoS One, 2012. **7**(5): p. e37416.

161. Burger, A.M., Hartung, G., Stehle, G., Sinn, H., and Fiebig, H.H., *Pre-clinical evaluation of a methotrexate–albumin conjugate (MTX-HSA) in human tumor xenografts in vivo.* International Journal of Cancer, 2001. **92**(5): p. 718-724.

162. Lächelt, U., and Wagner, E., *Nucleic Acid Therapeutics Using Polyplexes: A Journey of 50 Years (and Beyond).* Chemical Reviews, 2015. **115**(19): p. 11043-11078.

163. Lee, D.-J., He, D., Kessel, E., Padari, K., Kempter, S., Lächelt, U., Rädler, J.O., Pooga, M., and Wagner, E., *Tumoral gene silencing by receptor-targeted combinatorial siRNA polyplexes.* Journal of Controlled Release, 2016. **244**: p. 280-291.

164. Müller, K., Klein, P.M., Heissig, P., Roidl, A., and Wagner, E., *EGF receptor targeted lipo-oligocation polyplexes for antitumoral siRNA and miRNA delivery.* Nanotechnology, 2016. **27**(46): p. 464001.

165. Zhang, W., Müller, K., Kessel, E., Reinhard, S., He, D., Klein, P.M., Höhn, M., Rödl, W., Kempter, S., and Wagner, E., *Targeted siRNA Delivery Using a Lipo-Oligoaminoamide Nanocore with an Influenza Peptide and Transferrin Shell.* Adv Healthc Mater, 2016. **5**(12): p. 1493-504.

166. Morys, S., Urnauer, S., Spitzweg, C., and Wagner, E., *EGFR Targeting and Shielding of pDNA Lipopolyplexes via Bivalent Attachment of a Sequence-Defined PEG Agent.* Macromolecular Bioscience, 2017. **18**(1): p. 1700203.

167. Akinc, A., Querbes, W., De, S., Qin, J., Frank-Kamenetsky, M., Jayaprakash, K.N., Jayaraman, M., Rajeev, K.G., Cantley, W.L., Dorkin, J.R., Butler, J.S., Qin, L., Racie, T., Sprague, A., Fava, E., Zeigerer, A., Hope, M.J., Zerial, M., Sah, D.W., Fitzgerald, K., Tracy, M.A., Manoharan, M., Kotliansky, V., Fougères, A., and Maier, M.A., *Targeted delivery of RNAi therapeutics with endogenous and exogenous ligand-based mechanisms.* Mol Ther, 2010. **18**(7): p. 1357-64.

168. Lundqvist, M., Stigler, J., Elia, G., Lynch, I., Cedervall, T., and Dawson, K.A., *Nanoparticle size and surface properties determine the protein corona with possible implications for biological impacts.* Proc Natl Acad Sci U S A, 2008. **105**(38): p. 14265-70.

169. Caracciolo, G., Callipo, L., De Sanctis, S.C., Cavaliere, C., Pozzi, D., and Lagana, A., *Surface adsorption of protein corona controls the cell internalization mechanism of DC-Chol-DOPE/DNA lipoplexes in serum.* Biochim Biophys Acta, 2010. **1798**(3): p. 536-43.

170. Albrecht, M., Henke, J., Tacke, S., Markert, M., and Guth, B., *Influence of repeated anaesthesia on physiological parameters in male Wistar rats: a telemetric study about isoflurane, ketamine-xylazine and a combination of medetomidine, midazolam and fentanyl.* BMC Veterinary

Research, 2014. **10**(1): p. 310.

171. Albrecht, M., Henke, J., Tacke, S., Markert, M., and Guth, B., *Effects of isoflurane, ketamine-xylazine and a combination of medetomidine, midazolam and fentanyl on physiological variables continuously measured by telemetry in Wistar rats*. BMC Vet Res, 2014. **10**: p. 198.

172. Constantinides, C., Mean, R., and Janssen, B.J., *Effects of isoflurane anesthesia on the cardiovascular function of the C57BL/6 mouse*. Ilar j, 2011. **52**(3): p. e21-31.

173. Bazak, R., Hourri, M., Achy, S.E., Hussein, W., and Refaat, T., *Passive targeting of nanoparticles to cancer: A comprehensive review of the literature*. Molecular and Clinical Oncology, 2014. **2**(6): p. 904-908.

174. Hoshyar, N., Gray, S., Han, H., and Bao, G., *The effect of nanoparticle size on in vivo pharmacokinetics and cellular interaction*. Nanomedicine (Lond), 2016. **11**(6): p. 673-92.

175. Valentine, M.T., Fordyce, P.M., and Block, S.M., *Eg5 steps it up!* Cell Div, 2006. **1**: p. 31.

176. Edinger, D., Kläger, R., Troiber, C., Dohmen, C., and Wagner, E., *Gene silencing and antitumoral effects of Eg5 or Ran siRNA oligoaminoamide polyplexes*. Drug Deliv Transl Res, 2014. **4**(1): p. 84-95.

177. Judge, A.D., Robbins, M., Tavakoli, I., Levi, J., Hu, L., Fronda, A., Ambegia, E., McClintock, K., and MacLachlan, I., *Confirming the RNAi-mediated mechanism of action of siRNA-based cancer therapeutics in mice*. J Clin Invest, 2009. **119**(3): p. 661-73.

178. National Cancer Institute. *NCI Drug Dictionary*. 2018 [cited 2018 10 august]; Available from: <https://www.cancer.gov/publications/dictionaries/cancer-drug/search?contains=true&q=tubulysin>.

179. Kaur, G., Hollingshead, M., Holbeck, S., Schauer-Vukasinovic, V., Camalier, R.F., Domling, A., and Agarwal, S., *Biological evaluation of tubulysin A: a potential anticancer and antiangiogenic natural product*. Biochem J, 2006. **396**(2): p. 235-42.

180. Rajabi, M., and Mousa, S.A., *The Role of Angiogenesis in Cancer Treatment*. Biomedicines, 2017. **5**(2).

181. Carmeliet, P., and Jain, R.K., *Molecular mechanisms and clinical applications of angiogenesis*. Nature, 2011. **473**: p. 298.

182. Lee, D.J., Kessel, E., Edinger, D., He, D., Klein, P.M., Voith von Voithenberg, L., Lamb, D.C., Lächelt, U., Lehto, T., and Wagner, E., *Dual antitumoral potency of EG5 siRNA nanoplexes armed with cytotoxic bifunctional glutamyl-methotrexate targeting ligand*. Biomaterials, 2016. **77**: p. 98-110.

183. Hanahan, D., and Weinberg, R.A., *The hallmarks of cancer*. Cell, 2000. **100**(1): p. 57-70.

184. Hanahan, D., and Weinberg, R.A., *Hallmarks of cancer: the next generation*. Cell, 2011. **144**(5): p. 646-74.
185. Keith, C.T., Borisy, A.A., and Stockwell, B.R., *Multicomponent therapeutics for networked systems*. Nat Rev Drug Discov, 2005. **4**(1): p. 71-8.
186. Shah, M.A., and Schwartz, G.K., *The relevance of drug sequence in combination chemotherapy*. Drug Resist Updat, 2000. **3**(6): p. 335-356.
187. T., D.V., C., Y.R., and P., C.G., *Combination versus single agent chemotherapy: A review of the basis for selection of drug treatment of cancer*. Cancer, 1975. **35**(1): p. 98-110.
188. Zimmermann, G.R., Lehár, J., and Keith, C.T., *Multi-target therapeutics: when the whole is greater than the sum of the parts*. Drug Discovery Today, 2007. **12**(1): p. 34-42.
189. Zhao, R., Diop-Bove, N., Visentin, M., and Goldman, I.D., *Mechanisms of membrane transport of folates into cells and across epithelia*. Annu Rev Nutr, 2011. **31**: p. 177-201.
190. Lächelt, U., Wittmann, V., Müller, K., Edinger, D., Kos, P., Höhn, M., and Wagner, E., *Synthetic polyglutamylation of dual-functional MTX ligands for enhanced combined cytotoxicity of poly(I:C) nanoplexes*. Mol Pharm, 2014. **11**(8): p. 2631-9.
191. Otrocka, M., Verschueren, H., and Malicka-Błaszkiwicz, M., *The effect of methotrexate on actin and invasiveness of hepatoma Morris 5123 cells in culture*. Acta Biochim Pol, 2001. **48**(4): p. 1051-60.
192. Mazur, A.J., Nowak, D., Mannherz, H.G., and Malicka-Błaszkiwicz, M., *Methotrexate induces apoptosis in CaSki and NRK cells and influences the organization of their actin cytoskeleton*. European Journal of Pharmacology, 2009. **613**(1): p. 24-33.
193. Liao, G., Nagasaki, T., and Gundersen, G.G., *Low concentrations of nocodazole interfere with fibroblast locomotion without significantly affecting microtubule level: implications for the role of dynamic microtubules in cell locomotion*. J Cell Sci, 1995. **108 (Pt 11)**: p. 3473-83.
194. Danowski, B.A., *Fibroblast contractility and actin organization are stimulated by microtubule inhibitors*. J Cell Sci, 1989. **93 (Pt 2)**: p. 255-66.
195. Krendel, M., Zenke, F.T., and Bokoch, G.M., *Nucleotide exchange factor GEF-H1 mediates cross-talk between microtubules and the actin cytoskeleton*. Nat Cell Biol, 2002. **4**(4): p. 294-301.
196. Emilienne Soma, C., Dubernet, C., Bentolila, D., Benita, S., and Couvreur, P., *Reversion of multidrug resistance by co-encapsulation of doxorubicin and cyclosporin A in polyalkylcyanoacrylate nanoparticles*. Biomaterials, 2000. **21**(1): p. 1-7.
197. Mayer, L.D., and St-Onge, G., *Determination of free and liposome-*

associated doxorubicin and vincristine levels in plasma under equilibrium conditions employing ultrafiltration techniques. Anal Biochem, 1995. **232**(2): p. 149-57.

VIII. APPENDIX

1. Publications

Morys, S., Krhac Levacic, A., Urnauer, S., Kempter, S., Kern, S., Rädler, J.O., Spitzweg, C., Lächelt, U., Wagner, E. (2017) **Influence of Defined Hydrophilic Blocks within Oligoaminoamide Copolymers: Compaction versus Shielding of pDNA Nanoparticles**, *Polymers* 2017, 9(4), 142.

Truebenbach, I., Gorges, J., Kuhn, J., Kern, S., Baratti, E., Kazmaier, U., Wagner, E., Lächelt, U. (2017) **Sequence-Defined Oligoamide Drug Conjugates of Pretubulysin and Methotrexate for Folate Receptor Targeted Cancer Therapy**, *Macromol Biosci.* 2017 Oct; 17(10) 1600520.

Klein, P.M., Klinker, K., Zhang, W., Kern, S., Kessel, E., Wagner, E., Barz, M. **Efficient Shielding of Polyplexes Using Heterotelechelic Polysarcosines**. *Polymers* 2018, 10, 689.

Klein, P.M., Kern, S., Lee, D.J., Schmaus, J., Höhn, M., Gorges, J., Kazmaier, U., Wagner, E. **Folate receptor-directed orthogonal click-functionalization of siRNA lipopolyplexes for tumor cell killing in vivo**. *Biomaterials* 2018, 178, 630-642.

Kern, S., Truebenbach I., Höhn, M., Gorges, J., Kazmaier, U., Zahler, S., Vollmar, A. M., Wagner, E. **Combined Antitumoral Effects of Pretubulysin and Methotrexate**. *Pharmacology research & perspectives*, 2019. 7(1): p. e00460-e00460.

Truebenbach I., Kern, S., Loy, D., Gorges, J., Kazmaier, U., Wagner, E. **Combination chemotherapy of L1210 tumors in mice with pretubulysin and methotrexate**. Manuscript submitted.

2. Abstracts and Posters

2.1. Poster

Kern, S., Klein, P.M., Lee, D.J., Zhang, W., Wagner, E. **Folate receptor-directed siRNA lipopolyplexes for tumor-targeted gene silencing in vivo.** CeNS Workshop 2017 "Design and Control of NanoSystems", Venice, Italy, September 2017

2.2. Abstract

Kern, S., Klein, P.M., Lee, D.J., Zhang, W., Wagner, E. **Folate receptor-directed siRNA lipopolyplexes for tumor-targeted gene silencing in vivo.** CeNS Workshop 2017 "Design and Control of NanoSystems", Venice, Italy, September 2017

IX. ACKNOWLEDGEMENTS

Many people contributed to the completion of this thesis. Without all of you, this project would not have been possible!

First of all, I would like to thank Prof. Dr. Ernst Wagner for being my mentor and giving me the opportunity to perform this work on his chair. Thank you for your support and advice, but most importantly for the confidence you had in me concerning the animal facility and *in vivo* experiments.

I would like to express my gratitude to Prof. Dr. Eckhard Wolf, for being my veterinary supervisor and accepting this thesis at the department of veterinary medicine.

Teamwork has always been very important in our lab. Therefore, I would like to highlight especially Ines Truebenbach and Philipp Klein for the cooperation in numerous experiments. Also, my special thank goes to DJ Lee and Johannes Schmaus for assistance during animal experiments.

Furthermore, I would like to thank Markus Kovak for the maintenance and the good atmosphere in the animal facility, Wolfgang Rödl for technical support at all times and Olga Brück for secretary work. My special thank goes to Miriam Höhn who spent so much time and effort in supporting me with histologic evaluations and covered cell culture for *in vivo* experiments whenever she could.

I would like to express my gratitude to the whole team for creating such a good atmosphere, especially during the last year. It was great enjoying your company not only in a professional way, but also during various activities apart from work, for example during ski trips, carnival, Wiesn or in the famous Rendez vous bar! Special thanks to Jasmin, making the time in our “creative office” unforgettable, Johannes for all the lunch breaks we spent outside even at the tiniest ray of sunlight, Ines, Philipp and Sören for the careful proofreading of this work.

Moreover, I would like to thank Silja for a great friendship and a lot of support. It was great enjoying your companionship while writing this thesis, but more importantly during unforgettable lunch breaks and after-work hours

for frozen yogurt near the Eisbach.

These past few years would not have been the same without the company of my friends from university times who were not all always present (Fay!) but always there for me to share the ups and downs.

My special thank goes to my parents who have always supported and encouraged me on my way. Thank you for your trust in my decisions, your open ear at all times, and for being there for me with a warm advice whenever I need it!

Finally, I would like to thank Georg. With your caring, even-tempered and cheerful manner, you have always succeeded in calming me down and making me smile, especially during the last few weeks. Thank you for your constant support and for being by my side!